Terms and Conditions of Use of Digitised Theses from Trinity College Library Dublin

Copyright statement

All material supplied by Trinity College Library is protected by copyright (under the Copyright and Related Rights Act, 2000 as amended) and other relevant Intellectual Property Rights. By accessing and using a Digitised Thesis from Trinity College Library you acknowledge that all Intellectual Property Rights in any Works supplied are the sole and exclusive property of the copyright and/or other IPR holder. Specific copyright holders may not be explicitly identified. Use of materials from other sources within a thesis should not be construed as a claim over them.

A non-exclusive, non-transferable licence is hereby granted to those using or reproducing, in whole or in part, the material for valid purposes, providing the copyright owners are acknowledged using the normal conventions. Where specific permission to use material is required, this is identified and such permission must be sought from the copyright holder or agency cited.

Liability statement

By using a Digitised Thesis, I accept that Trinity College Dublin bears no legal responsibility for the accuracy, legality or comprehensiveness of materials contained within the thesis, and that Trinity College Dublin accepts no liability for indirect, consequential, or incidental, damages or losses arising from use of the thesis for whatever reason. Information located in a thesis may be subject to specific use constraints, details of which may not be explicitly described. It is the responsibility of potential and actual users to be aware of such constraints and to abide by them. By making use of material from a digitised thesis, you accept these copyright and disclaimer provisions. Where it is brought to the attention of Trinity College Library that there may be a breach of copyright or other restraint, it is the policy to withdraw or take down access to a thesis while the issue is being resolved.

Access Agreement

By using a Digitised Thesis from Trinity College Library you are bound by the following Terms & Conditions. Please read them carefully.

I have read and I understand the following statement: All material supplied via a Digitised Thesis from Trinity College Library is protected by copyright and other intellectual property rights, and duplication or sale of all or part of any of a thesis is not permitted, except that material may be duplicated by you for your research use or for educational purposes in electronic or print form providing the copyright owners are acknowledged using the normal conventions. You must obtain permission for any other use. Electronic or print copies may not be offered, whether for sale or otherwise to anyone. This copy has been supplied on the understanding that it is copyright material and that no quotation from the thesis may be published without proper acknowledgement.

Optical and Electrical Properties of Modified Conjugated Polymer Thin Films

Malcolm Stephen Lipson

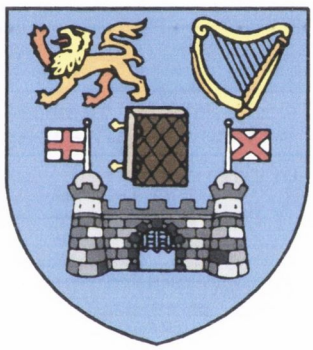

A thesis submitted for the degree of Doctor of Philosophy

Department of Pure and Applied Physics

University of Dublin

Trinity College

Dublin 2

Ireland

November 2001

Declaration

This thesis is submitted to the University of Dublin, Trinity College for the degree of Doctor of Philosophy. The work described herein is entirely my own, with the exception of the assistance mentioned in the acknowledgements.

This thesis has not been submitted as an exercise for a degree to this or any other university.

I agree that the University of Dublin, Trinity College Library may lend or copy this thesis upon request.

Stephen Lipson

Stephen Lipson

November 2001

Dedication

To my parents, for their tireless love and support.

"Pain is the feeling of weakness leaving the body."
Patrick Walsh DUHAC athlete 1996/97.

"There is more to being here than the medals. There is more to running than winning, there is just the rhythm of it."
Sonia O'Sullivan, commenting on her sixth place in the 10000m at the Sydney 2000 Summer Olympic Games.

Abstract

The ability to control both the spectral and electrical stability of polymer light emitting devices are just two of the parameters that are paramount to their commercial viability. The presence of water vapour and oxygen in such devices can be detrimental to both the short and long term performance of the device. In this thesis a numbers of different thin film processing techniques were employed to remove air from thin films of the conjugated polymer poly(*meta*-phenylenevinylene-co-2,5-dioctlyoxy-*para*-phenylenevinylene) [PmPV] to enhance its photostability. Each processing technique was calibrated for photoluminescence intensity. One technique, which required solution degassing, inert atmosphere spinning and a vacuum baking environment, showed significantly improved properties and was studied in depth using photoinduced absorption spectroscopy. Polaron formation and excited state absorptions were found to strongly influence the photoluminescence efficiency. The control of aggregation and thus interchain separation enabled the photoluminescence efficiency to be varied by the control of thin film morphology. The electrical properties of PmPV films prepared using this preparation technique were measured and some were found to be improved relative to conventional preparation techniques. The use of both alternating and direct current measurement techniques allowed a deep understanding of the changes in the electrical properties to be understood. Single layer light emitting devices were fabricated utilising polymer films prepared using this technique. They were found to have a larger current density for a given operating electric field giving significantly brighter devices. Additionally it was noted that the device operating lifetimes were improved. In conclusion the changes in film morphology resulting from the novel preparation of thin films of the polymer PmPV provided an insight to the photophysics of polymeric materials. The technique improved the photoluminescence efficiency and photostability of the material whilst increasing the positive charge carrier mobility of the material under the application of an electric field, leading to the fabrication of significantly enhanced light emitting devices utilising PmPV.

Acknowledgements

Firstly I would like to thank my supervisor Professor Werner Blau for giving me the opportunity to do a Ph.D. His help and support over the last five years, combined with the travel opportunities and the trust bestowed on me to give a number of talks on his behalf, including an invited talk, have been appreciated. I would also like to thank Professor Donal Bradley and Dr. Paul Lane for giving me the opportunity to perform the photoinduced absorption measurements at the University of Sheffield.

Amongst the administrative and technical staff in the Physics Department a special thanks must go to the following people: Tom Burke and John Kelly for processing all the paperwork associated with doing a Ph.D. and ordering equipment and supplies, Jeannette for all her help with booking flights and accommodation at short notice, James Egan for always making time to do the jobs requested of him, Michelle, Natalie, Susan and Liz for helping to solve problems, never questioning my use of the photocopying card and keeping me supplied with swift post labels and transparencies.

Within the group I would like to thank the following people for overseeing my work and guiding me through my years in the group: Kieran Ryder for supervising my 4th year project, Kevin Kretsch for guiding me through the early days, Dr. Diarmuid O'Brien for directing me through the middle two years and Dr. Jonathon Coleman for overseeing the final year. On the chemistry side of things Anna Drury deserves a special thank you for not only putting up with the constant bombardment of chemistry questions but for continuing to answer them after my numerous public lambastings of the quality of the PmPV emerging from her lab.

Outside the group I would like to thank Dr. Hugh Byrne for allowing me pretty much unlimited access to his spectroscopy lab and for all his help and guidance. Dr. Sean Martin for allowing me easy access to the FTIR machines and Dr. Jenny Boyle for making the vacuum oven available at times that suited me.

In the University of Sheffiled I would also like to thank Ashley Cadby and Dr. David Lidzey for allowing me to use the PA equipment and the integrating sphere respectively. Also for their guidance, help and advice on using the equipment. Also not forgetting Alasdair Campbell and Rob Fletcher.

Back within the group I would like to thank the following members past and present for their help, hindrance, patience, attachments etc. etc. Adam, Adrian, Alan, Alexander, Andy, Bernd, Brendan, Brian, Catrina, Colin, Dave, Donna, Elizabeth, Francesco, Georg, Janet, Jean, Keith, Lucia, Manual, Marc, Margaret, Marie, Martin, Michael, Orla, Patrick, Rob, Robert, Shay, Sean, Stefanie, Take and Valerie. My apologies to anyone that I have forgotten. Within physics but outside of the group I would also like to thank Dr. Vincent Weldon, Gordan Chambers and Kieran Henderson.

Outside of physics I would like to thank all the members of DUHAC, past and present, most of whom think I'm part of the furniture within college and a damn sight older than I actually am, for providing me with endless miles of fun and challenges during my eight years in the club.

Also, to Derek for advising me that the smoke was getting very thick and that I really should get out of the house, as I grabbled to disconnect all the cables from the back of the PC before the house burnt down, only to discover that most of the data on it was potentially useless if the two lab books lying in the middle of my bedroom floor had not survived. They got hit by the fireman's hose and didn't suffer the fate of my desk and even more luckily they dried out without all the pages sticking together. Also to Ronan who managed to rescue all the data from my seemingly dead hard drive a matter of weeks prior to submission, and for his amazing lack of annoyance when he discovered that my hard drive had fried his motherboard and hard drive. I later discovered why he wasn't too perturbed; he had everything backed up on several hard drives!

Table of Contents

Chapter 1

Introduction

1.1 Introduction

The conventional perception of polymers is what are commonly known as 'plastics'. At a molecular level these materials are long organic molecules with simple repeat units. The term conjugated is used to describe a material where carbon single bonds alternate with carbon multiple bonds along a molecule. The multiple carbon bonds form π molecular orbitals, which combine along the chain to form a large delocalised molecular orbital. This high delocalisation of the π- electrons is the source of the large non-linear optical parameters measured in conjugated polymers[1,2,3].

Since the doping of polyacetylene in 1977[4] there has been great interest in conjugated organic materials for electrical, opto-electronic and optical applications. Previously organic materials had been used to make optical waveguides and had exhibited fluorescence amplification in doped polymeric waveguides[5]. Organic materials emerged in the late 1970s as a possible alternative to semiconductors and glasses for integrated non-linear optical switching[2]. A large non-linear optical figure of merit, high optical damage thresholds, ultra fast responses, architectural flexibility and ease of fabrication have made conjugated polymers the subject of non-linear optical research over the last two decades.

It soon became apparent that conjugated polymers were efficient emitters of light across the visible spectrum. Once they were discovered to be semiconducting, electroluminescence was demonstrated[6]. This lead to considerable effort being directed towards the development of flat displays and research in this area is ongoing. Also light emission at the UV/blue end of the spectrum was a priority because of the difficulty in developing inorganic light emitting devices (LEDs) in this region of the spectrum.

Lasing has also been observed in solutions[7] of conjugated polymers and in the solid state[8]. The production of bright, long life organic LEDs has developed to the stage where limited colour small area displays are commercially available. For full colour displays these properties must be attained across the visible spectrum. Inorganic LEDs right across the visible spectrum are now commercially available, but organic LEDs are significantly cheaper than their inorganic equivalent and once high efficiency, long lifetime organic LEDs have been achieved they will offer a viable alternative. Additionally the development of an electrically pumped organic or polymer laser will open up another sector of the market. For example the fabrication of an economically affordable blue emitting laser will revolutionise the world of data storage and optical communications.

Another area of active research is in non-linear optical switching. The factor currently limiting 'fibre to the home' from reaching every home is the cost of putting the fibres in the ground. The potential to replace the expensive electrical switches with not only cheaper but also faster optical switches, which double up as cheap fibre couplers, could prove the way forward. All-optical switching provides a means to overcome the limitations imposed by electronics. The ultrafast or instantaneous phase shifts available through all optical interactions have been demonstrated in demultiplexing at the receiver end of Optical Time Division Multiplexing systems[9], optical clock recovery[10], and optical modulation of laser sources[11]. Because the effect is instantaneous it is then possible to increase the bit rate as required without significant alteration to the transmitter or receiver ends of the fibre link. The instantaneous non-linear phase shifts and waveguiding properties associated with conjugated polymers makes them ideal candidate materials.

With the worlds fossil fuel supplies due to run out by the middle of this century, the need for alternative and renewable energy sources is currently at its highest level. Hydro, wind and solar energy are three abundant sources of renewable and environmentally friendly energy that if harnessed efficiently can provide a cheap and viable alternative to fossil fuels and other potentially less environmentally friendly sources of energy such as nuclear power. Inorganic solar cells are currently used to convert solar energy into electricity, but the cost of producing these cells is expensive,

making the process uneconomical. Fabrication of cheap high efficiency organic solar cells could offer a viable alternative[12].

Nanoelectronics is another area of active research. The quest for ever smaller electrical components, such as transistors for electronic circuit boards, has lead researchers to look to alternative materials. The possibility of using a single molecule in a switching geometry is still several years away, but when achieved will reduce the dimensions of electronic circuitry.

At the low tech end of the scale the use of synthetic materials is evident in every day life. From the clothes we wear, to the packaging on the food we buy, to the casings on most household electrical goods. The low weight, high strength properties associated with some synthetic composite materials is vastly superior to that of any inorganic material. From cling film to bulletproof vests, the versatility and processability of these materials has made them an integral part of everyday life.

1.2 Background and Motivation

Photoluminescence degradation in organic materials upon exposure to visible radiation, be it from the sun, room lights or a visible laser source, is a big concern, as the long term commercial usage and viability of these materials in optical and electrical devices will involve exposure to visible radiation sources. The ability to survive this exposure is essential to the viability of such materials for some applications. Long device operating lifetimes and spectral emission stability are two of the important parameters that must be met prior to a material becoming commercially viable for use in optical and electrical devices. The industry standard for device operating lifetimes is a minimum of 10000 hours. Spectral stability is essential for display clarity over the operating lifetime. These parameters can prove difficult to attain, especially if a material photo-degrades through its own emission. The emission spectrum of polymeric materials tends to blue shift upon photo-degradation. This problem can be eliminated if photostable materials can be attained.

Prior to performing the work presented in this thesis amplified spontaneous emission measurements in waveguide geometries were being performed on poly phenylene vinylene (PPV) derivatives and on PPV model compounds[13,14]. The rate of photo-degradation, particularly in the polymeric materials, was causing problems in performing the gain narrowing threshold measurements. As the pump power increased the rate of photo-degradation increased and the photoluminescence efficiency decreased. This meant that more power was required to maintain the same levels of optical gain, giving rise to inaccurate measurements. At this juncture it was decided to study photo-degradation in polymeric materials to gain an understanding of what was happening, with a view to developing experimental techniques for minimising its effects.

The primary aim was to study the effects of air, both in the atmosphere and trapped within the film, on the rate of photo-degradation. The results of this work revealed some very interesting results that warranted further study, namely the magnitude of the photoluminescence efficiency increase observed, which was significantly larger than expected and the apparent change in film morphology, both of which warranted an explanation. The explanation derived lead to a complete electrical characterisation of PmPV thin film structures.

Any thin film fabrication technique that fabricates more photoefficient and photostable films with no negative effects on the electrical properties of the polymer will advance the science of organic light emitting devices significantly.

1.3 Thesis Outline

Chapter one details the basic introduction to polymer physics followed by the background and motivation to the work presented in this thesis. The thesis outline is also presented. Chapter two deals with the photophysics of organic materials. The differences between the photophysical properties of metals, semiconductors and insulators is detailed. The doping of organic materials and their resultant conduction properties along with a number of conduction models are outlined. Finally the synthesis of poly(m-phenylenevinylene-co-2,5-dioctlyoxy-p-phenylenevinylene) [PmPV], the material used in this thesis, is described. Chapter three details photo-degradation in

polymeric materials. Thin film fabrication techniques for increasing photoluminescence efficiency and stability are explored. Chapter four uses photoinduced absorption to probe the photophysics of PmPV, enabling the factors influencing the photoluminescence efficiency to be interpreted. Chapter five has three main experimental sections. Direct Current Current-Voltage measurements are used to calculate electrical parameters. These parameters and some additional ones are then calculated using Impedance Spectroscopy. The chapter concludes with the fabrication of single layer light emitting devices. Chapter six presents the conclusions for the thesis and outlines possibilities for future work leading to further development of the experimental results presented. A list of publications is given in appendix A.

1.4 References

1. C. Sauteret, J. P. Hermann, R. Frey, F. Pradere, J. Ducuing, R. H. Baughman and R. R. Chance, 'Optical nonlinearities of polymerized diacetylenes,' Optics Communications 18 (1976) 55-56.

2. C. Sauteret, J. P. Hermann, R. Frey, F. Pradere, J. Ducuing, R. H. Baughman and R. R. Chance, 'Optical nonlinearities in one-dimensional-conjugated polymer crystals,' Phys. Rev. Lett. 36 (1976) 956-959.

3. G. P. Agrawal, 'Nonlinear optical properties of one-dimensional semiconductors and conjugated polymers,' Phys. Rev. B 17 (1978) 776-789.

4. C. K. Chiang, C. R. Jr Fincher, Y. W. Park, A. J. Heeger, H. Shirakawa, E. J. Louis, S. C. Gau and A. G. MacDiarmid, 'Electrical conductivity in doped polyacetylene.' Phys. Rev. Lett. 39 (1977) 1098-1101.

5. R. Ulrich and H. P. Weber, 'Solution-deposited thin films as passive and active light-guides.' Appl. Optics 11 (1972) 428-434.

6. J. H. Burroughes, D. D. C. Bradley, A. R. Brown, R. N. Marks, K. Mackay, R. H. Friend, P. L. Burns and A. B. Holmes, 'Light-emitting diodes based on conjugated polymers.' Nature 347 (1990) 539-541.

7. W. Holzer, A. Penzkofer, S-H. Gong, A. P. Davey and W. J. Blau, 'Laser performance studies of para-(phenylene-ethynylene) polymers in organic solvents.' Optical & Quantum Electronics 29 (1997) 713-724.

8. N. Tessler, G. J. Denton and R. H. Friend, 'Lasing from conjugated polymer microcavities.' Nature 382 (1996) 695-697.

9. D. M. Patrick, A. D. Ellis and D. M. Spirit, 'Bit-rate flexible all-optical demultiplexing using a nonlinear optical loop mirror,' Electron Lett. 29 (1993) 702-703.

10. A. D. Ellis, K. Smith and D. M. Patrick, 'All-optical clock recovery at bit rates up to 40Gbit/s,' Electron Lett. 29 (1993) 1323-1324.

11. A. D. Ellis, W. A. Pender, T. Widdowson and D. J. Richardson, 'All-optical modulation of a 40GHz beat frequency conversion soliton source,' Electron Lett. 31 (1995) 1362-1364.

12. U Bach, D. Lupo, P Comte, J. E. Moser, F. Weissortel, J. Salbeck, H. Spreitzer and M. Gratzel, 'Solid-state dye-sensitized mesoporous TiO_2 solar cells with high photon-to-electron conversion efficiencies,' Nature 395 (1998) 583-585.

13. F. Hide, B. J. Schwartz, M. A. Diaz-Garcia and A. J. Heeger, 'Conjugated polymers as solid state laser materials,' Synth. Met. 91 (1997) 35-40.

14. K. P. Kretsch, C. Belton, S. Lipson, W. J. Blau, F. Z. Henari, H. Rost, S. Pfeiffer, A. Teuschel, H. Tillmann and H-H Horhold, 'Amplified spontaneous emission and optical gain spectra from stilbenoid and phenylene vinylene derivative model compounds,' J. Appl. Phys. 86 (1999) 6155-6159

Chapter 2

Photophysics, Electrical Properties and Synthesis of Organic Materials

2.1 Outline

This chapter can be divided into three main sections. The first deals with the photophysics of organic materials. Band structure in metals, semiconductors and insulators is discussed. The formation of excited states in organic materials along with the absorptions and emissions associated with them are described in detail. The second section deals with electronic conduction and outlines models for conduction in organic materials. Doping of organic materials is also discussed. The third and final section briefly outlines the development of polymeric synthesis over the last four decades. The synthesis of the organic polymer, poly(m-phenylenevinylene-co-2,5-dioctlyoxy-p-phenylenevinylene) [PmPV], used in this thesis, is detailed.

2.2 Photophysics of Organic Materials

2.2.1 Introduction

Organic Chemistry is the study of carbon compounds. There is no definite distinction between organic and inorganic chemistry as the principles that explain the simplest inorganic compounds are also the principles that explain the most complex organic compounds. The only distinguishing characteristic of organic chemistry is that all organic compounds contain the element carbon. Carbon, either on its own or with other atoms such as Nitrogen, Oxygen and Sulphur, has the ability to bond together to form rings and long chains. This ability allows the structure of organic molecules to be chemically engineered, enabling their optical and electrical properties to be easily altered. This has many applications for the optoelectronics industry.

Organic polymers are substances consisting of macromolecules formed by linking together low molecular weight repeat units called monomers. This one dimensional structure leads to several important differences between semiconducting polymers and conventional three dimensional inorganic semiconductors.

2.2.2 Energy Bands

The electrons on isolated atoms can only have discrete energy levels. When two identical atoms are far apart they both have the same energy, but in doubly degenerate energy levels. As the two atoms are brought closer together the doubly degenerate energy level splits into two levels due to the interaction between the atoms. When N atoms are brought together, as in a crystal, the N-fold degenerate level will split into N separate but closely spaced levels due to atomic interaction. This results in an essentially continuous band of energy. Thus for each discrete energy level in an atom a continuous band of energy is formed. These bands are separated by regions which possess energies that the electrons are forbidden to have. These regions are called *energy gaps* or *band gaps*. The upper band is called the conduction band and the lower band is called the valence band. The energy band diagrams for an insulator, a semiconductor and a metal are shown in Figure 2. 1.

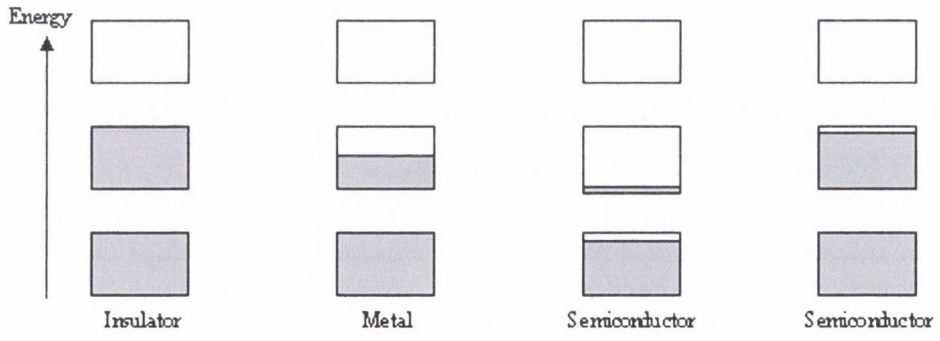

Figure 2. 1: Electron occupancy of allowed energy bands for an insulator, metal and semiconductor. The vertical extent of the boxes indicates the allowed energy regions. The shaded areas indicate the regions filled with electrons. A pure semiconductor becomes an insulator at absolute zero. The left of the two semiconductors shown is at finite temperature, with carriers excited thermally. The other semiconductor is electron deficient because of impurities. Reproduced from reference[1]

2.2.3 Electronically Excited States and Photo-Physical Processes of Organic Molecules

The large difference in mass between electrons and nuclei combined with the fact that nuclei move much more slowly than electrons, means that their motions can be treated separately according to the Born-Oppenheimer approximation. This approximation allows electrons to be visualised as moving in the potential field of static nuclei, giving the total energy of a molecule as

$$E_{Total} = E_{Electronic} + E_{Vibrational} + E_{Rotational} \qquad \textit{Equation 2. 1}$$

Photo-processes resulting from exposure to radiation in the ultra-violet and visible regions of the electromagnetic spectrum involve two steps: The production of an excited electronic state followed by its deactivation. Pure electronic transitions should produce discrete line spectra with natural linewidth broadening[2]. However vibrational and rotational excitations in molecules result in electronic transitions becoming indistinguishable through the broadening and overlap of neighbouring transitions to form broad bands. An electronic state with anti-parallel spins is a *singlet* state and that with parallel spins is a *triplet* state. Transitions are only allowed between states of the same spin multiplicity as spin angular momentum is conserved. The ground state of most organic polymers is singlet. Several different systems are used for the assignment of electronic states. The *Enumerative system* labels the states according to their spin multiplicity and increasing energy. The *Molecular orbital system* labels states by the molecular orbital involved. The *Group theory system* is used when symmetry considerations are important[3].

The energy of an electronic state can be represented by a Morse curve[3], with the vibrational states as horizontal lines as shown in Figure 2. 2. Transitions between electronic states are considered as transitions between vibronic states. The intensity of a transition band is governed by the Frank-Condon principle, which states that the electronic transition of highest probability is that from the ground vibronic level of the lower electronic state to the vibronic level of the higher electronic state lying vertically above it. This implies that an electronic transition occurs so rapidly in comparison with the vibration frequencies that no change occurs in inter-nuclear separation during the course of a transition. In terms of quantum mechanics the

intensity of a vibronic transition is proportional to the square of the overlap integral between the two vibrational wave functions involved in the transition. With increasing vibrational quantum number the electron wave functions have larger amplitudes near the limits of their displacement, giving them higher transition probabilities. Selection rules for electronic transitions should really be viewed as transition probabilities, instead of strictly allowed or forbidden transitions. Transitions do occur between electronic states of different spin multiplicity but the transition probability is usually small. However in the presence of heavy atoms, spin orbit-coupling increases, giving rise to a higher transition probability. Electronic transitions lead to changes in electron distribution, leading to changes in the equilibrium internuclear separation.

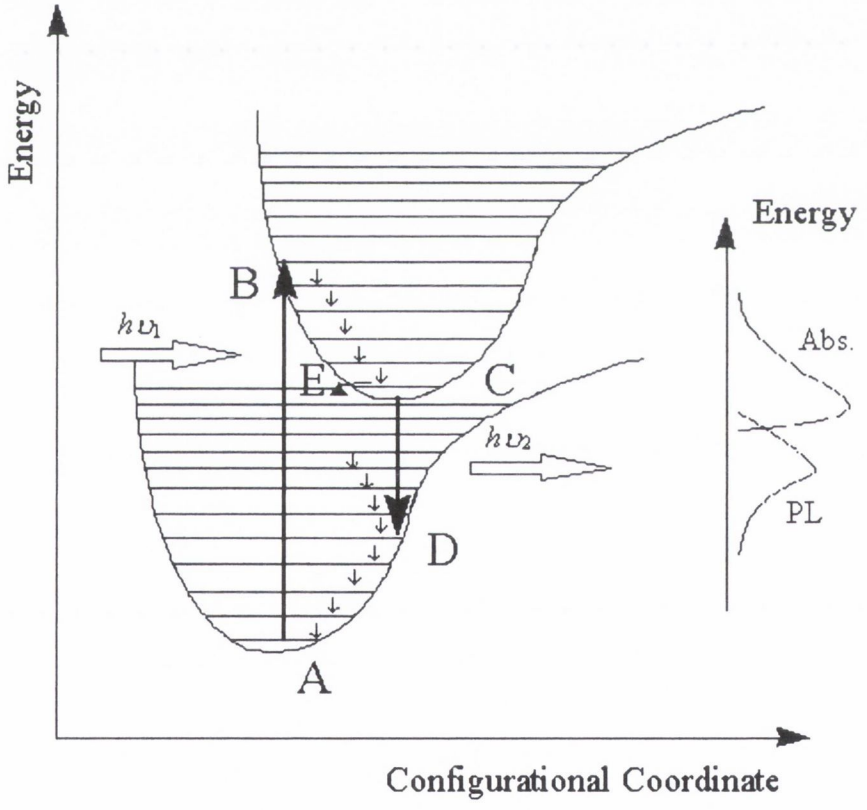

Figure 2. 2: Two level electronic model showing Absorption (AB), Luminescence (CD), Vibrational relaxation (BC, EDA) and Internal Conversion (CE).

Vibrational relaxation occurs from any vibronic state to the vibrational ground state within the same electronic state on the 10^{-13}-10^{-12} second time scale. This occurs through vibrational motion of the molecule. After relaxing to the lowest vibrational

state the electron can return to the ground state by emitting its excess energy as a photon or by non-radiative decay through internal conversion between the excited electronic state and the ground state, of states with the same spin multiplicity. These two decay routes have different lifetimes with luminescence lifetimes ranging from 10^{-10}-10^{-8} seconds and internal conversion lifetimes ranging from 10^{-13}-10^{-12} seconds, making luminescence the least preferred decay route. Luminescence becomes the dominant decay route in materials if the internal conversion lifetime is longer than the luminescence lifetime. The emitted photon is of longer wavelength than that of the absorbed light with the absorption and emission spectra being mirror images of each other. The difference between the position of the absorption and luminescence maxima is called the *Stokes shift*. Alternatively the electron can decay by intersystem crossing from the first excited singlet state to the first excited triplet state. Intersystem crossing is the non- radiative transition between electronic states of different multiplicity, although spin forbidden it takes place due to spin-orbit coupling. The rate of intersystem crossing increases in the presence of either high atomic weight atoms or paramagnetic molecules. Characteristic lifetimes range from 10^{-8}-10^{-5} seconds. Phosphorescence is the spin-forbidden emission of radiation between electronic states of different multiplicity, usually from the lowest energy triplet state to the singlet ground state. The emission band occurs at longer wavelengths than fluorescence and has typical lifetimes ranging from 10^{-4}-10^{1} seconds.

The situation however for polymeric systems is more complicated. Polymer systems have been modelled as one-dimensional periodic chains using band theory and within the framework of the molecular orbital description just described for small molecules, but both systems are incomplete. Examinations of the optical spectra of polymers show vibronic resolution in both absorption and emission spectra. This indicates the existence of strong electron-phonon coupling interactions. Hence, in longer conjugated polymer systems, localisation of excited electronic states on the polymer chain are present in the form of solitons, polarons, bipolarons, or excitons, depending on the symmetry of the polymer chain and the charge of the excitation[4].

2.2.4 Hybridisation

The most important bond in organic chemistry is the covalent bond, formed by an overlapping of atomic orbitals. When a pair of atomic orbitals, from two atoms, are combined, a pair of molecular orbitals is produced, one higher and one lower in energy than the atomic orbitals. It is the interactions between the valence electrons in the outer atomic orbital that form molecular orbital bonds. The type of molecular orbital bond formed depends on the type of atomic orbital involved and their orientation. The two bond types formed are sigma (σ) bonds and pi (π) bonds.

Carbon based materials have very distinct electronic properties based on what is known as the hybridisation of atomic orbitals. Each carbon atom has six electrons, which occupy the 1s, 2s, and 2p atomic orbitals. The 1s orbital contains two strongly bound electrons, known as core electrons. The four electrons that occupy the 2s and 2p orbitals are more weakly bound and are called valence electrons. Valence electrons give rise to 2s, $2p_x$, $2p_y$, $2p_z$ orbitals which are important for forming covalent bonds in carbon materials. Hybridisation is the mathematical combination of s and p orbitals, leading to a changing of the occupation of these orbitals so as to enhance the binding energy of the carbon with its neighbouring atoms. The hybridisation of the 2s orbital with n = 1, 2, 3 electrons in the 2p orbital is known as sp^n hybridisation. The concept of hybridisation explains how carbon bonds are formed, as the hybrid orbitals are unsymmetrical about the nucleus resulting in one of the two lobes of an sp^n orbital being much larger than the other, thus allowing a better overlap with other orbitals when bonds are formed. As a direct result of this hybrid orbitals form stronger bonds than unhybridised s and p orbitals.

The type of hybridisation determines whether an organic material is saturated or unsaturated with the former being non-conjugated and the latter being conjugated.

2.2.5 Non-Conjugated Polymers

Polymers that are formed as the result of the sp^3 hybridisation of the carbon atoms on its backbone are non-conjugated. Each carbon atom has two σ bonds to two other

carbon atoms on the chain and two σ bonds to side groups, such as hydrogen atoms or methyl groups. In this type of polymer the electrons are highly localised between atoms and can play little part in any conduction process. i.e. There is very little delocalisation of the electronic wavefunctions in sp^3 hybridised materials. Polymers of this nature are normally very good insulators with a large energy gap between the valence and conduction bands. A good illustration of this is the polymer polyethylene, shown in Figure 2. 3, which is known to be an excellent insulator. The backbone of a non-conjugated polymer is said to be saturated.

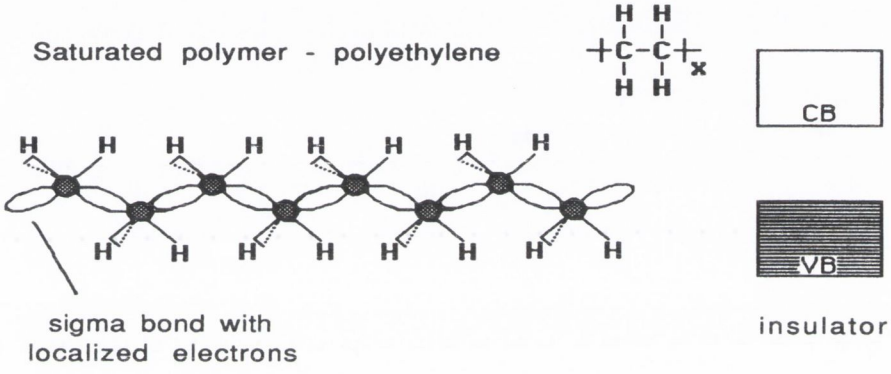

Figure 2. 3: sp^3 hybridisation leading to the saturated backbone structure and large band gap seen in the electrically insulating polymer polyethylene.

2.2.6 Conjugated Polymers

Polymers that are formed as the result of the sp^2 and sp hybridisation of the carbon atoms on its backbone are conjugated. That is they have carbon single bonds alternating with either carbon double or carbon triple bonds. Each carbon atom has two σ bonds to two other carbon atoms on the chain and for sp^2 hybridisation one σ bond to a side group, such as a hydrogen atom or a methyl group. In the case of sp^2 hybridisation this leaves one electron per atom in a p_z orbital, which is perpendicular to the backbone of the polymer chain. These orbitals overlap to form π bonds. In sp hybridisation two electrons per atom, in p_y and p_z orbitals, π bond to form carbon triple bonds. In both cases the π bonds form an extended π molecular system. These carbon double and triple bonds are unsaturated.

In order for an organic system to be considered semi-conducting or even bordering on conducting, the bonding system not only needs to establish the molecular structure of the molecule but must also provide a pseudo-continuous system of energies that can approach each other closely enough to allow the formation of delocalised electronic states. This is achieved in both sp^2 and sp hybridised systems as the overlap between the π orbitals allows carrier delocalisation along the length of the polymer chain making these materials into quasi-one dimensional systems. The π molecular orbitals have one electron per site, the lower lying half of these orbitals being occupied (π, bonding orbitals) and the upper half unoccupied (π^*, anti bonding orbitals). An excellent example of an sp^2 hybridized system is the polymer trans-polyacetylene, which is shown in Figure 2. 4.

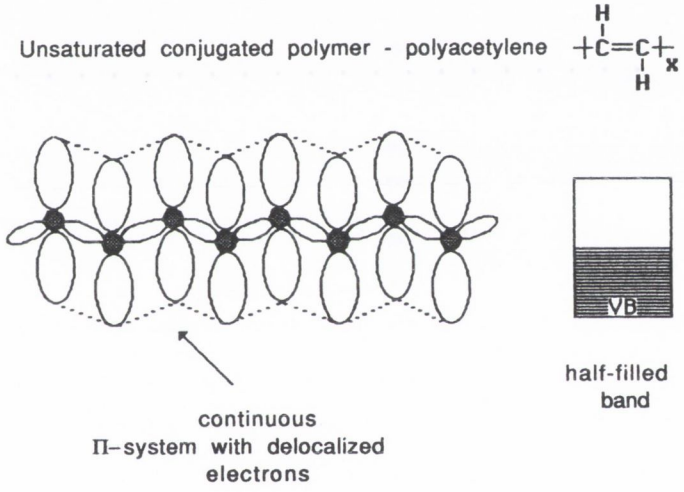

Figure 2. 4: sp^2 hybridisation leading to the unsaturated backbone structure in trans-Polyacetylene. (Hydrogen atoms have been omitted for clarity.) Complete delocalisation would result in a one-dimensional metal with a half filled conduction band.

2.2.6.1 Degenerate Ground State Polymers

Degenerate ground state polymers possess two possible bonding configurations in the ground state, meaning that single and double bonds can be swapped without altering the energy of the polymer chain. The simplest conjugated polymer is trans-polyacetylene (*t*-PA) and an infinite chain of it has two possible ground state configurations as shown in Figure 2. 5a. In fact both of these configurations can occur on the same chain as indicated in Figure 2. 5b. In this case the forth electron

on the carbon atom at the interface between the two configurations is non-bonding. The band structure of *t*-PA has been modelled by various groups[5,6] but the model most widely used is the Su, Schrieffer and Heeger (SSH)[7,8] model. This is a tight binding model, with cyclic boundary conditions that neglect electron-electron interactions. The chain was modelled as a series of carbon atoms joined by springs with an effective force constant k. Electron phonon interactions were incorporated using a nearest neighbour overlap integral. For equally spaced carbon atoms this model predicts a half filled highest energy band as shown in Figure 2. 4. This is what is expected for a linear polymer backbone consisting of a large number of equally spaced, strongly interacting p_z orbitals. Each p_z orbital can accommodate two electrons but each carbon atom donates only one electron to the band, giving rise to a half filled band, which would make *t*-PA a one-dimensional metal.

Figure 2. 5: a) The two possible orientations of trans-polyacetylene in the ground state on infinite chains. b) on the same chain.

If this were the case *t*-PA would have a completely delocalised electron wavefunction. It was however proposed by Peierls that such a metal would be unstable. In one-dimensional systems, the chain can more efficiently lower its energy by introducing bond alternation, also called dimerisation. This alternation of carbon single and double bonds limits the extent of electron delocalisation that can take place along the backbone. Bond alternation is a direct consequence of the strong coupling that exists between the π-electrons and the phonon modes of the backbone and is characteristic of many quasi one-dimensional systems. The reason

for the alternation, as shown by Peierls, is that the reduction in electronic energy due to the filled states being lowered when an energy gap is formed is more than the energy required to distort the lattice. Bond alternation in *t*-PA is shown in Figure 2. 6.

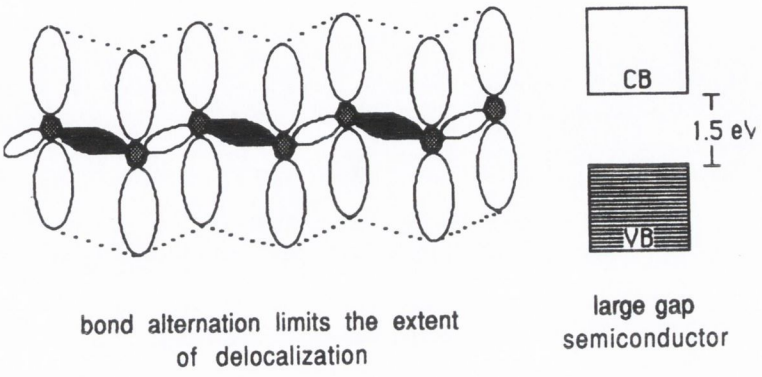

Figure 2. 6 Alternation of bond lengths in trans-polyacetylene due to Peierls distortion (about 0.07 Å for trans-polyacetylene) results in the opening of a band gap.

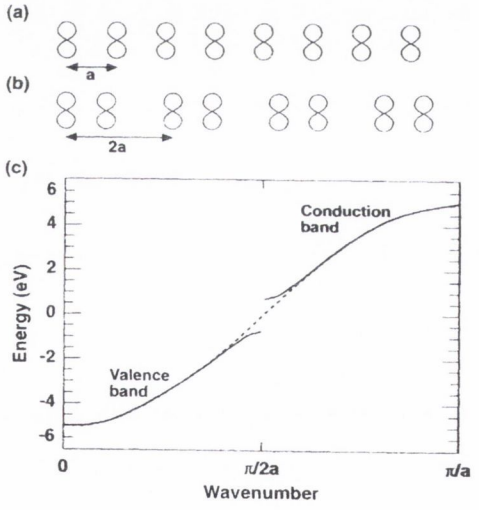

Figure 2. 7: a) p_z orbitals on an undimerised trans-polyacetylene chain and b) on a dimerised chain. c) Energy versus wavenumber for the π-band is shown as a dashed line for an undimerised chain and as a solid line for a dimerised chain. The energy gap opens up in the dispersion curve at wavevector $k = \pi/2a$. Diagram taken from reference[9]

Figure 2. 7a shows equally spaced p_z orbitals, with distance *a* between the carbon atoms, on a *t*-PA chain. The band structure of the one-dimensional metal is shown by the dashed line in Figure 2. 7c. The chain dimerisation is shown in

Figure 2. 7b, with lattice constant $2a$. The dimerisation causes an energy gap to open in the middle of the π-band as indicated by the solid line in Figure 2. 7c. In chemical terminology the lower band is called the π-band and the upper band, the π*-band, also known as the valence and conduction bands in semiconductor terminology. For a detailed theoretical analysis of bond alternation in conjugated polymers see Soos *et al*[10].

2.2.6.1.1 Solitons

As stated previously, the two degenerate ground state configurations of *t*-PA can occur on the same chain as shown in Figure 2. 5b. The two configurations are then separated by a *domain wall* with a bond distortion taking place over approximately 14 bonds along the backbone, (as opposed to the two indicated in the diagram) as predicted by the SSH model, which is called a soliton.

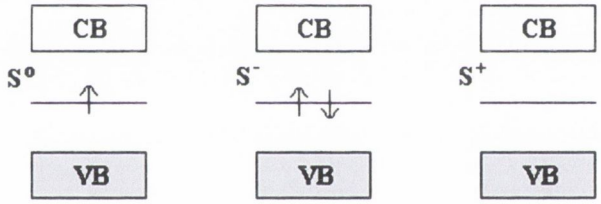

Figure 2. 8: Schematic representation showing the filling of the energy level for neutral and charged solitons.

Solitons occur in all *t*-PA chains with an odd number of C-H's, as the chains are more stable with double bonds at both ends[10]. These solitons are neutral as they occur without adding any charges to the chain. The fourth electron of the carbon at the centre of the soliton is neither bonding nor anti-bonding. It occupies a non-bonding midgap level. If an electron is added to the chain it could occupy this level, creating a negatively charged soliton (S^-). Alternatively if the original bound electron is removed from the soliton, a positive soliton is created (S^+). The three different soliton types are depicted in Figure 2. 8. Solitons are mobile and thus move along the polymer chain. Soliton defects can be added to the chain in pairs. This leads to a splitting of the midgap level with

the eventual formation of a midgap soliton band as the average soliton separation decreases. It should also be pointed out that solitons can only exist in degenerate ground state polymers.

2.2.6.2 Non-Degenerate Ground State Polymers

Non-degenerate ground state polymers only possess one possible bonding configuration in the ground state. The alternative configuration possesses a higher energy. The majority of conjugated polymers have non-degenerate ground states. In poly(*p*-phenylenevinylene) [PPV] type polymers these different energy configurations are called aromatic and quinoid, as shown in Figure 2. 9, with the aromatic configuration being lower in energy. The quinoid configuration only forms in the vicinity of a charge excitation.

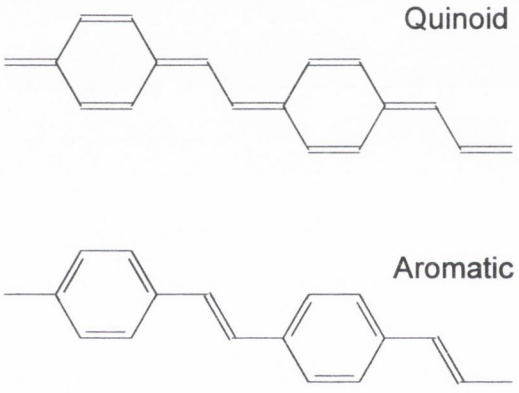

Figure 2. 9: Aromatic and quinoid forms of PPV. The quinoid form is of higher energy and is therefore not stable over large lengths of polymer chain.

The relatively large band gap in this type of polymer is not due solely to Peirels distortion. The non-degenerate ground state introduces a contribution to the energy gap, which is added to the Peierls contribution[7,8]. The band gap in this type of polymer can be as large as 3 eV. The SSH model predicts that this extra contribution will introduce defect states into the energy gap[11]. These defects can be thought of in terms of the interaction between an excited state and the polymer backbone. The equilibrium positions of the nuclei along the chain are not the same in the vicinity of an excitation as in the ground state. The result is a local bond alteration that minimises energy and is due to the strong electron phonon

interactions. The charged excitations of a non-degenerate ground state polymer are termed polarons or bipolarons and represent localised states on the polymer chain, with an accompanying local rearrangement of bond alternation.

2.2.6.2.1 Polarons and Bipolarons

The addition of a single electron to the conduction band (or hole to the valance band) in a conventional semiconductor results in this electron contributing to transport if there is no empty level in the valance band for it to decay into. In a non-degenerate ground state polymer the electron will cause the chain to deform around it if there is no space in the valance band for it to decay into. This results in a characteristic bond deformation over about 20 bonds along the backbone. This deformation involving the addition of an electron (or a hole) is called a polaron and is shown in Figure 2. 10. In this deformation process a level is pulled out of the valence band with two electrons and a level is pulled out of the conduction band containing the electron that was added to the chain, creating two levels in the band gap. The stability of the polaron is due to the energy gained when the electron moves from the conduction band into a lower level exceeding the elastic energy required to form this level. Despite its energy levels being in the band gap the polaron can still move freely on its chain, its chain distortion moving with it[12].

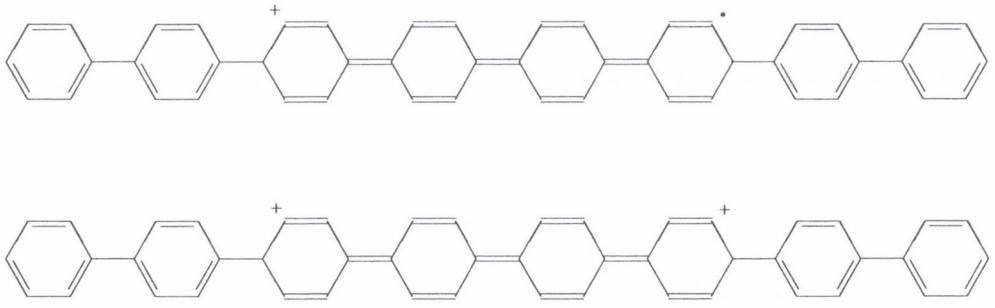

Figure 2. 10: a) Polarons and b) Bipolaron in poly(para-phenylene).

The addition of two electrons on to two separate parts of a polymer chain results in the formation of two separate, negatively charged, polarons. If these two polarons come together they can combine to form a single distortion called

a bipolaron, which has two band gap levels filled by four electrons. In non-degenerate ground state polymers a bipolaron is more stable than a polaron[13].

The creation of an electron and a hole through the absorption of a photon results in the formation of a singlet exciton, which evolves into a polaron-exciton due to coupling to the polymer backbone[14,15]. Likewise two energy levels are formed in the band gap that are singly occupied.

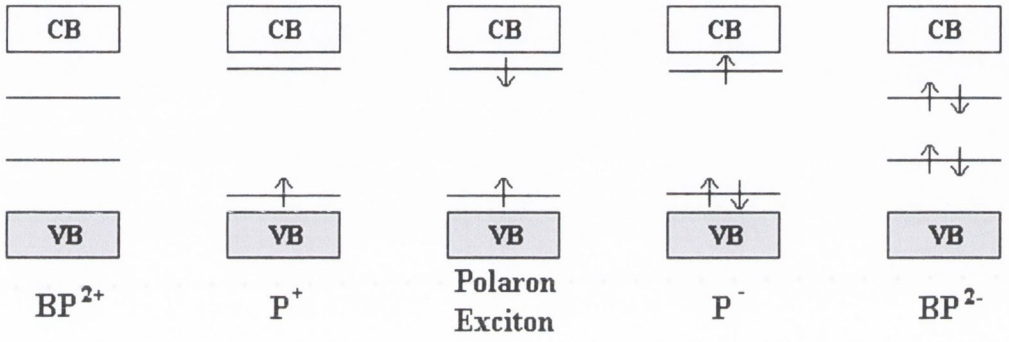

Figure 2. 11: Positive bipolaron, positive polaron, polaron-exciton, negative polaron and negative bipolaron energy levels in a non-degenerate ground state polymer.

In conclusion these levels can be occupied by 0, 1, 2, 3, 4 electrons, giving a positive bipolaron, positive polaron, polaron-exciton, negative polaron or negative bipolaron respectively. These are depicted graphically in Figure 2. 11. The presence of these new states gives rise to new optical absorptions at energies below the energy gap.

A detailed study on conjugated polymers can be found in reference[16] and [17].

2.2.7 Excitons

The migration of the photo-generated exciton to lower energy segments of the polymer chain prior to luminescent decay results in a lower energy fluorescence relative to the energy initially absorbed to create the exciton. This coupled with the Stokes shift, as discussed previously, leads to the presence of clearly resolved vibronic structure in the fluorescence spectrum. An exciton is a bound electron-hole

pair and is classed by its electron-hole separation. A Frenkel exciton is located on one molecular unit, a Mott-Wannier exciton extends over many molecular units and charge transfer excitons extend over a few adjacent molecular units. The Frenkel exciton is associated with molecular systems, whereas due to its relatively low effective mass the Mott-Wannier exciton is associated with polymer systems. Fesser, Bishop and Campbell[18] included the electron-lattice interaction in their model of the Mott-Wannier exciton in polymers but the model wasn't in good agreement with experiment, as shown by Friend, Bradley and Townsend[4]. A complete model must include the electron-electron interaction as shown by Shuai *et al*[19] and by Beljonne *et al*[20]. A consequence of incorporating this interaction is a lowering in energy of the triplet exciton and a reduction in the radius of the triplet exciton. A detailed study of excitons in solid-state systems can be found in reference[21].

2.3 Electronic Conduction in Organic Materials

2.3.1 Introduction

As discussed previously the highest occupied band in a metal is partially filled whereas in semiconducting materials the highest occupied band is completely filled. This enables the charge carriers to move freely under the application of an electric field in metals but not in semiconductors, as there are no states in the filled band for carriers to move into. For conduction to take place an electron must be promoted from the full valence band to the empty conduction band. Only then can it move under an applied field, whereas the free motion of an electron in a metal is impeded only by scattering due to phonons and impurities.

The optical bandgap of most conjugated polymer materials is between 1.5 - 3.0 eV[22]. This is the amount of energy required to promote an electron from a π to a π^* state, which in a conjugated material is an excitation of the molecule due to the π delocalisation, but the extent of the delocalisation is limited by electron-phonon coupling. The bandgap is significantly larger than the thermal energy, hence very few carriers are thermally excited across it. The limited number of carriers that are present are due to the presence of impurities indicating that the easiest way to artificially

increase the conductivity is by increasing the carrier density. This process is commonly called doping.

2.3.2 Impurities in Organic Materials

Conducting polymers differ from conventional inorganic semiconductors in the way in which they accept impurities. In conventional semiconductors an impurity atom with one extra or one less valence electron than the bulk semiconductor atom, goes into the lattice substitutionally, with the extra electron or hole being free to contribute to conduction at room temperature. Additionally some impurities go into the lattice interstitially, providing deep levels for electrons and holes. The situation is somewhat different in polymers. Impurities do not go into the polymer chain substitutionally. The quasi one dimensionality of polymer chains allows impurities to line up in columns between the chains. The impurities that act as dopants will either give up an electron to the chain or accept an electron from the chain, to form solitons, polarons or bipolarons as previously discussed in sections 2.2.6.1.1 and 2.2.6.2.1, which are localised excited states, unlike the delocalised states formed in inorganic semiconductors. Due to the nature of impurity substitution into polymer systems, higher impurity concentrations can be achieved compared to inorganic semiconductors. Due to the high doping concentrations that can be achieved it is possible for polymers to achieve conductivity values comparable with metals[23].

2.3.2.1 Doping of Organic Molecules

The easiest way to increase the free charge density of an organic material is through the introduction of dopant atoms or molecules into the material. Suitable dopants find it energetically favourable to transfer charge to the organic material via oxidisation or reduction. Oxidising agents such as I_2, PF_6, BF_4, $FeCl_3$ and As_5 accept electrons from the polymer chain and so act as p-type dopants. Reducing agents such as Na, K, Li and Ca donate electrons to the chain and so act as n-type dopants. Conservation of charge is observed, as all dopants are initially neutral.

Doped polyacetylene has been largely studied since conductivity values of 100 Scm^{-1}, upon doping with iodine were reported[24]. In fact the conductivity of polyacetylene can be varied by a factor of 10^{14}, with the conducting properties of the material ranging from those of an insulator to those of a metal[25].

2.3.3 Electronic Conduction Models in Organic Materials

Organic materials are highly disordered compared to inorganic semiconductors, giving rise to energy levels within the band gap as discussed throughout section 2.2.6. This results in at least two possible conduction models within organic materials. The first is the band model with conduction via the delocalised states in either the conduction or valence band. The second is some form of tunnelling or hopping conduction between the localised energy levels in the band gap.

The first model can be pictured as an excited charge tunnelling over a distance of many molecules, in a band model with varying potential. This model allows the tunnelling of an excited charge from its excited state on one molecule into an unoccupied state on a neighbouring molecule. Energy is conserved in the process as shown in Figure 2. 12. The potential barrier between neighbouring molecules is shaped by the various Coulomb forces acting on the charge and is best represented by a triangular shaped barrier[26]. The decreasing barrier width with increasing energy explains various charge carrier properties, but falls short in explaining several others leading to the development of several other models.

The Hopping model as shown in Figure 2. 12 is sometimes used instead of the tunnelling model, as it incorporates multiple phonon scattering, allowing a carrier to randomly move from one molecule to another by jumping over the potential barrier separating them. The electron-phonon interaction dictates whether charge carrier conduction through organic materials takes place coherently according to the band model or via a series of random hopping between localised states near the band edge. The electron-phonon interaction can be either intermolecular (lattice) of intramolecular (nuclear) and the electron relaxation time, τ_e, relative to these two vibrational periods influences which conduction model charge carriers will follow.

The intramolecular vibrational period, τ_n, is approximately two orders of magnitude quicker than the intermolecular vibrational period, τ_l, in organic materials[27]. This gives rise to two possibilities.

1.) $\tau_e < \tau_n < \tau_l$: Meaning that any vibrational motion can be considered to be stationary relative to the electron motion. Hence electrons can be thought of as waves that travel over large distances before being scattered. These characteristics are signatures of the band model.

2.) $\tau_n < \tau_e < \tau_l$: Meaning that the nuclei vibrate while an electron is on a given site. This enables nuclei to move to new equilibrium positions, leading to the formation of a polaron. This can lead to self-trapping due to the formation of self-induced potential wells resulting from polarising electron-phonon interactions. Conduction can then take place by hopping from one potential well to the next, provided the electron can acquire enough energy to overcome the potential barrier.

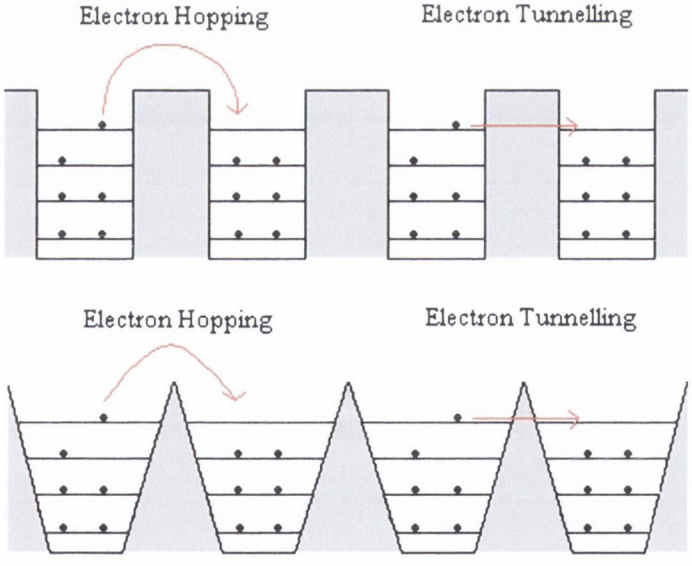

Figure 2. 12: Electron hopping across and electron tunnelling through a square and a triangular potential barrier. Hole hopping and tunnelling takes place in the opposite direction.

2.3.3.1 Variable Range Hopping

The conductivity of semiconductors goes to zero as the absolute temperature approaches zero, as there is no thermal energy present to generate any charge carriers. Organic materials have energy levels in the band gap and it was Mott who proposed that conduction in such materials was dominated by *variable range hopping*[28,29] where hopping is short for phonon assisted quantum mechanical tunnelling.

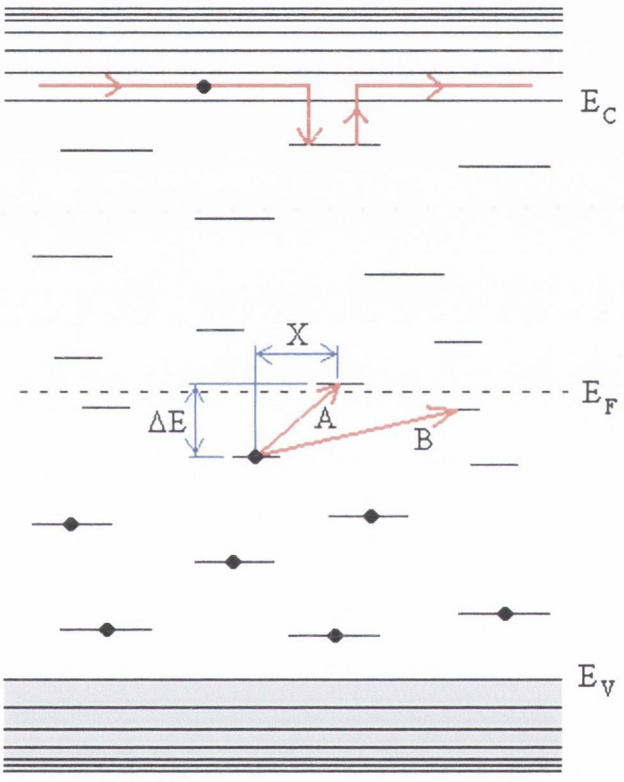

Figure 2. 13: Variable range hopping is represented by arrows A and B. Transition A is characterised by the energy difference ΔE and the distance X, between the two energy states. Band transport with trapping and detrapping is also shown.

Figure 2. 13 shows both band transport in extended states which is interrupted by trapping sites and hopping transport between localised states in the band gap. The hopping transition (A) indicted, is characterised by the energy difference ΔE and the distance X, between the two energy states. For $\Delta E > 0$ (as shown in Figure 2. 13) a phonon must be absorbed during a hop. Since phonons are required

to supply energy, the hopping conductivity vanishes as the absolute temperature goes to zero. For an electron in a given gap state, surrounded by other localised states at various distances and energies, the hopping rate to any of these states is proportional to the probability of finding the electron at a distance X from its initial state. The hopping rate is also proportional to the probability that the electron can either absorb or emit a phonon of energy equal to the energy separation between these states. This implies that the transition probability, P, is proportional to two exponential factors as shown in Equation 2. 2.

$$P \propto \mathbf{exp}\left[-2\alpha X - (\Delta E / kT)\right] \qquad \textit{Equation 2. 2}$$

where α is the inverse localisation length that describes the exponential decay of the electronic wavefunction at large distances, R, from the electron site [$\psi(R)= \psi_0 \exp(\alpha R)$], k is the Boltzmann constant and T is the absolute temperature. In the low temperature limit the second factor is due to the electrons need for energy conservation through the absorption or emission of a phonon, which is proportional to the number of phonons of energy ΔE at temperature T.

The nature of the hopping is temperature dependent. At high temperatures there are a high number of phonons available, which makes short distance, large energy difference hops the dominant hopping transition. At low temperatures the number of available phonons is limited meaning that hops have to take place over larger distances in order to find a state separated by the energy available in one of the phonons. Stated differently, the lower the temperature the more difficult it is to overcome a large energy difference and hence the more desirable it becomes to hop further to find a lower energy difference between the initial and final states. It is obvious that for a given temperature there will be a combination of ΔE and X for which a hop is most likely. This enables the most probable hopping radius, R_{hop} to be calculated

$$R_{hop} \propto \left[\alpha k T n(E_F)\right]^{-1/4} \qquad \textit{Equation 2. 3}$$

where $n(E_F)$ is the carrier density at the fermi level. It can be clearly seen that the hopping range varies with temperature. Assuming that the hopping conductivity is

dominated by the most probable hops, the conductivity is given by Mott's equation for Variable Range Hopping

$$\sigma = \sigma_0 \exp\left(\frac{-C}{T^{1/4}}\right) \qquad \textit{Equation 2. 4}$$

where

$$C = \left[\frac{\alpha^3}{k\,n(E_F)}\right]^{1/4} \qquad \textit{Equation 2. 5}$$

Mott's equation includes the dimensionality of the system. There are four dimensions, three space and one energy, which are represented in the ¼ temperature dependence. An electron can only hop to a site which is close by in (x, y, z, E) four-space. In d space dimensions, the ¼ dimensions is replaced by 1/(d+1).

Variable range hopping is the predominant method of conduction in polymers due to their predominantly semi-crystalline nature. Other conduction models that are valid in amorphous (non-crystalline) semiconductors are also valid in some polymeric materials and are outlined briefly below.

2.3.3.1.1 The Poole-Frenkel Effect

Defined as the field enhanced thermal excitation of trapped charge due to the lowering of the potential energy of a trap due to the application of an electric field. This can be explained by treating the material as a system of neutral atoms. On the ionisation of an atom the electron moves freely among the neutral polarisable atoms in the field of the positive ion and any other external fields. Due to the screening of the field by the polarisability of the atoms the expression for the conductivity is given by [30,31]

$$\sigma = \sigma_0 \exp\left[\left(\frac{e^3}{\pi\varepsilon}\right)^{1/2}\left(\frac{E^{1/2}}{2kT}\right)\right] \qquad \textit{Equation 2. 6}$$

where the conductivity is dependent of the square root of the field. This effect is bulk limited and is very similar to the Schottky Effect, which is an electrode

limited process. Some shortcomings when applied to conjugated polymers are outlined in reference [32].

2.3.3.1.2 Fluctuation Induced Tunnelling

Fluctuation induced tunnelling takes place between crystalline regions within the polymer, if the crystalline regions are close enough and the insulating barrier between them sufficiently thin[33,34,35,36]. The model takes into account tunnelling through potential barriers of varying height due to local temperature fluctuations and the conductivity is given by

$$\sigma = \mathbf{exp}\left[\frac{-T_1}{(T+T_0)}\right] \qquad \textit{Equation 2. 7}$$

where T is the temperature, $T_1 = wA\varepsilon^2 / 8\pi k$, $T_0 = 2T_1 / \pi w\chi$, $\chi = \sqrt{2mV_0^2 / h^2}$, $\varepsilon = 4V_0 / ew$, k is the Boltzmann constant, m and e are the electron mass and charge, w is the spacing between crystalline regions, A is the area of the capacitance formed between crystalline regions and V_0 is the potential barrier height. The expression for the conductivity can be distinguished from that of variable range hopping by its field dependence.

2.4 Design and Synthesis of Organic Materials

2.4.1 Introduction

The conventional perception of a polymer is what are commonly known as 'plastics'. At a molecular level these materials are long organic molecules with simple repeat units. Interest in opto-electronic polymers developed in the 1960s with the objective of obtaining organic semiconductors[37]. Initially conjugated polymers tended to be rigid-like molecules that were insoluble in common organic solvents, making thin film fabrication impossible[17].

Electro-polymerisation was initially used, resulting in films forming on the electrode from a solution that contained both an electrolyte and the monomer. Films produced

by this method tended to be highly doped. However the technique was successfully used for controlled doping of polymers such as polyacetylene[38].

Polymer synthesis then developed into a two step, indirect synthesis. By this method a non-conjugated monomer which can be easily converted into a conjugated polymer, was used as a precursor. A good precursor is stable, easily processable and can be purified and characterised prior to polymerisation. Initially polymers such as trans-polyacetylene[39] and poly-phenylenevinylene[40,41] as synthesised by the Durham and Wessling routes respectively, formed polymer layers that were either free-standing or could be deposited on to a suitable substrate. Due to the instability of polyacetylene in air, much research has centred on poly-phenylenevinylene. In the 1980s new synthesis ideas have lead to polymers that are easily soluble in common organic solvents[42]. This is commonly achieved through the substitution of flexible alkyl or alkoxy chains on to the polymer backbone to form sidechains. This has lead to polymers that are easily processable, making for easy thin film fabrication. Solubility can be improved further by substituting PPV asymmetrically. One of the more extensively studied PPVs with asymmetrically sidechains is poly(2-methoxy-5-(2'-ethyl-hexyloxy)-p-phenylenevinylene) [MEH-PPV]. For a full study on the properties of sidechain substitution on PPV and its derivatives the reader is referred to reference[43,44].

Much research has centred on organic polymers due to their potential applications in display technology and organic lasers because they are easily tuneable. In the early 1990s there was a concerted effort to develop blue emitting polymers as until the late 1990s there were no cheap inorganic light emitting devices emitting in the blue end of the spectrum commercially available. The number of polymers that exhibited blue emission was limited until the mid 1990s. Attempts were made to modify existing polymers so as to blue shift their emission. A shortening of conjugation length was found to blue shift emission in PPV and its derivatives[45]. This has been achieved by a number of techniques including the incorporation of non-conjugated co-polymer units, the use of meta linkages on the backbone and through the use of steric effects.

2.4.2 Poly (m-phenylenevinylene-co-2,5-dioctyloxy-p-phenylenevinylene)

In this thesis the majority of work was performed on the relatively new copolymer poly(m-phenylenevinylene-co-2,5-dioctlyoxy-p-phenylenevinylene) [PmPV] which has been synthesised with alternating m-phenylenevinylene and 2,5-dialkoxy-p-phenylenevinylene units along its backbone as shown in Figure 2. 14.

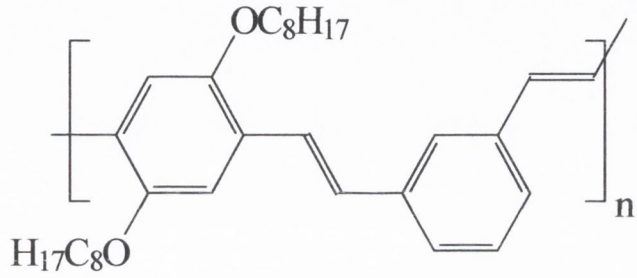

Figure 2. 14: Repeat unit structure of poly(m-phenylenevinylene-co-2,5-dioctlyoxy-p-phenylenevinylene)

The incorporation of the meta linkage on the phenylenevinylene co-unit is in an attempt to blue shift the absorption and luminescence spectra relative to para-phenylenevinylene (PPV) by reducing the effective conjugation length through increasing the disorder along the polymer backbone and thus limiting exciton diffusion to lower energy segments of the polymer chain. The limiting of exciton diffusion along the polymer backbone also acts to increase the efficiency of the material by reducing non-radiative decay via quenching sites[46]. A blue shift of the absorption and PL maxima compared to the corresponding all para-phenylenevinylene copolymers has been observed[47].

The PmPV used in this thesis was synthesised by the Organic Materials Synthesis section of Materials Ireland Polymer Research Centre in Trinity College Dublin[48]. A total of four different reactions have been employed to synthesise the polymer as shown in Figure 2. 15.

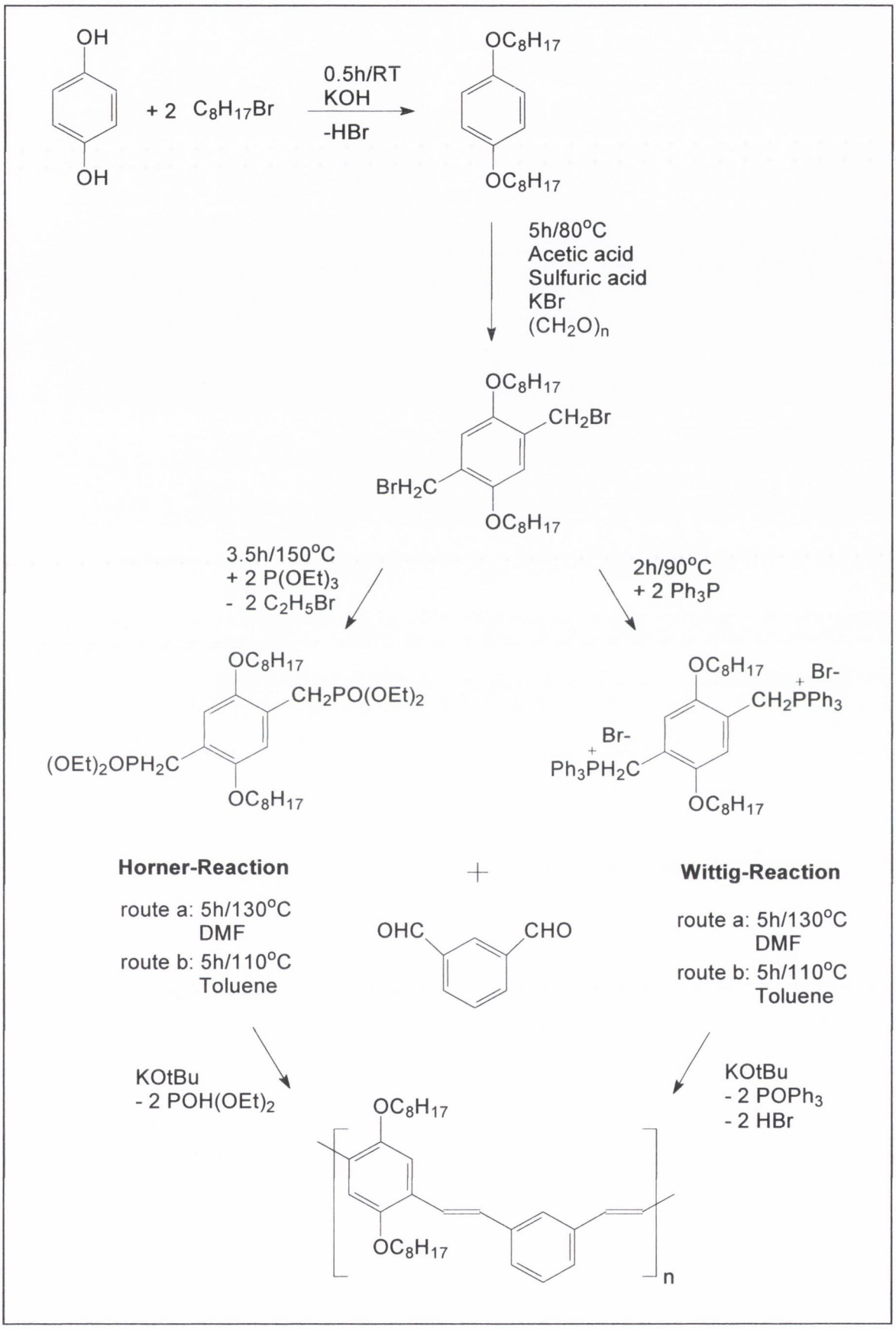

Figure 2. 15: Synthesis of poly(meta-phenylenevinylene-co-2,5-dioctlyoxy-para-phenylenevinylene).

The alkoxy side groups are introduced by alkylation of hydroquinone using the method of Johnson and Rose[49]. The resulting 1,4-di-n-octoxybenzene is then reacted with paraformaldehyde and Potassium Bromide in acetic acid and sulfuric acid to give 1,4-bis(2,5-dialkoxy)benzylbromide. This is reacted in dry toluene with triphenylphosphine to give the phosphonium salt. The salt can then be used in a Wittig polycondensation reaction[50] in either dry toluene or dry Di-Methyl Formaldehyde (DMF) to produce two polymers, Wittig toluene PmPV and Wittig DMF PmPV. 1,4-bis(2,5-dialkoxy)benzylbromide can also be used to generate a phosphonate ester (by reaction with triethylphosphite), which can be used in a Horner-Emmons polycondensation reaction[51] to give two more polymers, Horner toluene PmPV and Horner DMF PmPV. The results of the ^{1}H and ^{12}C nuclear magnetic resonance (NMR) measurements (in deuterated chloroform) clearly indicate that the polymer structure is as proposed.

The Horner toluene synthesis route was used to make the PmPV for this thesis. The ratio of the cis to trans bond orientation on the vinylene linkage is low for PmPV prepared using this reaction route. In this conformation the material interacts with carbon nanotubes to separate them from the graphitic particles produced during their production[52], making this an interesting material for characterisation. Previously, its molecular mass characteristics were analysed using gel permeation chromatography, referenced to narrow molecular weight polystyrene standards. The weight average molecular weight (M_w) and number average molecular weight (M_n) were measured to be 141547 and 71213 respectively, giving a polydispersivity index of 1.98 and a number average (n_{av}) chain length of 155. It should be pointed out that there are batch to batch variations and that the values presented above are representative.

Polymers are far from the idealised one-dimensional chains represented by chemical formula. In general, samples will have a range of molecular weights and will also contain various defects both chemical and conformational. Optical and electronic properties are highly dependent on the nature and quantity of these defects. Hence by changing the route to the polymer, these properties to some extent may be controlled.

For a detailed analysis of the affects on the polymeric properties of PmPV prepared by the four synthesis routes outlined above, the reader is referred to reference[53].

In order to gain an idea as to the possible conformation of the polymer chains, standard HyperChem software was used and the structures modelled using molecular mechanics. The molecular mechanics system developed for organic molecules was used without altering the parameters to perform a geometry optimisation. In this system the forces between non-bonded atoms were calculated using bond dipole interactions. Approximate bond lengths and angles[54] were used to construct the polymer chains. In total, three different chain types were constructed. The chain constructed of repeat units takes on a coiled geometry due to the meta linkage, whereas a chain constructed from repeat units that have been alternately flipped gives a comparatively linear backbone.

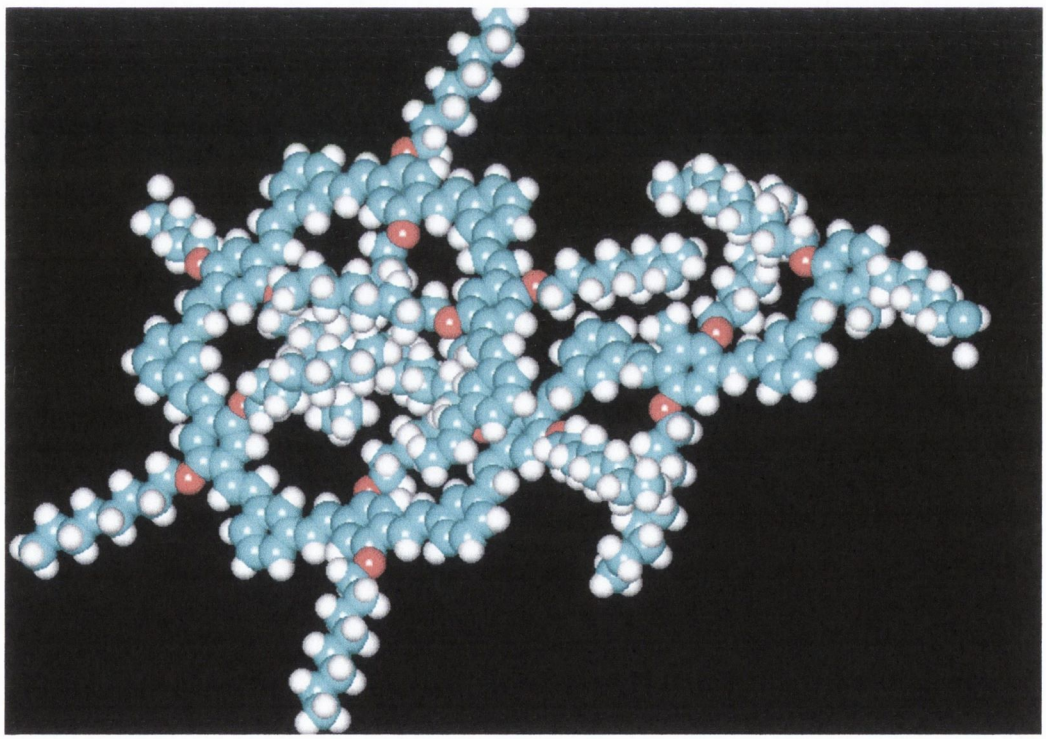

Figure 2. 16: PmPV backbone structure showing the possible coiled and linear alignment of the backbone. The coil is due to the meta linkage on the backbone, whereas the linear segment is due to the alternate flipping of the repeat unit.

These orientations are to some extent dictated by the cis and trans orientation on the vinylene bonds as these can act to distort the chain conformations through steric

hindrance. In reality the polymer chains would not be ordered and would be more likely to contain both geometries on the same chain due to the presence of both cis and trans bonds on the vinylene linkage. The diagram shown in Figure 2. 16. contains five repeat units in a coiled geometry attached to three repeat units that are alternately flipped to give a linear geometry. The modelling results show how the meta-phenylene linkage and the orientation of the repeat monomer unit have a significant affect on the geometry of the polymer chain.

2.5 Conclusions

The photo-physical properties of organic materials have been detailed and the differences between them, inorganic semiconductors and metals have been discussed. The changes to the photo-physical properties that occur in the transition from molecular organics to polymer organics have also been detailed. For conjugated polymers the differences between degenerate and non-degenerate ground states have been outlined using polyacetylene and poly(phenylenevinylene) as examples. The interactions incorporated into the various theoretical models and the deficiencies of the models due to the absence of some interactions has been briefly outlined. Doping of organic polymers and its effect on the electrical conduction in these materials along with several models for charge carrier conduction have been outlined. Additionally a brief overview of polymer synthesis was presented along with the synthesis of the polymer poly(m-phenylenevinylene-co-2,5-dioctlyoxy-p-phenylenevinylene) [PmPV], which is to be studied extensively in this thesis.

2.6 References

1. C. Kittel, 'Introduction to Solid State Physics'. 7th Edition, John Wiley & Sons (1996).

2. H. Haken and Ch. Wolf, 'The physics of atoms and quanta,' Springer Berlin 2000.

3. J. Kopecký, 'Organic Photochemistry: A visual Approach', VCH Publishers (1992).

4. R. H. Friend, D. D. C. Bradley and P. D. Townsend, 'Photo-excitation in conjugated polymers', J. Phys. D: appl. Phys 20 (1987) 1367-1384.

5. M. J. Rice, 'Charged Pi -phase kinks in lightly doped polyacetylene', Phys. Lett. A, 71A, (1979) 152-154.

6. A. J. Heeger, S. Kivelson, J. R. Schrieffer and W. P. Su, 'Solitons in conducting polymers', Rev. Mod. Phys. 60, (1988) 781-850.

7. W. P. Su, J. R. Schrieffer and A. J. Heeger, 'Solitons in polyacetylene'. Phys. Rev. Lett. 42 (1979) 1698-1701.

8. W. P. Su, J. R. Schrieffer and A. J. Heeger, 'Soliton excitations in polyacetylene', Phys. Rev. B –Con. Matt. 22 (1980) 2099-2111.

9. 'Handbook on Semiconductors Vol 1: Basic properties of semiconductors'. Elsevier Science Publishers (1992).

10. Z. G. Soos, S. Ramasesha, D. S. Galvão, R. G. Kepler and S. Etemad, 'Electronic excitations and alternation of conjugate polymers', Synth. Met. 54 (1993) 35-47.

11. S. A. Brazovski and N. N. Kirova, 'Excitons, polarons and bipolarons in conducting polymers'. J. Expt. Theoretical Phys. 33 (1981) 6-10.

12. E. M. Conwell, H-Y. Choi and S. Jeyadev, 'Interchain polaron transport in trans-polyacetylene,' Synth. Met. 49 (1992) 359-65.

13. Y. Shimoi and S. Abe, 'Competition between polarons and bipolarons in non-degenerate conjugated polymers,' Phys. Rev. B-Con. Mat. 50 (1994) 14781-14784.

14. M. Hartmann, M. Schreiber, H. W. Streitwolf and S. Mukamel, 'Nonlinear optical excitations in femtosecond spectroscopy of conjugated polymers,' J. of Luminescence 66-67 (1995) 97-101.

15. J. Fagerström and S. Stafström, "Inter- and intrachain electron-hole recombination in polythiophene," Synth. Met. 85 (1997) 1065-1068.

16. 'Handbook of Organic Conductive Molecules and Polymers,' Vol 2 and 4, John Wiley & Son, (1997).

17. 'Handbook of conducting polymers,' Edited by T. A. Skotheim, R. L. Elsenbaumer and J. R. Reynolds, 2nd Edition, Marcel Dekker INC (1998).

18. K. Fesser, A. R. Bishop and D. K. Campbell, 'Optical absorption from polarons in a model of polyacetylene,' Phys. Rev. B-Con. Mat. 27 (1983) 4804-25.

19. Z. Shuai, J. L. Bredas and W. P. Su, 'Nature of photoexcitations in poly(paraphenylene vinylene) and its oligomers'. Chem. Phys. Lett. 228 (1994) 301-6.

20. D. Beljonne, Z. Shuai, R. H. Friend and J. L. Bredas, 'Theoretical investigation of the lowest singlet and triplet states in poly(paraphenylene vinylene) oligomers'. J. Chem. Phys. 102 (1994) 2042-2049.

21. J. T. Devreese and F. Peeters, Editors, 'Polarons and Excitons in Polar Semiconductors and Ionic Crystals,' NATA ASI Series B, Vol. 108, Plenum Press, New York (1984).

22. F. Meyers, A. J. Heeger and J. L. Bredas, 'Fine tuning of the band gap in conjugated polymers via control of block copolymer sequences,' J. Chem. Phys. 97 (1992) 2750-2758.

23. D. R. Gagnon, J. D. Capistran, F. E. Karasz, R. W. Lenz and S. Antoun, 'Synthesis, doping and electrical conductivity of high molecular weight poly(*p*-phenylene vinylene),' Polymer 28 (1987) 567-573.

24. C. K. Chiang, C. R. Jr. Fincher, Y. W. Park, A. J. Heeger, H. Shirakawa, E. J. Louis, S. C. Gau and A. G. MacDiarmid, 'Electrical conductivity in doped polyacetylene'. Phys. Rev. Lett. 39 (1977) 1098-1101.

25. N. Theophilou, D. B. Swanson, A. G. MacDiarmid, A. Chakraborty, H. H. S. Javadi, R. P. McCall, S. P. Treat, F. Zuo and A. J. Epstein, 'Highly conducting polyacetylene,' Synth. Met. 28 (1989) D35-42.

26. G. Kemeny, B. Rosenberg, 'Theory of the pre-exponential factor in organic semiconductors,' J. Chem. Phys. 52 (1970) 4151-4153.

27. K. C. Kao and W. Hwang, 'Electrical Transport in Solids; with particular reference to organic semiconductors', Pergamon Press (1981).

28. N. F. Mott and E. A. Davis, 'Electronic processes in non-crystalline materials'. 2nd Edition, Oxford University Press (1979).

29. R. Zallen, 'The Physics of Amorphous Solids', Wiley-Interscience, (1983).

30. J. Frenkel, 'On pre-breakdown phenomena in insulators and electronic semi-conductors,' Phys. Rev. 54 (1938) 647-648.

31. N. F. Mott, 'Conduction in non-crystalline systems; Non-ohmic behaviour and switching'. Philos. Mag. 24 (1971) 911-934.

32. W. D. Gill, 'Drift mobilities in amorphous charge-transfer complexes of trinitrofluorenone and poly-*n*-vinylcarbazole,' J. Appl. Phys. 43 (1972) 5033-5040.

33. Ping Sheng, E. K. Sichel, and J. I. Gittleman, 'Fluctuation-Induced Tunneling Conduction in Carbon-Polyvinylchloride Composites,' Phys. Rev. Lett. 40 (1978) 1197–1200.

34. B. Lundberg, W. R. Salaneck and I. Ludstrom, 'Pressure, temperature and field dependence of hopping conduction in polyaniline.' Synth. Met. 21 (1987) 143-147.

35. G. Paasch, G. Lehmann and L. Wuckel, 'A novel barrier model for fluctuation induced tunnelling in highly conductive polyacetylene.' Synth. Met. 37 (1990) 23-32.

36. B. E. Kilbride, J. N. Coleman, J. Fraysse, P. Fournet, M. Cadek, A. Drury, S. Hutler, S. Roth and W. J. Blau, 'Experimental observation of scaling laws for alternating current and direct current conductivity in polymer-carbon nanotube composite thin films,' J. Appl. Phys. 92 (2002) 4024-4030.

37. B. F. Pamplin, 'Opto-electronics - a survey,' Electronic Equipment News 12 (1970) 12-16.

38. T. C. Clarke, A. F. Diaz and G. B. Street, 'Conducting polyacetylene with controlled doping levels and doping gradients,' IBM Technical Disclosure Bulletin 23 (1980) 772.

39. D. C Bott, C. S. Brown, J. H. Edwards, W. J. Feast, D. Parker and J. N. Winter, 'Some aspects of the chemistry of the two step Durham route to polyacetylene'. Molecular Crystals & Liquid Crystals, 117 (1985) 9-14.

40. R.A Wessling and R. G. Zimmerman, U.S Patent 3401152 (1968).

41. R.A. Wessling and R.G. Zimmerman, U.S. Patent 3406677 (1972).

42. W. J. Feast, I. S. Millichamp, R. H. Friend, M. E. Horton, D. Phillips, S. D. D. V. Rughooputh and G. Rumbles, 'Optical adsorption and luminescence in poly(4,4'-diphenylenediphenylvinylene)'. Synth. Met. 10 (1985) 181-91.

43. S. Maier, Diploma, Trinity College Dublin 1997.

44. S. Maier, Ph.D Thesis, Trinity College Dublin 2000.

45. K. S. Wong, D. D. C. Bradley, W. Hayes, J. F. Ryan, R. H. Friend, H. Lindenberger and S. Roth, 'Correlation between conjugation length and non-radiative relaxation rate in poly(p-phenylene vinylene): a picosecond photoluminescence study,' J. Phys. C: Solid State Phys. 20 (1987) L187-194.

46. R. H. Friend, D. D. C. Bradley and P. D. Townsend, 'Photo-excitation in conjugated polymers', J. Phys. D: appl. Phys 20 (1987) 1367-1384.

47. D. F. O'Brien, A. Bleyer, D. G. Lidzey, D. D. C. Bradley T. Tsutsui, 'Efficient multiplayer electroluminescence devices with poly(m-phenylenevinylene-co-2,5-dioctyloxy-p-phenylenevinylene) as the emissive layer.' J. Appl. Phys. 82 (1997) 2662-2670.

48. A. P. Davey, A. Drury, S. Maier, H. J. Byrne and W. J. Blau, 'Synthesis and Optical Properties of Phenylene-vinylene Copolymers', Synth. Met. 103 (1999) 2478-2479.

49. R. A. W. Johnstone and M. E. Rose, 'A rapid, simple, and mild procedure for alkylation of phenls, alcohols, amides and acids'. Tetrahedron 35 (1979) 2169-2173.

50. R. N. McDonald, T. W. Cambell, J. Am. Chem. Soc. 82 (1960) 4669.

51. H. Rost, A. Teuschel, S. Pfeiffer and H. H. Horhold, 'Novel light emitting and photoconducting polyarylenevinylene derivatives containing phenylene arylamine and phenylene oxide units in the main chain'. Synth. Met. 84 (1997) 269-270.

52. A. B. Dalton, J. N. Coleman, M. in het Panhuis, B. McCarthy, A. Drury, W. J. Blau, B. Paci, J. M. Nunzi and H. J. Byrne, 'Controlling the optical properties of a conjugated co-polymer through variation of backbone isomerism and the introduction of carbon nanotubes,' J. PhotoChemistry. PhotoBiology A: Chemistry 5678 (2001) 1-11.

53. A. B . Dalton, Ph.D Thesis, Trinity College Dublin 1999.

54. H. Hart, L. E. Craine and D. J. Hart, 'Organic Chemistry.' 9th Edition, Houghton Mifflin Company, (1995).

Chapter 3

Investigation and Minimisation of Photo-degradation in Organic Materials

3.1 Outline

This chapter starts by outlining the problems associated with degradation in organic conjugated polymers and goes on to explain the theory behind photo-degradation in such materials. Experimental data is presented to verify the method of photo-degradation in PmPV. A detailed experimental section follows in which various techniques were used in an attempt to prepare neat thin films of PmPV with significantly enhanced photostability. Results are presented which show enhanced photo-stability and photoluminescence efficiency in neat thin films of PmPV. The third and final section outlines the conclusions derived from the above work.

3.2 Photo-degradation in Conjugated Organic Materials

3.2.1 Introduction

The discovery that conjugated organic polymers could be used to make electroluminescence (EL) devices[1], opened up endless possibilities in the field of lightweight, large area, full colour flexible displays[2,3,4] and light emitting devices. The advantages of organic polymers over their inorganic semiconductor counterparts include ease of processability, wavelength tuneability[5,6] and potentially low manufacturing costs. Unfortunately device stability and reliability are two important issues affecting organic light emitting devices (OLED). Other issues include device efficiency[7,8] and luminosity[9,10]. Photo-degradation of the active layer in an OLED, through exposure to radiation from external sources[11] and through its own emission[12], affect device stability. Oxygen dependant phenomena play a significant part in OLED failure, with devices failing faster when operated in the presence of

oxygen and water vapour as opposed to an inert gas or vacuum[13]. This has lead to a need for a better understanding of the mechanism of photo-degradation in organic polymers, enabling the design of organic materials that resist photo-degradation and helping in the preparation of OLEDs with significantly enhanced stability. Degradation of the electrodes[14], for example through the presence of impurities, is another source of device failure but this chapter will focus on photo-degradation in organic polymers.

3.2.2 Theory

In 1982 it was suggested that singlet oxygen might be involved in the photo-degradation of polyacetylene[15]. The discovery of electroluminescence in poly(*p*-phenylenevinylene) [PPV] in 1990, resulted in renewed interest in polymer photo-degradation and stability. In 1991 it was shown that the photo-excitation of poly(3-alkylthiophenes) produces singlet oxygen, which can react with these polymers[16,17]. In 1994 studies on PPV showed that photo-degradation in air resulted in the formation of carbonyl groups on the PPV backbone resulting in decreased photoluminescence (PL) efficiency, while the same experiment conducted under nitrogen had no effect on the carbonyl groups population and hence the PL efficiency[18]. In 1995 detailed studies on the photo-degradation of poly(2,5-bis(5,6-dihydrocholestanoxy)-1,4-phenylenevinylene) [BCHA-PPV] were published by two independent groups[11,19]. Both groups explained in detail how ground state triplet oxygen can be excited to form singlet oxygen which breaks the vinylene bond on the polymer backbone leading to reduced conjugation lengths and hence reduced PL efficiency through an increase in the number of non-radiative recombination sites. They also show that the bulky side chains, added to PPV to increase solubility, are also involved in the photo-degradation of the polymer.

The oxygen molecule (dioxygen) possesses a high degree of symmetry and has degenerate frontier molecular orbitals, as seen in Figure 3. 1a. The frontier orbitals of the ground state are singly occupied by electrons with parallel spins, in accordance with Hund's Rule. This makes the ground state of the oxygen molecule (O_2) a triplet state, denoted by T_1 $\left({}^3\Sigma_g^-\right)$, with the symbol ${}^3O_2$. The lowest energy excited states are

two singlet states, (Figure 3. 1b), with anti-parallel electron spins denoted by $S_1\left({}^1\Delta_g\right)$ and $S_2\left({}^1\Sigma_g^+\right)$. The electronic transitions ${}^1\Sigma_g^+ \rightarrow {}^3\Sigma_g^-$ and ${}^1\Delta_g \rightarrow {}^3\Sigma_g^-$ are forbidden and hence both of the singlet states have long lifetimes. Dioxygen in the triplet state is a biradical and undergoes 'one-electron' reactions[20]. In its singlet state it is called 'Singlet Oxygen' with the symbol ${}^1O_2$. The energy levels of $\left({}^1\Sigma_g^+\right)$ ${}^1O_2$ and $\left({}^1\Delta_g\right)$ ${}^1O_2$ are 1.63eV and 0.98eV[21] respectively. The excitation of ground state triplet oxygen to form excited state singlet oxygen is by Dexter energy transfer[22,23] from a photosensitizer, which in this thesis is the polymer PmPV. The singlet excited state of the polymer is responsible for light emission, but with a lifetime on the nanoseconds time scale it is too short lived to transfer energy to ${}^3O_2$ efficiently. The non-emissive triplet spin state of the polymer has a greater lifetime and is lower in energy than the singlet state. The triplet energy level of most PPV derivatives is about 1.55eV [21] in solution and is slightly lower in the solid state, as measured by two-photon photoemission[24], due to changes in the orbital overlap of the π system due to higher polymer concentrations and conformational constraints. This energy is sufficient to produce $\left({}^1\Delta_g\right)$ ${}^1O_2$. It has been shown in BCHA-PPV that the triplet state of the polymer is quenched by oxygen, thus verifying that the polymer triplet state is the precursor to singlet oxygen.

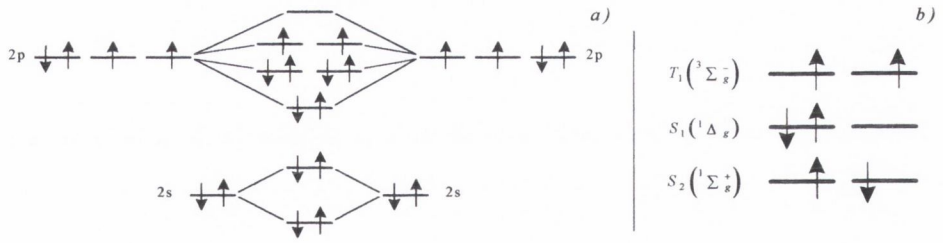

Figure 3. 1: a) The degenerate frontier orbitals of the oxygen molecule, dioxygen. b)The ground state of dioxygen is triplet, T_1. The lowest energy excited states are two singlet states, S_1 and S_2.

${}^1O_2$ is electrophilic in nature and undergoes 'two-electron' reactions and is thus highly reactive. The conjugated / semi-conjugated nature of PPV and its derivatives means that it has vinylene (carbon double) bonds on its backbone. These are electron rich areas and are hence very susceptible to attack from ${}^1O_2$. The large electron

affinity of singlet oxygen favours [2+2] cycloaddition reactions with electron rich vinylene bonds (alkenes) on the polymer backbone to produce 1,2 dioxetanes, in which $^1O_2$ is an acceptor of electrons. (Where a cycloaddition reaction is an addition that produces rings and the [2+2] is the number of electrons involved in the reaction from each reacting species). The 1,2 dioxetanes can decompose to form two terminal aldehydes and this is what happens in pure PPV[25] due to the absence of sidechains. They can also decompose to produce a biradical intermediate which can react with the sidechains in alkoxy-substituted PPV to form esters or acids[21]. The biradical intermediate can act to abstract hydrogen atoms from the aliphatic sidechains (non aromatic sidechains), thus initiating the formation of hydroperoxides, which decompose to form esters and hydroxyl groups. The abstraction of hydrogen from the carbon adjacent to the ether oxygen is favoured as the resulting radical is stabilised by the oxygen lone pairs. Figure 3. 2 shows the degradation procedure described above. It also shows a proposed decomposition of the hydroxyl groups to form aldehydes. In alkyl-substituted PPV the 1,2 dioxetanes decompose to form two terminal aldehydes, as no ester signatures are observed in the infrared spectra. The end product, in all PPVs, is chain scission and the formation of terminal aldehydes (carbonyl groups [C=O]) at the vinyl double bond on the polymer backbone.

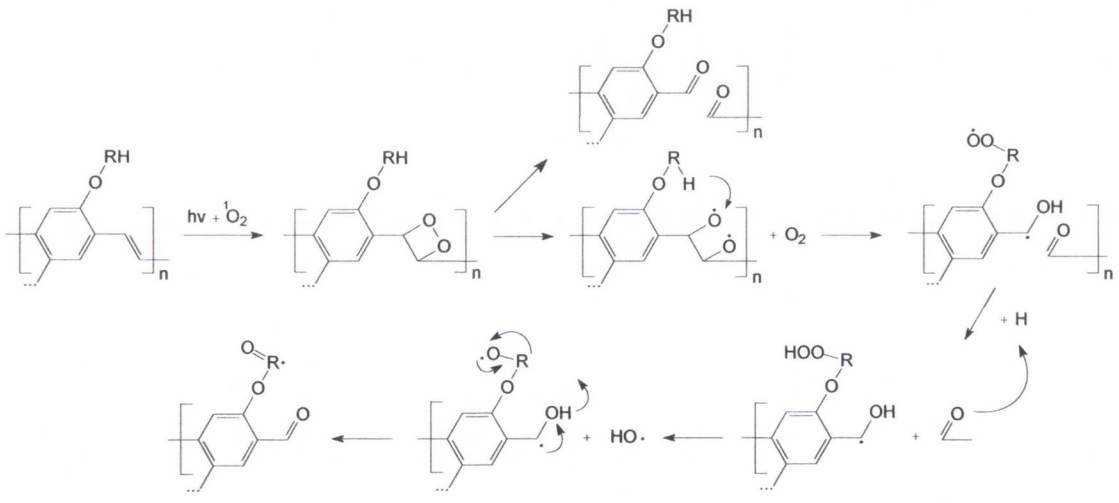

Figure 3. 2: Proposed oxidation mechanism for alkoxy-substituted PPV derivatives, showing the formation of esters, aldehydes and alcohols. (Reproduced from Reference [21])

The chain scission can be verified using Gel Permeation Chromatography, which shows a reduction in the molecular weight of the polymer after photo-degradation[19]. Fourier Transform Infrared Spectroscopy (FTIR) can also be used to study the effects of photo-degradation on the structure of the polymer. Infrared spectral signatures (bands) allow us to study the formation of new functional groups in the polymer. The bands of main interest are the *cis*-vinylene C-H out of plane bending band which is at 691cm^{-1}, the *trans*-vinylene C-H out of plane bending band intensity at 965cm^{-1}, the C-O-C band at 1200cm^{-1} the C-O peak at 1278cm^{-1}, the C=O band ranging from 1695cm^{-1} in aldehydes to 1745cm^{-1} in esters and the O-H band from 2400-3500cm^{-1}. Additionally, changes in the conjugation length of polymer chains can be observed in the absorption and photoluminescence spectra. As the conjugation length shortens, due to chain scission caused by photo-degradation, the absorption and photoluminescence peaks blue shift and reduce in intensity[26].

3.2.2.1 Infrared Vibrations

When infrared radiation is passed through an organic material, certain wavelengths or frequencies are absorbed. The absorption bands talked about in the previous section refer to energy transitions within an organic material. Absorption in the infrared region of the spectrum is associated with vibrational changes within the organic material and is sometimes called vibrational spectroscopy. The vibrations correspond to stretching or bending vibrations and thus enable scientists to distinguish between different organic bonds. Stretching absorptions appear at higher energies than the corresponding bending absorptions of the same bond. Additionally, the vibrational frequency of a bond increases with bond strength and with decreasing reduced mass, as defined by Hooke's Law:

$$\nu = \frac{1}{2\pi}\sqrt{\frac{k}{\mu}} \qquad \textit{Equation 3. 1}$$

where ν is frequency (s^{-1}), k is bond strength (Nm^{-1}) and μ is the reduced mass (kg). The absorption bands are usually referred to by wavenumber, as opposed to frequency or wavelength, where wavenumber is defined as the reciprocal of the wavelength in centimetres (cm^{-1}). Stretching absorptions can be *symmetric* or *anti-symmetric*, while bending absorptions can be *in-plane* or *out-of-*

plane. In-plane bending is called either *scissor*, where the bonds bend towards each other, or *rock*, where the bonds bend in the same direction. Out-of- plane bending is called either *twist*, where the bonds bend out of different sides of the plane, or *wag*, where the bonds bend out of the same side of the plane. Some of these vibrational modes may have the same frequency which means that they can't be distinguished. Additionally, in order to see an absorption band in the infrared, the vibration must have a fluctuating dipole. i.e. the bond must be polar. For example the C=C of the vinylene bond on the PPV back bone can't be detected using infrared spectroscopy as it is a non-polar bond, but the vibrations of the hydrogen atoms attached to the C=C can be detected and can be used to infer the existence of the vinylene bond. Finally, a given bond doesn't have a fixed vibrational frequency. A bond's frequency can vary according to its environment. Conformational constraints, vibrational coupling and hydrogen bonding can all alter the frequency at which a bond vibrates. A detailed study of infrared spectroscopy can be found in 'Organic Spectroscopy'[27].

3.2.3 Experimental Methods and Procedures

To verify the method of photo-degradation in PmPV and in particular that chain scission was taking place, a film was spun from a filtered (0.8μm pore diameter) 25g/l toluene solution, at 600rpm for 60 seconds on a polished Potassium-Bromide (KBr) substrate and was dried overnight under vacuum ($\sim 6\times10^{2}$ Nm^{-2}). An FTIR spectrum was recorded using a Nicolet FTIR spectrometer before, during and after exposure to the expanded 457.9 nm beam of an Innova 90 Coherent water cooled Argon Ion laser at 50mW/cm^2 for one hundred and twenty five (125) minutes.

3.2.3.1 Fourier Transform Infrared Spectroscopy (FTIR)

The name is derived from the fact that the initial interferograms are converted from the time domain to the frequency domain using Fourier Transforms. A scanning Michelson interferometer is used, meaning that all wavelengths can be passed through the sample simultaneously, thus allowing fast scan times. Any absorbed light due to the presence of an absorbing sample will result in reduced

intensities at the absorbed frequencies in the interferogram. Sample dimensions of about 1 cm in diameter are required. The sample thickness required depends on how absorbing the sample is. The spectral range scanned usually extends from 500 - 4000 cm^{-1} (2.5 - 20 μm).

3.2.4 Results and Analysis

The initial and final spectra are plotted in Figure 3. 3. The change in the local environment in the vicinity of the vinylene bond when it degrades will result in changes to the vibrations of both the *cis* and the *trans* vinylene C-H vibrations. The *trans*-vinylene C-H out of plane bending band intensity at 965cm^{-1} is decreased after exposure, indicating the breaking of the vinyl double bond, thereby shortening the conjugation length. There is also a weak absorption at 691cm^{-1} due to the *cis*-vinylene C-H out of plane bending band. This also decreases, indicating chain scission at the vinyl double bond, but due to a *cis/trans* ratio of 0.38[28], the absorption at 691cm^{-1} is weak. The weak signal allows meaningful information only to be obtained from the absorption band at 965cm^{-1}. At the same time there is a substantial increase in the aldehyde (C=O) stretch at 1710cm^{-1}. It should be noted that C=O is a highly polar bond, resulting in a large absorption in comparison with the small reduction observed in the *cis & trans* vinylene C-H out of plane bending at the C=C bond on the PmPV backbone. The band at 1600cm^{-1}, is a phenyl quadrant ring stretching which broadens upon chain scission. The absence of a C-O peak at 1278cm^{-1} and an O-H band from 2400-3500cm^{-1} indicates no carboxylic acid formation. The absence of the C-O peak also indicates no ester formation. The slight reduction in the strong C-O-C absorption peak at 1200cm^{-1} is indicative of possible changes taking place in the sidechains during photo-degradation. All these changes are consistent with chain scission and the formation of terminal aldehydes at the vinylene bond on the PmPV backbone. The O-H band from 3400-4000cm^{-1} is due to the presence of water vapour in the atmosphere and the film. This is discussed in more detail in section 3.3.3.

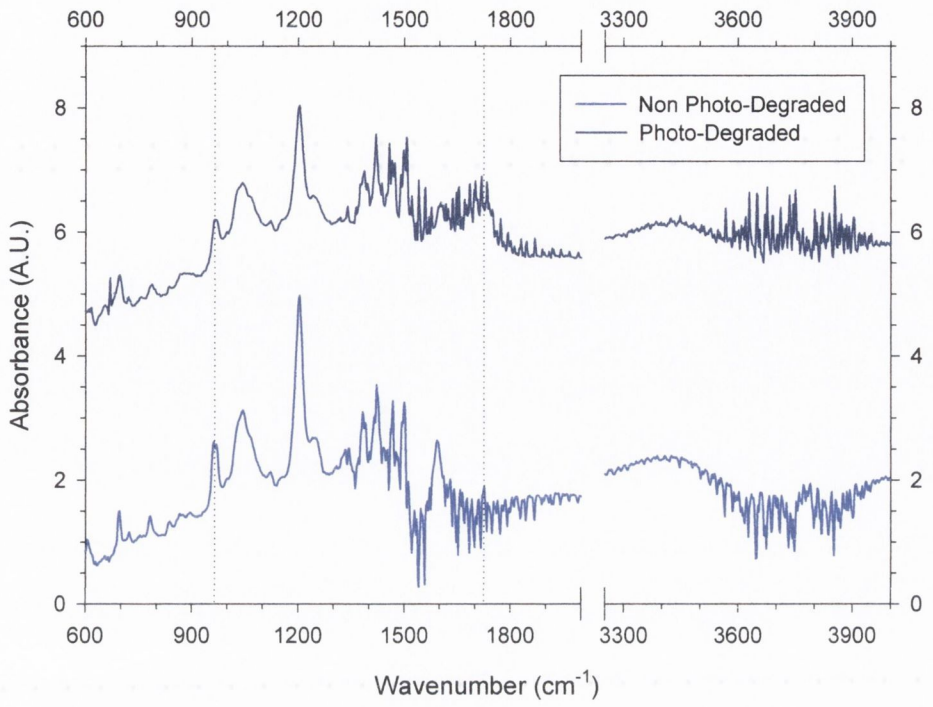

Figure 3. 3: FTIR spectrum for a PmPV film before (blue) and after (dark blue) 125 minutes exposure to the 457.9 nm line of an Ar ion laser at 50 mW/cm^2. The reduction in the trans-*vinylene out of plane bending band at 965cm^{-1} and the appearance of the C=O peak at 1710cm^{-1} are marked by the vertical dashed lines. The photo-degraded spectrum has been offset vertically for clarity.*

3.2.5 Discussion

It is clear from reading the literature that the presence of oxygen in polymer solutions and films and in the atmosphere causes the polymer to photo-degrade when photo-excited[29,30,31]. The mechanism has been studied in detail and has lead to several ways to reduce the effects of photo-degradation in organic materials. Material synthesis has lead to the design of materials that are more resistant to photo-degradation. The long conjugation lengths in PPV and PPV derivatives combined with long alkyl/alkoxy sidechains makes these materials more susceptible to attack from singlet oxygen. Stilbene, the monomeric two phenyl ring model compound for PPV does not appreciably react with singlet oxygen[19,32]. The incorporation of electron withdrawing groups on the vinylene bond acts to decrease the susceptibility of PPV type polymers to attack from singlet oxygen. Nitrile groups attached to the vinylene bond in poly(2-methoxy,5-(2'-ethyl-hexyloxy)-1,4-phenylene vinylene) [MEH-PPV] were found to

dramatically improve its photo-stability[21]. Phenyl groups also act to help stabilise the vinylene bond against attack. However it should be pointed out that such alterations to a material could alter the desired photophysical effects that made the material attractive to researchers in the first place. Small molecules tend to be very photo-stable as a result of reduced conjugation. Photo-degradation measurements were performed on the small molecule 1,4-bis-(α-cyanostyryl)-2,5-dimethoxybenzene (referred to as G33) in a polystyrene matrix and compared to measurements performed on PmPV in a polystyrene matrix. These results showed that the small molecule was more resistant to photo-degradation than the polymer and will be presented later.

OLED stability has been partially addressed through device encapsulation[33,34], structure and the use of more photo-stable polymers and small molecules. OLED design and the materials used in OLEDs are being continually optimised to minimise photo-degradation and to improve efficiency, stability and reliability. The next step is to look at thin film formation techniques to see what can be done to eliminate air from polymer thin films and to see what strides can be taken to improve thin film efficiency and stability, in an effort to optimise every aspect of an OLED.

3.3 Development of Thin Polymer Film Preparation Techniques to Minimise Photo-degradation in PmPV

3.3.1 Introduction

There has been rapid development of OLEDs in recent years, with long lifetimes, high efficiencies and large luminance values achieved[10,35,36,37]. However improvement in polymer stability is still an important issue. Photo-degradation in conjugated polymers results in lower photoluminescence (PL) efficiencies. At present the effect of this degradation is minimised by device encapsulation. Although encapsulation dramatically improves device lifetime through the exclusion of oxygen and water, it does not improve the inherent polymeric properties of stability and efficiency. In this section novel polymer thin film preparation techniques are employed in an attempt to understand the requirements necessary for the removal of

air from thin polymer films in an effort to minimise the effects of photo-degradation due to oxygen in the polymer films. By doing this it is hoped that the stability and lifetime of OLEDs can be significantly increased.

3.3.2 Experimental Methods and Procedures

For the removal of exciton quenching agents from polymer thin films, inert baking and spinning environments along with solution degassing were tried separately and combined together to determine the necessary requirements. In all, eight different types of film were fabricated and are summarised in Table 3. 1. All the techniques are compared to film type; Conventional (C). All the films were spun at 600 rpm for sixty seconds on to 50 mm diameter borosilicate crown glass (BK-7) substrates from a 25 g/l toluene solution of PmPV. The films were baked at 70°C for a minimum of two hours in three separate atmospheres: air, argon and vacuum (~6×10^2 Nm^{-2}).

Table 3. 1: Techniques used to prepare each film type. ✓ indicates an experimental procedure was carried out. × indicates an experimental procedure was not carried out. The ultimate vacuum achieved was of the order of 6×10^2 Nm^{-2}.

FILM TYPE	SOLUTION DEGASSED	INERT SPINNING ENVIRONMENT	BAKING ENVIRONMENT
Conventional	×	×	Atmosphere
Film 2	×	×	Vacuum
Film 3	×	×	Argon atmosphere
Film 4	✓	×	Atmosphere
Film 5	✓	×	Argon atmosphere
Film 6	✓	×	Vacuum
Film 7	✓	✓	Argon atmosphere
Treated	✓	✓	Vacuum

The solution was degassed by bubbling argon gas through the solution immediately prior to spinning. Inert spinning was performed by fitting an adapter on top of the spincoater and purging the chamber with argon gas prior to, during and after spinning. Inert baking was carried out in a container that had a constant argon feed at

atmospheric pressure. A vacuum oven was used for baking under vacuum. The oven was evacuated using a two-stage rotary pump.

The set-up shown in Figure 3. 4 was used to monitor the degradation lifetime of films prepared by techniques Conventional through to Treated and to record their integrated PL intensities. A Bragg diffraction grating and an aperture were used to select the 457.9 nm line from a multi-line air cooled Ar^+ laser. A glass microscope slide was used to take off a reference beam so as to enable the output of the laser to be monitored using a silicon photodiode. A 10 cm focal length convex lens was used to focus the beam directly onto the polymer film. The beam diameter at the sample was measured by placing a narrow slit in front of a silicone photodiode and scanning through the beam. The beam power at the sample was also measured using a power meter. The fluorescence from the sample was collected and collimated using a 5 cm diameter planar convex lens with a 5 cm focal length. The fluorescence was then

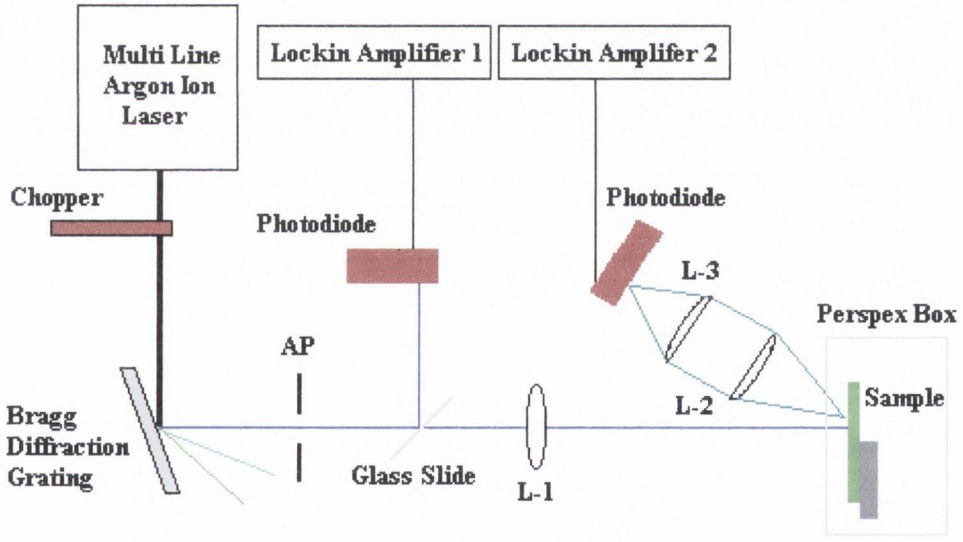

Figure 3. 4: Experimental set up for photo-degradation measurements. The figure labels are as follows: AP ~ Aperture; L-1 ~ Convex lens f = 10 cm; L-2 ~ Planar convex lens ϕ = 5cm, f = 5 cm; L-3 ~ Planar convex lens ϕ = 5cm, f = 10 cm.

focused onto a large area silicon photodiode using a 5 cm diameter, 10 cm focal length planar convex lens. The pump beam was chopped at 287 Hz and both the optimised luminescence signal and the laser beam reference signal were recorded

using lockin-amplifiers. The sample was encased in a perspex box with a constant argon feed for inert atmosphere measurements.

Integrating sphere measurements were also carried out so as to calculate the absolute efficiency, the number of photons emitted from the material per photon absorbed[38,39]. The efficiency measurements were performed using an integrating sphere at an excitation wavelength of 354 nm from a Helium-Cadmium laser at 0.1 mW/cm^2. The films were spun on 20 mm diameter Spectrosil B substrates at 400 rpm. Measurements were performed in a nitrogen atmosphere and were repeated twice for reproducibility. Spectra were recorded with and without the sample in the sphere. The spectra were integrated to calculate the area of the laser and the PL spectra with the sample in the sphere and the area of the laser spectrum without the sample in the sphere. These areas were used to calculate the amount of the laser light absorbed by the sample and the relative efficiency of the sample. Corrections were made to take several factors into account including the spectral response of the sphere[39].

The solid state absorption and photoluminescence spectra were recorded before and after photo-degradation of Conventional and Treated films. The films were exposed, in air, to the expanded 457.9 nm beam of an Innova 90 Coherent water cooled Argon Ion laser at 2 mW/cm^2 for forty five minutes, after which time the photoluminescence from the film had decreased significantly. The lower beam power relative to previous measurements was as a result of the beam having to be expanded so as to photo-degrade a large area of the film for the absorption measurements. A Shimadzu UV-2101PC absorption spectrometer and Perkin Elmer LS50B luminescence spectrometer were used to record the absorption and photoluminescence spectra respectively. An excitation wavelength of 458 nm was used for the PL measurements. The design of the sample holder in the luminescence spectrometer meant that the intensities recorded couldn't be compared directly, thus rendering the measurements unsuitable for measuring relative PL efficiencies, but spectral shifts could still be observed in the normalised spectra.

3.3.2.1 Ultra Violet-Visible Absorption Spectrometer

Shimadzu UV-2101PC Absorption Spectrophotometer: The Shimadzu UV-2101PC is a double beam, direct ratio photometric measuring system using a dynode feedback method. It has a photometric range of -4 to ~5 in Absorbance, 0 to ~99.99% in Transmittance. It employs a 50W halogen lamp and a Deuterium lamp. Spectra are dispersed by a Czerny-Turner monochrometer with a high performance blazed holographic grating, and detected by an R-928 photomultiplier. The instrument has a range of 190 - 900 nm.

3.3.2.2 Luminescence Spectrometer

Perkin Elmer LS50B Luminescence Spectrometer: The LS50B is a computer controlled ratioing luminescence spectrometer. Excitation is provided by a pulsed Xenon discharge lamp, with a full width half maximum of <10 ms and a pulse power of 20 kW. The source is monochromated using a Monk - Gillieson type monochrometer and can be scanned over the range 200 - 800 nm. The luminescence is passed through a similar monochrometer, which can be scanned over the range 200 - 900 nm and is detected using a photomultiplier. The excitation slits (2.5 - 15 nm) and the emission slits (2.5 - 20 nm) can be varied in 0.1 nm increments.

PL spectra were also taken in solution before, during and after bubbling argon through the solution. The solution was pumped using two 1 mW Ultra Violet diodes, $\lambda_{max} = 373$ nm, and the PL spectra were recorded using a CCD camera. These measurements were performed to ascertain if the removal of air from polymer solutions had any affect on the PL.

To test the longevity of the improved PL efficiency measured in the Treated film type, it was exposed to atmosphere over hundreds of hours and its PL intensity recorded on a number of occasions.

Films were prepared at different spin speeds using the conventional and treated technique and their relative PL intensities recorded, to see what effect film thickness

had on the results. Film thickness and surface roughness were examined using optical profilometry.

3.3.2.3 Optical Profilometer

A Zygo *New View 100* scanning white light interferometer was used for all film thickness measurements in this thesis. The machine operates a lot like the FTIR spectrometer discussed earlier. Incoming white light is split inside an interferometer with one beam going to an internal reference surface and the other one going to the sample. When the beams recombine they form a 3D interferogram on a CCD array, which is then transformed, using Fourier transforms, into the frequency domain to form a quantitative 3D image. The depth resolution is 1 nm.

Raman spectroscopy was performed on films prepared in this report, in an attempt to study the vinylene bond and carbonyl group intensities before and after photo-degradation, in films of type Conventional and Treated but problems were encountered which meant that this experimental technique was unsuitable. The problems included a rapidly degrading signal and the fact that carbonyl groups are not very Raman active.

PmPV (25g/l in toluene) solutions containing 0%, 10%, 20% and 30% mass fraction of multiwall carbon nanotubes were made up. The solutions were placed under a sonic tip for 30 seconds to help disperse the carbon nanotubes in the solution and to help break up any amorphous carbon. The solutions were then placed in a sonic bath for 3 hours and then left to settle for 48 hours. The solutions were then decanted, thus separating the polymer and suspended carbon nanotubes from the amorphous carbon which settles at the bottom. PmPV has been used previously as a host material for carbon nanotubes[40]. These solutions were made in order to investigate whether carbon nanotubes acted to reduce the rate of photo-degradation in PmPV. Films were prepared by drop casting onto microscope slides and gently heating the films on a hotplate to ensure that all solvent had been removed from the films. At the time of fabrication of these films it was though that it was not possible to prepare polymer-

carbon nanotube films by spin casting. This has subsequently been discovered not to be the case[41]. The preparation of these films can be compared to that of the Conventional film type as no solution degassing or inert atmosphere spinning was used and the films were baked in air.

3.3.3 Results and Analysis

Air acts as a space filler in polymer solutions and films. The rate of diffusion of air through polymer films or the extent to which air can propagate through a polymer film is relatively unresearched. Initially in this work films were prepared that involved only simple deviations from that of film type Conventional. Film 2 was baked under vacuum to see if air would diffuse out of the film during baking. Film 3 was baked in an argon (inert) atmosphere to see if argon would diffuse into the film during baking and displace the air trapped in the film during spinning. The initial integrated PL of these two films was recorded along with the integrated PL intensity over time while the films were photo-degraded and found to be similar to that of film type Conventional. It was clear that just altering the baking environment had no affect on the magnitude of the integrated PL or photo-degradation lifetime of the PmPV films.

Air trapped in polymer solutions can be replaced with another gas by displacement. Films 4, 5 and 6 were prepared from solutions of PmPV that had been degassed by displacing the air in the solution by bubbling argon gas through the solution immediately prior to spinning and were baked in atmosphere, argon atmosphere and under vacuum respectively. The initial integrated PL of these three films was recorded along with the integrated PL intensity over time while the films were photo-degraded. Film 4 was found to be similar to that of film type Conventional. Film 5 showed a 20% increase in its initial integrated PL intensity while film 6 showed a 70% increase in its initial PL intensity compared to film type Conventional. Additionally, within the time frame of the photo-degradation measurements film 6 hadn't degraded to the same integrated PL intensity as films of type Conventional. These results indicated that not only did solution degassing have an effect on the PL efficiency of PmPV films, but that the baking environment also played an important

role. It is clear from the above data that air has time to diffuse back into the films during the baking process.

Two more films were fabricated to investigate the effects of the spinning environment on the previous results. Film 7 was spun and baked in an argon atmosphere from a degassed solution. Its initial integrated PL intensity showed a 60% increase over that of film type Conventional. Film type Treated was spun in an argon atmosphere and baked under vacuum from a degassed solution. Its initial integrated PL intensity showed a 90% increase over that of film type Conventional. As with films 5 and 6, both films still had a higher integrated PL intensity than film type Conventional after photo-degradation. Film type 6 and Treated, which were baked under vacuum, have higher integrated PL intensities that their corresponding films 5 and 7 respectively, which were baked in an argon atmosphere.

The above results are shown in Figure 3. 5. The luminescence signal was normalised to the laser beam reference. Each film type was prepared twice and four points were monitored on each film, hence each decay curve is an eight point average of data obtained from two films. The measurements for film type Conventional were repeated on two newly prepared films and found to be similar to the original results and hence are not plotted in Figure 3. 5. The influence of film preparation on PL intensity is significant. It can be clearly seen that film type Treated has an initial PL intensity which is 90% greater than that of film type Conventional.

From this point forward it was decided to concentrate on the differences between films prepared by the Conventional and the Treated technique. It had been noted during the above measurements that the power of the laser varied on a day to day basis. The above photo-degradation measurements were repeated for these two film types and are replotted in Figure 3. 6. The measurements were carried out consecutively so as to perform them all at a constant power. The power was measured before and after the measurements and the beam intensity was calculated to be 50 $mWcm^{-2}$ on both occasions. The beam profile at the sample is shown in Figure 3. 7.

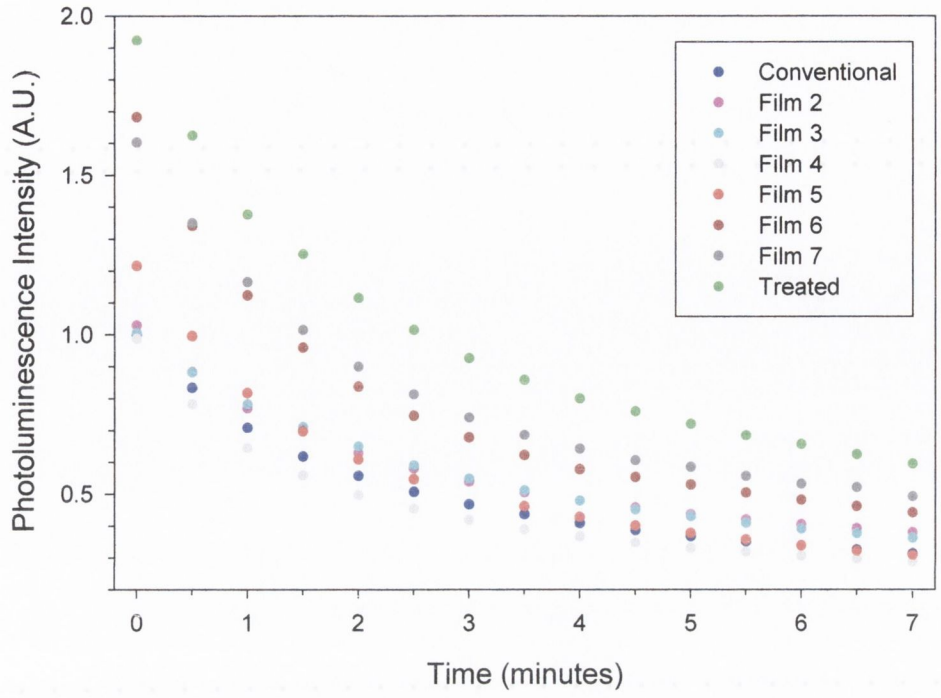

Figure 3. 5: Photoluminescence intensity and photo-degradation with time in air under continuous exposure to radiation at 457.9 nm from an air cooled Ar^+ laser for each film preparation technique as described in Table 3. 1.

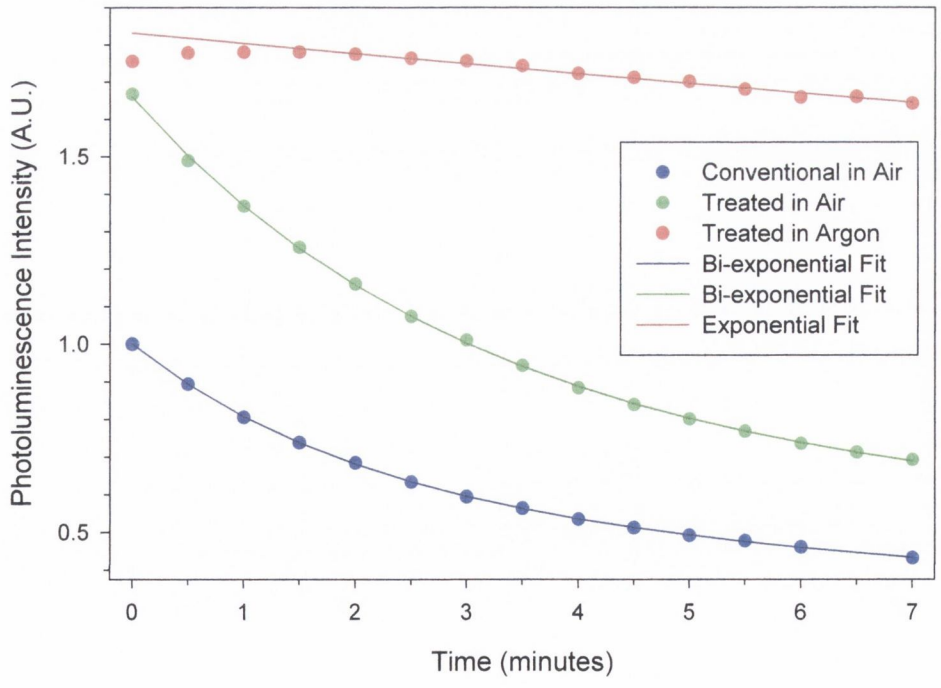

Figure 3. 6: Biexponential fit for film types Conventional and Treated in air and exponential fit for film type Treated in argon atmosphere, for photoluminescence degradation under continuous exposure to radiation at 457.9nm (50 $mWcm^{-2}$) from an air cooled Ar^+ laser.

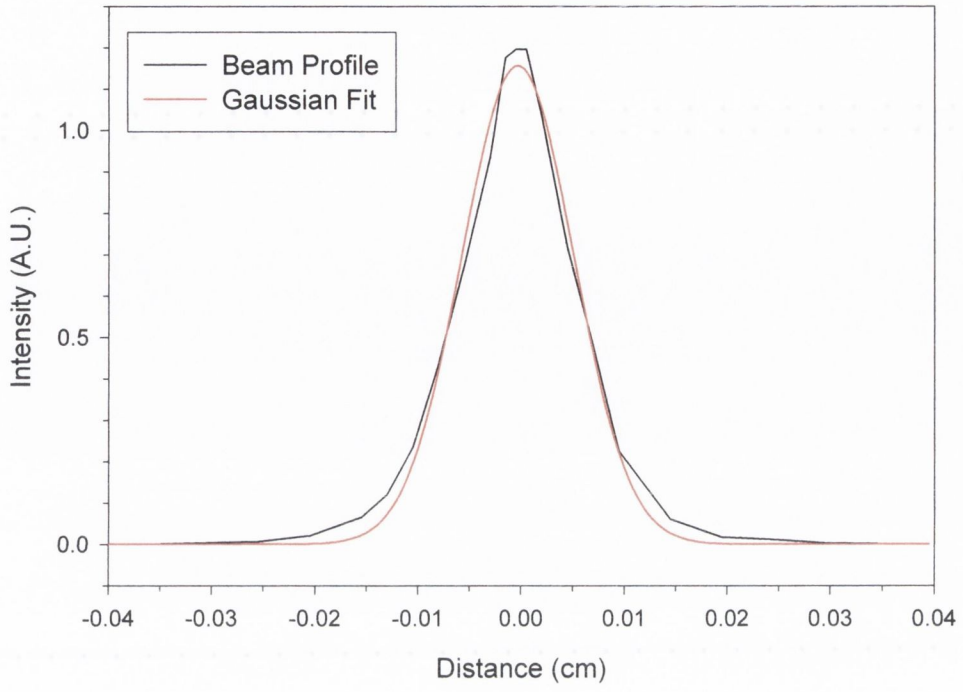

Figure 3. 7: Gaussian fit to Air cooled Argon Laser beam profile.

As previously, each film type was prepared twice and four points were monitored on each film. Film type Treated was also photo-degraded in an argon atmosphere. As can be seen from the graph, film type Treated has an initial PL intensity 70% greater than that of film type Conventional. This increase is lower than measured previously, but is still significantly greater than film type Conventional.

The luminescent decay of film types Conventional and Treated in atmosphere (Figure 3. 6) were modelled using a bi-exponential fit, as shown in Equation 3. 2 with two time constants, t_1 and t_2. The parameters a and b are the initial intensities of the individual decay curves and their sum is the initial PL intensity. The ratio of a/b is 0.83 and 1.44 for the conventional and treated films respectively.

$$y = ae^{t_1} + be^{t_2} \qquad \textit{Equation 3. 2}$$

In air, two different types of luminescence decay are evident. There is an initial rapid decay rate ($1/t_1$), followed by a second slower decay rate ($1/t_2$). Where t_1 and t_2 are time constants, defined as the time taken for the PL intensity to fall to 1/e of its initial value. The time constants are shown in Table 3. 2. It is evident that the preparation

techniques used for film type Treated reduce the decay rates substantially. Compared to film type Conventional, t_1 and t_2 were found to be 43 % and 105 % longer respectively. In an argon atmosphere an initial PL intensity increase is followed by a very gradual decay with a significantly smaller decay rate, ($1/t_{Ar}$). This decay was fitted with a single exponential fit. The decay is attributed to oxygen embedded in the film. These results suggest that in atmosphere the initial sharp decay is due to oxygen in the atmosphere and the second decay is related to oxygen trapped in the film during preparation.

Table 3. 2: Time constants, in seconds, for the decay in photoluminescence intensity. The magnitude of t_2 & t_{Ar} for the photo-degradation due to oxygen embedded in the Treated polymer film are of the same order of magnitude as expected.

	Conventional	**Treated**	**% INCREASE**
t_1	126	180	43
t_2	1538	3158	105
t_{Ar}	—	4000	—

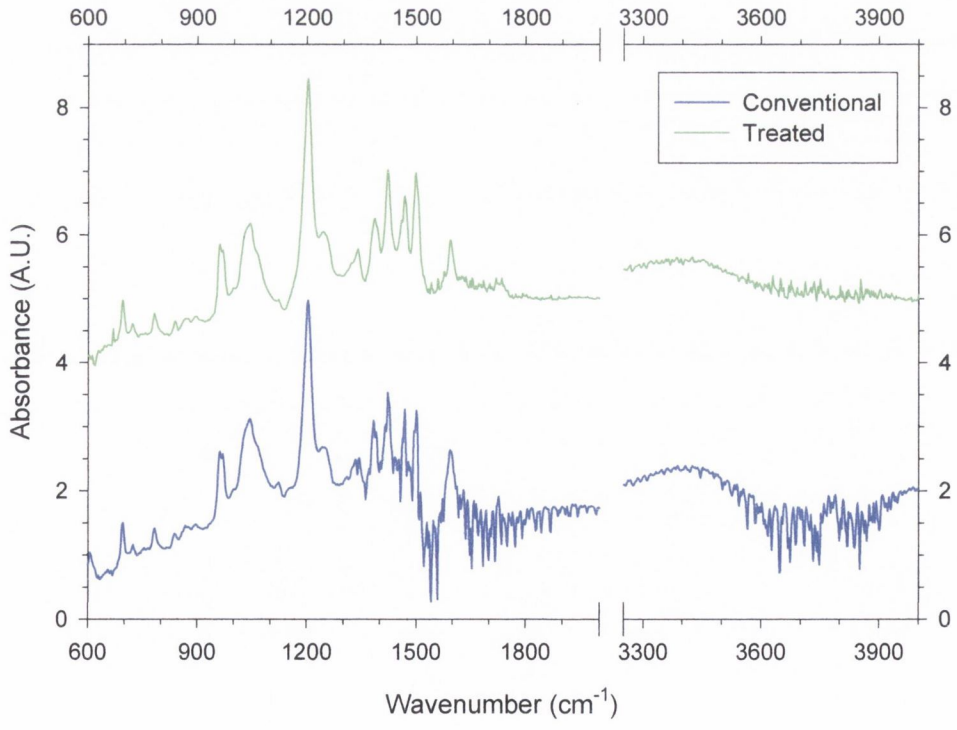

Figure 3. 8: FTIR spectra of film types Conventional and Treated. The significant reduction in the atmospheric signatures of water from 1500 - 2000 cm^{-1} and from 3400 - 4000 cm^{-1} are clearly visible. The Treated spectrum has been displaced for clarity.

Comparison of the FTIR spectrum for film types Conventional and Treated in Figure 3. 8 demonstrates the removal of air from film type Treated. This is inferred by the reduction in the atmospheric signatures of water from 1500 - 2000 cm^{-1} and from 3400 - 4000 cm^{-1}.

Average film thicknesses of 211.6 nm and 370.4 nm were recorded for the film types Conventional and Treated, presented in Figure 3. 5, respectively, with the latter being 75 % thicker. This represents a dramatic increase in film thickness between the two film preparation techniques. The increased thickness is not due to an altering of the polymer concentration due to solvent evaporation during solution degassing as consistent film thicknesses for film types Conventional and Treated have been measured for films prepared from the same polymer solution.

The absorbance spectra of film types Conventional and Treated were taken in the solid state before and after exposure, in air, to the expanded beam of an Innova 90 Coherent water cooled Argon Ion laser at 2 $mWcm^{-2}$ for forty five minutes and are plotted as absorption spectra in Figure 3. 9. It can be seen that there are two peaks in the absorption spectrum of PmPV. The peak at $\lambda = 407$ nm is due to the conjugation along the PmPV backbone. The absorption edge is at $\lambda = 465$nm. Consequently a pump wavelength of $\lambda = 457.9$ nm was chosen to test the PL properties of the polymer, as described above. It was also noted that the absorbance values for the Treated film type was greater than for the Conventional film type, indicating that there was more polymer in the Treated films. With the increased film thickness measurements in mind, the measured increase in PL intensity can not be solely accounted for by additional polymer in the Treated films, thus suggesting possible film morphology changes between the two film types. The PL spectrum of PmPV has two strong peaks, one at 510 nm and the second at 529 nm. The PL spectra have been normalised at their maxima. It can be clearly seen from the absorption spectra in Figure 3. 9 that chain scission has taken place. The 407 nm absorption peak has blue shifted by 12 nm in both film types. This is a direct result of the reduced conjugation caused by the chain scission resulting from photo-degradation. The peak at 336 nm shows no spectral shift after photo-degradation. The two absorption maxima have

also reduced in intensity indicating that the polymer chains have been damaged during photo-degradation.

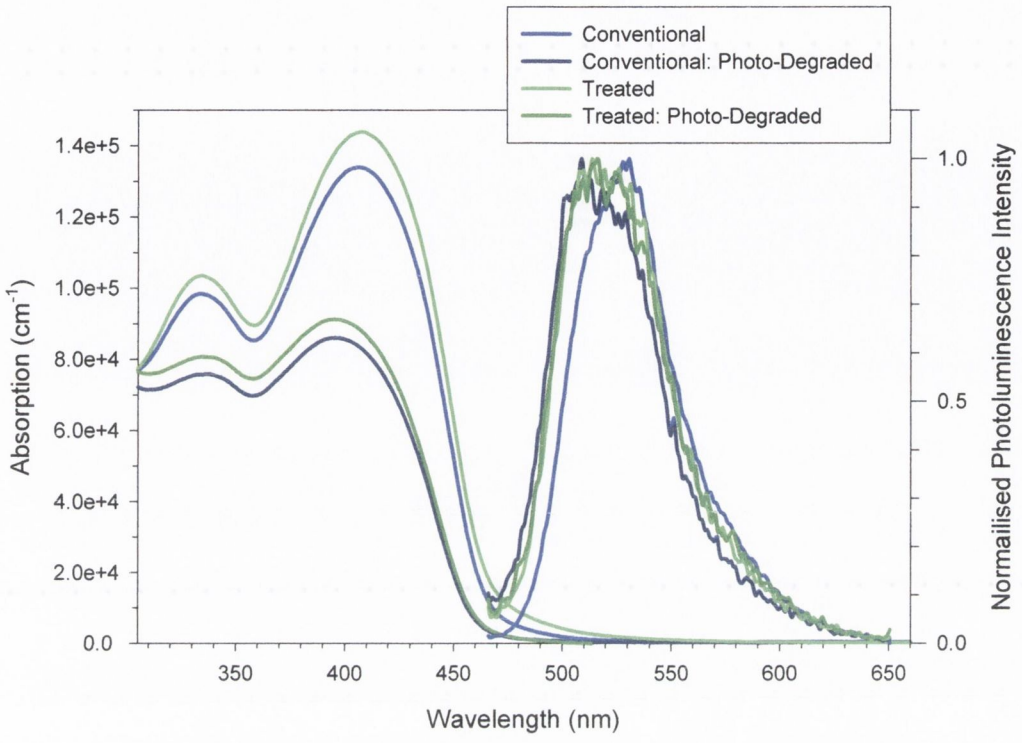

Figure 3. 9: Absorption and photoluminescence spectra for film types Conventional and Treated before and after exposure to radiation at 457.9nm are presented. Blue line: Conventional, Dark Blue line: Conventional Photo-degraded, Green line: Treated and Dark Green line: Treated Photo-degraded.

The PL spectra also show some very interesting changes. The PL spectra of both film types prior to photo-degradation show some distinct differences. The 510 nm peak in film type Conventional is quenched relative to film type Treated, resulting in the spectrum of the Treated film being broadened towards shorter wavelengths by 7 nm in comparison to the Conventional film. This is thought to be due to aggregation in the Conventional film that isn't observed in the Treated film, again suggestive of possible film morphology changes. The spectrum of film type Conventional after photo-degradation shows a blue shift of about 10-12 nm, with the 510 nm peak becoming the dominant peak. This blue shift is indicative of reduced conjugation length caused by chain scission. Interestingly the spectrum of the Treated film after photo-degradation shows no spectral changes. This implies that the Treated film is spectrally stable during photo-degradation. One would expect to observe a blue shift

in film type Treated after photo-degradation seeing as a shift was observed in the absorption spectrum.

To see if the broadening of the PL, in the Treated film, towards the blue was as a result of the removal of air from the solution prior to spinning or as a consequence of film morphology changes, PL spectra were taken in solution and their integrated PL intensity are shown in Table 3. 3. The degassed polymer solution showed no broadening of the PL spectrum towards shorter wavelengths. This indicates that the removal of air from the polymer solution was not responsible for the observed spectral shift. The solid state changes observed are possibly due to changes in film morphology, which act to prevent aggregation effects in the Treated film. It was noted that the increase in integrated PL intensity saturated relatively quickly and then remained constant for the duration of the experiment. A PL intensity increase of 21 % was observed in the degassed solution, showing that air acts to quench the PL in polymer solutions. Film preparation technique 5 shows that the removal of air from polymer thin films gives rise to a 20 % PL intensity increase relative to the Conventional type.

Table 3. 3: Relative integrated photoluminescence intensity for PmPV before (time = 0) and during (time > 0) solution degassing, by bubbling argon gas through the solution.

Time (minutes)	Relative Integrated Photoluminescence Intensity
0.0	1.000
3.5	1.191
6.5	1.215
9.0	1.218

The exposure of a Treated film to atmosphere resulted in a very gradual decrease in initial PL intensity. An initial PL intensity drop of 10 % was recorded over the first eighty hours followed by a further 10 % drop over the next three hundred hours. Meaning that even after three hundred and eighty hours exposure to atmosphere the treated film still has a PL intensity increase of 50 % over the Conventional film being used as the control sample. The films were stored in the dark in between

measurements to prevent photo-degradation. This decrease in initial PL intensity has been partly attributed to the diffusion of air back into the film. X-Ray diffraction measurements were performed on both Conventional and Treated films to study any differences in crystallinity between the two films types, but were inconclusive as the machine required thicker films than could be produced to get a meaningful signal. It was thought that a gradual recrytallisation of the treated film might be contributing to the reduction in PL intensity over time.

In order to monitor the diffusion of air back into Treated films over time, two films were prepared at 600 rpm for 60 s on KBr substrates and dried under vacuum to remove any remaining solvent. FTIR spectra were taken over the course of one month, during which time the two films were continually exposed to atmosphere. The two films were stored in the dark so as to prevent photo-degradation in between measurements. The spectra taken for one of the films, after zero, six and thirty days exposure, are plotted in Figure 3. 10. They have been offset vertically for clarity. As can be clearly seen the atmospheric signatures of water (OH) at 1500 - 2000 cm^{-1} and at 3400 - 4000 cm^{-1} have increased significantly after six days and continue to increase over the thirty day exposure period.

These result shows that Treated films are relatively stable in air for up to one week, before any significant drop off in PL intensity is observed and before the diffusion of air back into the film becomes noticeable. These results also add weight to the idea that the changes in film morphology are largely responsible for the increased PL intensity observed in Treated films as the diffusion of air into the treated films does not reduce the PL intensity of the Treated films to that of the Conventional films.

As reported earlier, films of type Treated were measured to be 75% thicker than films of type Conventional when prepared at 600 rpm. Films of type Conventional and Treated were prepared at 1000 rpm in order to establish whether a similar film thickness increase would be observed, along with the changes in PL spectra observed for the 600 rpm films. Film thicknesses of 136.1 nm and 154.3 nm were measured, showing that Treated film types were 13% thicker than Conventional films when spun at 1000 rpm. PL spectra showed no shifts relative to each other and were found

to be similar to that of Conventional film types, prepared at 600 rpm. It was also noted that the Treated film had an initial PL intensity increase of 17 % over the Conventional film, significantly lower than in the 600 rpm films. Hence the thinner the films the smaller the thickness increase between the two film types and hence the smaller the PL intensity increase. This corresponds with other evidence suggesting we are strongly altering the film morphology in Treated films. Additionally, the film thickness of film type 5 was also measured to be the same as that of the Conventional film type. This verifies that the removal of air from thin films of PmPV is partly responsible for the increased PL intensity observed as film type 5 showed a PL intensity increase of 20% and no increase in film thickness relative to the Conventional film type.

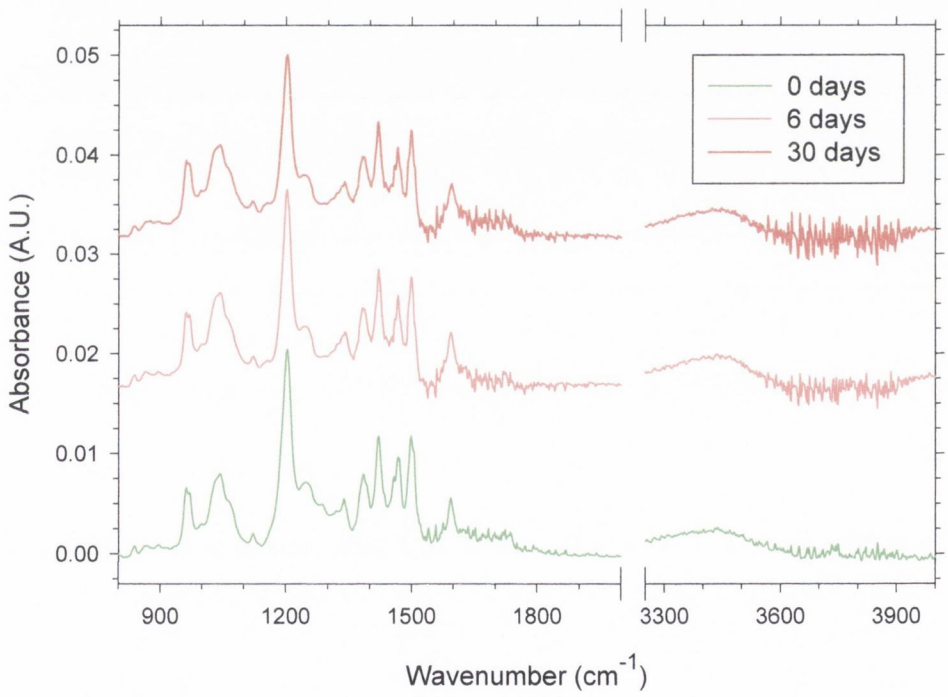

Figure 3. 10: FTIR spectra charting the diffusion of air back into a Treated PmPV polymer film. Spectra are shown after zero, six and thirty days exposure. The spectra have been displaced vertically for clarity.

3.3.3.1 Experimental Point to Note for this point forward in the Thesis

At this point in the experimental work a new batch of PmPV was synthesised to replace the previous batch that had run out. Absorption and PL spectra were

taken and all the peaks were found to be in the same position as expected. It should be pointed out that from this point forward all experimental work involving the use of PmPV was performed using this new batch of PmPV. It was noted that Treated films prepared at 600 rpm showed a significantly smaller PL intensity increase over Conventional films, than obtained previously and that negligible film thickness increases were being achieved. In an attempt to obtain Treated films with significant thickness increases over Conventional films, films were prepared at 400 rpm as opposed to 600 rpm, as had been the case up to this point. This resulted in a PL intensity increase of 54% being achieved combined with a film thickness increase of ~30%. Table 3. 4 shows the PL intensity and film thickness increase measured in films prepared at several different spin speeds for the new batch of polymer and the previous batch.

Table 3. 4: Percentage film thickness and photoluminescence increases comparisons between the old and new batch on PmPV. rpm indicates spin speed, C and T indicate Conventional and Treated films respectively, % d is percentage film thickness increase and % PL is percentage PL intensity increase. Film thicknesses are in nanometers.

	Old PmPV				New PmPV			
rpm	Film Thickness				Film Thickness			
	C	T	% d	% PL	C	T	% d	% PL
1000	136.1	154.3	13.3	17				
600	211.6	370.4	75	90	269	276	2.6	22
500					284	308	8.5	-
400					347	450	29.7	54

Integrating sphere measurements were performed on three samples, film types Conventional and Treated prepared at 400 rpm and a drop cast film containing carbon nanotubes at 10% mass fraction. The results are shown in Table 3. 5. The Treated film was found to be 26.7% more efficient than the Conventional film. This figure is somewhat smaller than the 54% PL intensity increase measured for films of this type.

Table 3. 5: Solid state photoluminescence efficiency values for Conventional and Treated PmPV films and a PmPV film doped with 10% mass fraction of carbon nanotubes.

	10% Nanotube	Conventional	Treated
PL Efficiency	5.00%	6.47%	8.20%

It was noted that the sample wasn't tested for five days after being prepared, but that they had been stored in the dark in an argon atmosphere or under vacuum during those five days. The discrepancy between the measured efficiency increase and the PL intensity increase can be accounted for by slight sample degradation over the five days prior to the efficiency measurements, but is most likely due to additional polymer in the treated films as shown by absorbance measurements. Additional polymer wouldn't influence the efficiency measurements but would give higher PL intensity readings due to the additional polymer. Using film thickness measurements, the absorption coefficient for film types Conventional and Treated combined with the assumption that the thickness increase in the Treated film is solely due to additional polymer and that both film types have the same PL efficiency, a PL intensity increase of ~2% and ~16% would be achieved at wavelengths of 354 nm and 457.9 nm respectively. This indicates that the measured PL intensity increase cannot be due solely to additional polymer. Using the measured values for the efficiencies these values increase to ~29% and ~47% respectively. Additionally, by allowing for some sample degradation of the Treated film prior to performing the efficiency measurements, the measured value would be even higher. It is clear from these calculations and the integrating sphere results that additional polymer in the Treated films is not solely responsible for the increased PL intensity observed.

The 22.7% efficiency decrease for the PmPV film containing 10% mass fraction of carbon nanotubes shows that the incorporation of large percentages of carbon nanotubes into PmPV acts to decrease PL efficiency. It has previously been shown that the incorporation of small percentages of carbon nanotubes acts to break up aggregation and increase PL efficiency in PmPV in solution[42]. This indicates that the quantity of carbon nanotubes added and the environment to which they are added is important for controlling aggregation and PL efficiency in PmPV.

3.3.4 Additional Photo-degradation Measurements

The incorporation of nanotubes into PmPV films had previously been shown to reduce the affects of photo-degradation[43] in PmPV. Photo-degradation measurements were performed in air, as outlined previously, on PmPV films containing 0%, 10%, 20% and 30% mass fraction of nanotubes. The results are graphed in Figure 3. 11 and the decay lifetimes, t_1 and t_2, obtained from the bi-exponential fits are shown in Table 3. 6.

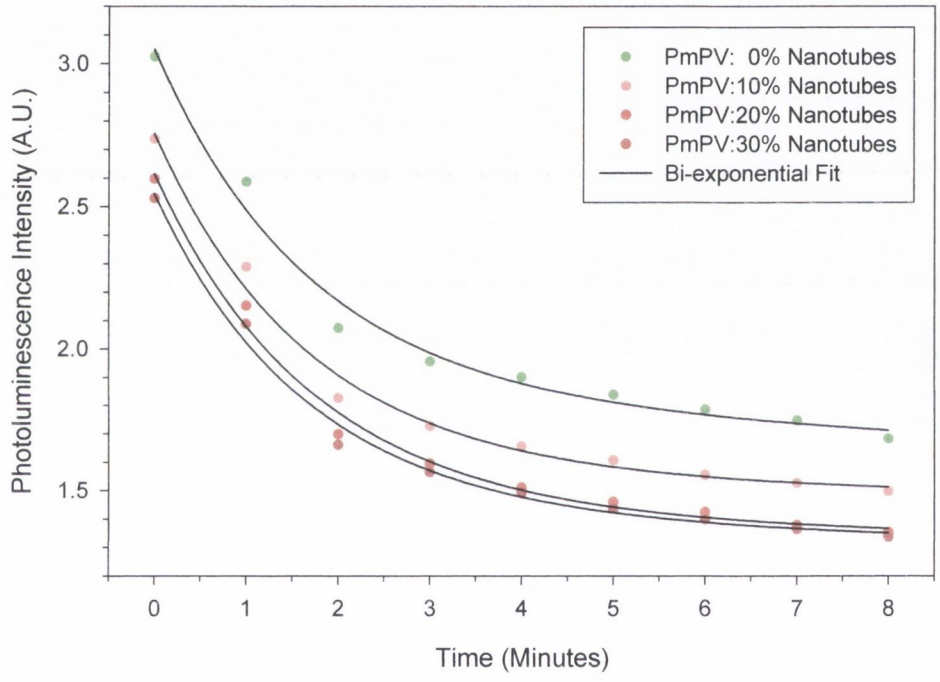

Figure 3. 11: Photoluminescence intensity and photo-degradation with time in air under continuous exposure to radiation at 457.9 nm from an air cooled Ar^+ laser for PmPV and PmPV:nanotube composite containing 10%, 20% and 30% mass fraction of nanotubes. Also shown is the bi-exponential fit to each data set.

As shown previously, there is an initial rapid decay due to the oxygen in the air, followed by a much slower decay, associated with the oxygen trapped in the film. The lifetime of the initial rapid decay (t_1) is similar in all four film types. However the lifetime of the slower secondary decay (t_2) shows a 113% increase for the 10% mass fraction nanotube film over the neat PmPV film. Similarly the 20% and the 30% mass fraction nanotube films show an 88% and 49% increase respectively over the neat PmPV film. These results clearly show that the incorporation of nanotubes

into PmPV films acts to reduce the rate of photo-degradation caused by air trapped in PmPV films.

Table 3. 6: Time constants, in seconds, for the decay in photoluminescence intensity for PmPV films containing 0%, 10%, 20% and 30% mass fraction of carbon nanotubes. $1/t_1$ is the initial decay rate due to air and $1/t_2$ is the decay rate due to air embedded in the films.

	Carbon Nanotube Mass Fraction			
Lifetime	0%	10%	20%	30%
t_1	101	101	104	100
t_2	6767	14409	12714	10070

The mass fraction of nanotubes added is also critical as the rate of the secondary photo-degradation increases with mass fraction of nanotubes. It should be pointed out that the actual mass fraction of carbon nanotubes is significantly less that the percentages quoted as the nanotube soot used was not 100% pure, but that the nature of the PmPV:nanotube soot interaction is such that only carbon nanotubes interact with the PmPV. It should also be noted that the results for the neat PmPV film presented in this paragraph differ from those presented previously. This is possibly due to the fact that these measurements were performed with a different batch on PmPV to the previous measurements and that the experimental set-up had been repositioned since the previous measurements.

Initially photo-degradation experiments were performed on the small molecule 1,4-bis-(α-cyanostyryl)-2,5-dimethoxybenzene (referred to as G33) in a polystyrene matrix. 1g/l G33 doped into 75g/l Polystyrene in o-xylene. Its chemical structure and degradation on exposure to radiation at 457.9 nm from an air cooled argon ion laser are shown in Figure 3. 12. It is immediately apparent from the graph that this material is very photo stable at 457.9 nm. Photo-degradation measurements were also observed for a 1g/l PmPV doped into 75g/l Polystyrene in toluene thin film. The rate of photo-degradation was observed to be very quick, as in neat films of PmPV, indicating that the incorporation of a material into a polystyrene matrix could not be responsible for the remarkable stability measured in G33, implying that the photo-stability in G33 was a material property. It is noted that there are electron

withdrawing nitrile groups attached to vinylene bonds on the backbone, which as discussed earlier, can dramatically improve the photo-stability of organic materials.

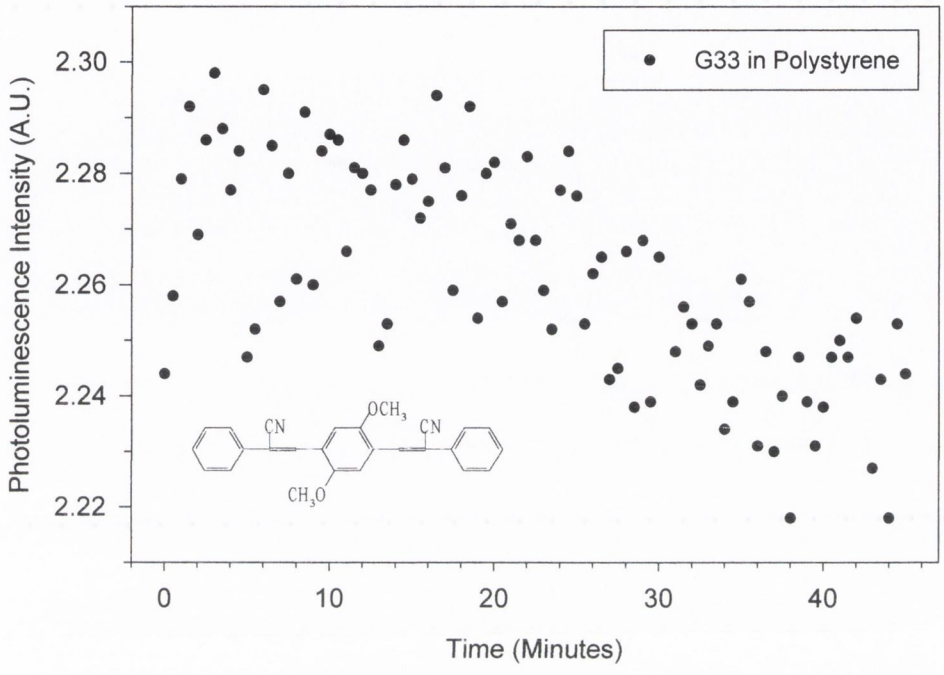

Figure 3. 12: Photoluminescence intensity and photo-degradation with time in air, for G33 doped into Polystyrene, under continuous exposure to radiation at 457.9 nm from an air cooled Ar^+ laser. The chemical structure of G33 is also shown.

3.3.5 Discussion

Increased PL intensity, film thickness, efficiency and photo-stability have all been achieved in Treated films over Conventional films. The solution and solid state PL spectra combined with the film thickness measurements indicate that the thin film preparation technique used to prepare the Treated films is altering the morphology of the film. Absorbance measurements indicate that there is additional polymer in the Treated films, but that it is not sufficient to account for the increased PL intensity measured. This is verified by the integrating sphere measurements and accounts for the difference between the PL intensity increase and the PL efficiency increase measured.

Increased PL efficiency implies that there are an increased number of radiative singlet decays, and hence fewer non-radiative singlet decays, either directly to the ground state or to the triplet state or both. Reduced intersystem crossing would result in the formation of less excited state singlet oxygen, thus acting to reduce the rate of photo-degradation. A significant reduction in the amount of air in Treated films would also have the same effect, hence the reduced rate of photo-degradation observed could result from one or both of these mechanisms. One mechanism for increased radiative singlet decay is a reduction in exciton quenching sites. These sites act to dissociate excitons, which then decay non-radiatively. Polymerisation reactions always leave functional groups on the ends of the polymer chains. These functional groups are usually esters and/or aldehydes, which contain carbonyl groups, which act as quenching sites. In the preparation of Treated films the synthesis of the polymer has not altered and hence the number of this type of quenching sites remains constant and can not be associated with a reduction in non-radiative decay. The close proximity of polymer chains to each other in the solid state results in the formation of inter-chain excitons, polarons and bipolarons. These excited state species all decay by non-radiative routes. To improve PL efficiency requires reducing the formation of these species. The PL efficiency of PmPV increases to 71%[44] in solution due to increased inter-chain separation. The PL efficiency of polymer films can also be increased by doping the polymer into an inert matrix such as Polystyrene (PS) or Poly(methyl methacrylate) (PMMA). Matrix films have higher efficiencies than neat polymer films[45], due to reduced aggregate formation resulting from increased interchain separation and reduced crystallinity compared to neat PmPV films[46]. Other techniques used to increase interchain separation through reduced aggregate formation include incorporating bulky side-chains[47,48,49]. Work involving changes in film morphology through the use of different solvents has been published[50]. Different solvents lead to different conformations in solution, that are carried over into film structure during spinning, leading to increased efficiency due to changes in film morphology. The incorporation of nano-particles such as nanotubes into a PmPV solution act to break up aggregation by increasing interchain separation. The results reported in this chapter indicate that increased inter-chain separation has been achieved in the Treated films. It is thought that the combination of saturating the solution with argon prior to spinning and baking the film under vacuum gives rise to

a foaming effect within the film, resulting in increased inter-chain separation. In order to achieve a better understanding of how the measured PL efficiency increase was obtained, pump and probe experiments were carried out and the results are detailed in Chapter 4.

The effect of polymer chain conformation on the photoluminescence in solutions of PmPV has been studied in detail[28]. Backbone configurations with predominantly *cis* and *trans* configurations show different optical properties. The extent to which interchain interactions in solution differ between the two conformations proves that polymer chain conformation resulting from synthesis can strongly influence solution luminescence efficiency. The aggregation effects have also been studied with increasing solution concentrations. It was found that the incorporation of carbon nanotubes could be used to control aggregation and hence luminescence efficiency, through the control of interchain separation. This result supports the solid state PL spectra, PL efficiency and film thickness measurements presented in this chapter and strongly advances the argument presented that the increased PL efficiency measured is due to changes in film morphology.

Spectral stability and high PL efficiency combined with a minimal fall off in luminance are three very important criteria for electroluminescent (EL) devices if they are to be utilised successfully in organic displays. Changes in spectral stability can be detrimental to the viability and quality of organic displays as they strongly affect the Commission Internationale de L'Eclairage (CIE) co-ordinates. Prior to preparing films by the Treated technique, PmPV demonstrated a blue shift after photo-degradation. Presently, no spectral shift is observed over time for Treated films. The time constants presented in Table 3. 2 clearly show that the removal of oxygen from polymer thin films doubles photo-degradation lifetimes. This problem is particularly relevant to EL devices as they can photo-degrade through their own emission[12]. A final advantage for EL devices from this preparation is the improvement of the PL quantum efficiency, as the EL external quantum efficiency is directly proportional to its PL counterpart. The results presented in this chapter show that the PL properties of PmPV, when prepared by the Treated technique, take a big step towards achieving these three criteria.

The possibility of recrystallisation in the treated films contributing to the decreases in PL intensity over time was looked at unsuccessfully. If it were the case that it was a factor then ways of counteracting it would include new polymer design and the incorporation of nanoparticles. It has been shown that incorporating asymmetric sidechains into the PmPV polymer significantly reduces the ability of the polymer to recrystallise[51]. Similarly the incorporation of nanoparticles, such as carbon nanotubes, SiO_2 and TiO_2, reduce aggregation effects in the polymer and can lead to an improvement in the EL efficiency through a redistribution of the electric field[52].

During the course of preparing treated films for this thesis it was noted that the percentage thickness increase in treated films was sometimes less than the value of ~30% presented in Table 3. 4 for 400rpm films. It should be pointed out that thickness increases of ~30% are recorded in most incidences but that differences can occur, due to two delays that may occur in the fabrication process for treated films. The two delays in question are the time lapse between pipetteing the degassed solution onto the substrate and the commencement of spinning and the time lapse between the completion of the spinning process and the start of the pumping down of the vacuum oven. An example of one of these delays would be if the substrate proved difficult to remove from the spincoater. Several films were fabricated that weren't presented in this thesis due to problems that arose with the devices in question. The problems included bad evaporations and poor film quality leading to devices that degraded upon the application of an electric field. These films, although not presented, enabled a better understanding of the observed thickness increase in treated films. It was noted that in films with reduced thickness increase, there had been delays as detailed above.

3.4 Conclusions

In this chapter the issues of solid state PL efficiency and photo-degradation lifetimes have be addressed, interpreted and improved. Device encapsulation is essential if EL devices are to reach the lifetimes necessary for commercial applications, but does not tackle the material properties of efficiency or photo-degradation lifetime. The

preparation techniques described in this chapter notably improve these device properties prior to encapsulation. Furthermore the stability of the fluorescence spectrum with time, a major issue with regards the future development of organic display technology, is increased significantly by reducing the formation of aggregates. It has been show that the removal of air from polymer thin films combined with changes in film morphology improves PL efficiency by at least 27%, and decay lifetimes t_1 and t_2 by 43% and 105% respectively, in air. This combined with the fact that these films don't significantly degrade on exposure to atmosphere for several hundreds hours, marks a significant step forward in the use of polymers for optoelectronic applications.

3.5 References

1. J. H. Burroughes, D. D. C. Bradley, A. R. Brown, R. N. Marks, K. Mackay, R. H. Friend, P. L. Burn and A. B. Holmes, 'Light-emitting diodes based on conjugated polymers', Nature 347 (1990) 539-541.

2. P. Yam, 'Plastics get wired', Sci. Am. 273 (1995) 74-79.

3. H. Kobayashi, S. Kanbe, S. Seki, H. Kigchi, M. Kimura, I. Yudasaka, S. Miyashita, T. Shimoda, C. R. Towns, J. H. Burroughes and R. H. Friend, 'A novel RGB multicolor light-emitting polymer display', Synth Met. 111-112 (2000) 125-128.

4. J. Kido, 'Organic displays', Physics World 12 (1999) 27-30.

5. P. L. Burn, A. B. Holmes, A. Kraft, A. R. Brown, D. D. C. Bradley, R. H. Friend, 'Light-emitting diodes based on conjugated polymers: control of colour and efficiency', Electrical, Optical, and Magnetic Properties of Organic Solid State Materials Symposium. Mater. Res. Soc. 1992, pp.647-654.

6. I. S. Millard, 'High efficiency polyfluorene polymers suitable for RGB applications'. Synth. Met. 111-112 (2000) 119-123.

7. N. C. Greenham, S. C. Moratti, D. D. C. Bradley, R. H. Friend and A. B. Holmes, 'Efficient light-emitting diodes based on polymers with high electron affinities.' Nature 365,(1993) 628-630.

8. L. C. Palilis, D. G. Lidzey, M. Redecker, D. D. C. Bradley, M. Inbasekaran, E. P. Woo, W. W. Wu, 'Bright and efficient blue and green light-emitting diodes based on conjugated polymer blends', Synth. Met. 111-112 (2000) 159-163.

9. A. W. Grice, D. D. C. Bradley, M. T. Bernius, M. Inbasekaran, W. W. Wu, E. P. Woo, 'High brightness and efficiency blue light-emitting polymer diodes', Appl. Phy. Lett. 73 (1998) 629-631.

10. R. B. Fletcher, D. G. Lidzey, D. D. C. Bradley, S. Walker, M. Inbasekaran and E. P. Woo, 'High Brightness conjugated polymer LEDs', Synth. Met. 111-112 (2000) 151-153.

11. B. H. Cumpston and K. F. Jensen, 'Photo-oxidation of polymers used in electroluminescent devices', Synth. Met. 73 (1995) 195-199.

12. T. Zyung and J. J. Kim, 'Photodegradation of poly(*p*-phenylenevinylene) by laser light at the peak wavelength of electroluminescence', Appl. Phys. Lett. 67 (1995) 3420-3422.

13. F. Cacialli, R. H. Friend, S. C. Moratti and A. B. Holmes, 'Characterization of properties of polymeric light-emitting diodes over extended periods', Synth. Met. 67 (1994) 157-160.

14. J. R. Sheats and D. B. Roitman, 'Failure modes in polymer-based light-emitting diodes', Synth. Met. 95 (1998) 79-85.

15. H. W. Gibson and J. M. Pochan, 'Chemical modification of polymers. Part 19: Oxidation of polyacetylne', Macromolecules 15 (1982) 242-247.

16. S. Holdcroft, 'A photochemical study of poly(3-hexylthiophene)', Macromolecules 24 (1991) 4834-4838.

17. M. S. A. Abdou and S. Holdcroft, 'Mechanisms of photodegradation of poly(3-alkylthiophenes) in solution', Macromolecules 26 (1993) 2954-2962.

18. M. Yan, L. J. Rothberg, F. Papadimitrakopoulos, M. E. Galvin and T. M. Miller, 'Defect Quenching of Conjugated Polymer Luminescence', Phys. Rev. Lett. 73 (1994) 744-747.

19. R. D. Scurlock, B. Wang, P. R. Ogilby, J. R. Sheats and R. L. Clough, 'Singlet Oxygen as a Reactive Intermediate in the Photodegradation of an Electroluminescent Polymer', J. Am. Chem. Soc. 117 (1995) 10194-10202.

20. J. Kopecky, 'Organic Photochemistry: a visual approach.' VCH (1992).

21. B. H. Cumpston and K. F. Jensen, 'Photo-oxidation of Electroluminescent Polymers', TRIP 4 (1996) 151-157

22. J. L. Sessler, B.Wang and A. Harriman, 'Photoinduced energy-transfer in associated but non-covalently linked photosynthetic model systems', J. Am. Chem. Soc. 117 (1995) 704-714.

23. A. M. Brun and A. Harriman, 'Energy-transfer and electron-transfer processes involving palladium porphyrins bound to dna', J. Am. Chem. Soc. 116 (1994) 10383-10393.

24. G. D. Hale, Triplet Exciton Dynamics in Conjugated Polymer Films, M.Sc.Thesis submitted to Rice University, Houston Texas, April 1997

25. F. Papadimitrakopoulos, K. Konstadinidis, T. Miller, R. Opila, E. A. Chandross and M. E. Galvin, 'The role of carbonyl groups in the photoluminescence of poly(*p*-phenylenevinylene)', Chem. Mater. 6 (1994) 1563-1568.

26. L. X. Chen, W. J. H. Jager, M. P. Niemczyk and M. R. Wasielewski, 'Effects of π-conjugation attenuation on the photophysics and exciton dynamics of poly(*p*-phenylenevinylene) polymers incorporating 2,2'-bipyridines', J. Phys. Chem. A 103 (1999) 4341-4351.

27. W. Kemp, 'Organic Spectroscopy' 3rd edition. Macmillan Education (1991).

28. A. B. Dalton, J. N. Coleman, M. in het Panhuis, B. McCarthy, A. Drury, W. J. Blau, B. Paci, J. M. Nunzi and H. J. Byrne, 'Controlling the optical properties of a conjugated co-polymer through variation of backbone isomerism and the introduction of carbon nanotubes', J. PhotoChemistry. PhotoBiology A: Chemistry 5678 (2001) 1-11.

29. A. T. H. Koch, N. T. Harrison, N. Haylett, R. Daik, W. J. Feast and R. H. Friend, 'Enhanced photostability of poly(1,3-phenylene diphenylvinylene)-derivatives by diphenyl-substitution,' Synth. Met. 100 (1999) 113-122.

30. H. Neugebauer, C. Brabec, J. C. Hummelen and N. S. Sariciftci, 'Stability and photodegradation mechanisms of conjugated polymer/fullerene plastic solar cells,' Solar Energy Materials & Solar Cells 61 (2000) 35-42.

31. L. Ma, X. Wang, B. Wang, J. Chen, J. Wang, K. Huang, B. Zhang, Y. Cao, Z. Han, S. Qian and S. Yao, 'Photooxidative degradation mechanism of model compounds of poly(p-phenylenevinylenes),' Chem. Phys. 285 (2002) 85-94.

32. J. Eriksen and C. S. Foote, 'Electron-Transfer Photooxygenation; Oxidation of Phenyl-Substituted Alkenes Sensitised by Cyanoanthracenes.' J. Am. Chem. Soc. 102 (1980) 6083-6088.

33. K. Yamashita, T. Mori and T. Mizutani, 'Encapsulation of organic light-emitting diode using thermal chemical-vapour-deposition polymer film,' J. Phys. D Appl. Phys. 34 (2001) 740-743.

34. R. Windisch, C. Rooman, S. Meinlschmidt, P. Kiesel, D. Zipperer, G. H. Dohler, B. Dutta, M. Kuijk, G. Borghs and P. Heremans, 'Impact of texture-enhanced transmission on high-efficiency surface-textured light-emitting diodes,' Appl. Phys. Lett. 79 (2001) 2315-2317.

35. J. R. Sheats, H. Antoniadis, M. Hueschen, W. Leonard, J. Miller, R. Moon, D. Roitman, and A. Stocking, 'Organic electroluminescent devices.' Science 273 (1996) 884

36. A. Dodabalapur, 'Organic Light Emitting Diodes', Solid State Communications 102 (1997) 259-267.

37. M.A. Baldo, D. F. O'Brien, Y. You, A. Shoustikov, S. Sibley, M. E. Thompson and S. R. Forrest, 'Highly efficient phosphorescent emission from organic electroluminescent devices'. Nature 395 (1998) 151-154.

38. Y. S. Liu, P. de Marco and W. R. Ware, 'Photophysics of polycyclic aromatic hydrocarbons absorbed on silica gel surfaces III Fluorescence quantum yields and radiative decay rate constants derived from lifetime distributions.' J. Phys. Chem. 97 (1993) 5995-6001.

39. N. C. Greenham, I. D. W. Samuel, G. R. Hayes, R. T. Philips, Y. A. R. R. Kessener, S. C. Moratti, A. B. Holmes and R. H. Friend, 'Measurements of absolute photoluminescence quantum efficiencies in conjugated polymers', Chem. Phys. Lett 241 (1995) 89-96.

40. S. A. Curran, P. M. Ajayan, W. J. Blau, D. L. Carroll, J. N. Coleman, A. B. Dalton, A. P. Davey, A Drury, B. Mcarthy, S Maier and A Strevens, 'A composite from poly(m-phenylenevinylene-co-2,5-dioctoxy-p-phenylene) and carbon nanotubes: a novel material for molecular optoelectronics.' Advanced Materials 10 (1998) 1091-1093.

41. P. Fournet, J. N. Coleman, B. Lahr, A. Drury, W. J. Blau, D. F. O'Brien and H-H Horhold, 'Enhanced brightness in organic light-emitting diodes using a carbon nanotube composite as an electron-transport layer,' J. Appl. Phys. 90 (2001) 969-75.

42. A. B. Dalton, H. J. Byrne, J. N. Coleman, S. Curran, A. P. Davey, B. McCarthy and W. J. Blau, 'Optical absorption and fluorescence of a multi-walled nanotube-polymer composite', Synth. Met. 102 (1999) 1176-1177.

43. A. B. Dalton, Private communication on unpublished work.

44. LUPO Project Report; A novel approach to solid state short wavelength laser generation using luminescent polymers, Part 1: First Phase Project Overview. Esprit Project 20038.

45. M. Yan, L. J. Rothberg, E. W. Kwock and T. M. Miller, Interchain Excitations in Conjugated Polymers', Phys. Rev. Lett. 75 (1995) 1992-1995.

46. B. McCarthy, 'Substrate mediated ordering in PmPV thin films', Proceedings of Materials Research Society, Boston, December 1999.

47. C. L. Gettenger, A. J. Heeger, J. M. Drake and D. J. Pine, 'A photoluminescence study of poly(phenylene vinylene) derivatives: The effect of intrinsic persistence length', J. Chem. Phys 101 (1994) 1673-1678.

48. C. H.Lee, G. Yu, D. Moses and A. J. Heeger, ' Dynamics of photoexcited carriers in poly(*p*-phenylenevinylene) and its soluble derivative', Synth. Met. 69 (1995) 429-430.

49. M. R. Andersson, M. Berggren, T. Olinga, T. Hjertberg, O. Inganaes and O. Wennerstroem, 'Improved photoluminescence efficiency of films from conjugated polymers.' Synthetic Metals 85 (1997) 1383-1384.

50. T. Q. Nguyen, V. Doan and B. J. Schwartz, 'Conjugated polymer aggregates in solution: Control of interchain interactions.' J. Chem. Phys. 110 (1999) 4068-4078.

51. C. R. Belton, Private communication on unpublished work.

52. P. W. M. Blom, H. F. M. Schoo and M. Matters, 'Electrical characterisation of electroluminescent polymer nanoparticle composite devices.' Appl. Phys. Lett. 73 (1998) 3914-3916.

Chapter 4

Investigation of Photoluminescence Efficiency in PmPV

4.1 Outline

This chapter starts by outlining the factors that influence photoluminescence (PL) efficiency in organic and polymeric materials. It goes on to outline ways of improving both solution and solid state PL efficiencies. A detailed section follows in which photoinduced absorption (PA) is discussed and the experimental results of PA measurements on Conventional, Treated and Matrix films are presented. The results explain the reason for the increased efficiency measured in Treated films. The third and final section outlines the conclusions derived from the above work.

4.2 Photoinduced Absorption

4.2.1 Introduction

Over the last decade polymers have been utilised successfully as the luminescent materials in organic light emitting devices. Polymers with excellent carrier transport properties and high photoluminescence efficiency have been synthesised[1,2,3]. Poly(*p*-phenylenevinylene) [PPV], along with many of its derivatives, has been extensively studied for potential use in display applications. As discussed previously, enhanced photoluminescence efficiency is a major goal for polymer synthesists and one method used is to reduce the conjugation length of organic polymers. The incorporation of *meta*-phenylene rings into the polymer backbone is one method of restricting conjugation length[4] and limiting exciton diffusion to quenching sites. PmPV is one such polymer that has a *meta*-phenylene ring incorporated into its backbone. Such polymers provide an opportunity to study the relationship between molecular

symmetry and electronic states. The electronic states in PPV have C_{2h} symmetry and are labelled as A_g or B_u, with the corresponding symmetry labels for molecular orbitals being a_g and b_u. Dipole selection rules dictate that transitions can only take place between levels of opposite parity. The incorporation of a *meta*-phenylene ring into PPV acts to break the C_{2h} symmetry, leading to modifications of the electronic structure of PPV. This has potential implications for the photophysics of PmPV as if the incorporation of the *meta* linkage significantly alters photophysical properties of the polymer, other than those associated with the restriction of its conjugation length, that are detrimental to the performance of the material in optical and electrical devices then other techniques may have to be used.

Developments in recent years have led to the investigation of polymers as suitable materials for an electrically pumped organic laser[5,6]. The question of whether polymers can be used successfully as solid state laser materials has raised numerous important issues in polymer science, one of which is excited state absorption by charged species[7]. The presence of a large excited state population with absorption close to the emission maximum will quench any lasing action and has been highlighted as a major problem in fabricating an electrically pumped organic laser[8,9].

In this chapter the photophysics of PmPV is studied, using photoinduced absorption (PA) spectroscopy. In the previous chapter, a variety of different thin film preparation techniques were calibrated for photoluminescence efficiency and photostability. One technique, known as the *treated technique*, was found to significantly improve these two properties. The improvement in these properties was directly correlated with increased film thickness, leading to speculation of increased interchain separation. This leads to a reduction in interchain interaction through increased interchain separation, giving rise to a reduction in the formation of polarons and non-radiative quenching routes, resulting in increased PL efficiency. Increased interchain separation in matrix films, where the luminescent polymer has been doped into a material such as polystyrene, can significantly enhance PL efficiency through reduced polaron formation[10]. A thin film formation technique that addresses this polymeric property would have important implications for the future development of organic optical devices. The aim of this chapter is to study the

relationship between film forming techniques and polaron formation for neat PmPV. Comparisons are made between PmPV thin films prepared by the conventional and treated techniques and with a PmPV/polystyrene blend which is known to have improved efficiency and increased interchain separation when compared to neat PmPV films.

Previously, techniques used to increase interchain separation include incorporating bulky side-chains, doping the organic material into an inert matrix and minimising aggregate formation through solvent choice[11]. All of these techniques succeed to some level in reducing the polaron population, but can alter other important polymer properties, such as charge carrier mobility.

4.2.2 Theory

The photophysics of organic polymers is influenced by a lot of factors. The photoluminescence efficiency of a polymeric material in solution is usually higher than in the solid state[12]. In low concentration solutions in which the individual polymer chains are isolated and thus free to relax into their lowest energy configuration, photoluminescence efficiency is higher than in concentrated polymer solution in which the chains aren't free to rotate. In these solutions the close proximity of neighbouring polymer chains leads to interactions between the chains. Such interactions include the formation of weakly bound excitons across the two chains. These interchain excitons may recombine on the same chain, or they may completely dissociate as they migrate along the chain to form a positive and a negative polaron on separate chains. Additionally they may interact with other interchain excitons and recombine to form singlet or triplet excitons. Interchain excitons are easily dissociated giving rise to lower photoluminescence efficiencies in organic materials with closely interacting polymer chains. Solid state thin films are the ultimate high concentration solution and exhibit significantly lower efficiencies than low concentration solutions of the same polymeric material. The formation of aggregates, closely aligned segments from two or more polymer chains, leads to the formation of low energy absorption tails in the solid state that aren't visible in solution. Excitons dissociate to form these lower energy absorbing species, as they

are energetically favourable. Excitons are continually looking for lower energy states in order to lower their energy. Interchain excitons and polarons are two such states. To summarise[13], the isolation of polymer chains in dilute solutions results in the formation of fewer non radiative excited state interchain species. This gives rise to higher efficiencies in dilute solution than in the solid state. For a detailed study on the photophysics of phenylenevinylene polymers the reader is referred to reference[14].

4.2.3 Experimental Methods and Procedures

Photoexcitation dynamics were studied by Photoinduced absorption (PA) spectroscopy. For PA measurements, the sample is excited by an amplitude-modulated pump beam and changes in the transmission of a probe beam are measured by lock-in amplification of a photodetector. The 457.9 nm line of a Spectra Physics 164 water cooled argon ion laser at a power density of 30 $mWcm^{-2}$ peak-peak, was used as the pump beam and a monochromated tungsten white light source was used as the probe. The probe light transmitted through the sample was passed through a monochromator set to the same wavelength as the probe beam. The use of multiple detectors and gratings enabled the PA spectrum to be investigated between 0.7 and 3.0 eV (~1.8 – 0.4 μm). Cooled silicon and germanium photodetectors were used for measurements between 0.4 - 1.2 μm and 1.0 - 1.8 μm respectively. The pump beam was modulated at 120 Hz by an acousto-optical modulator and the spectra were measured in a cryostat, under vacuum at 80 K. A vacuum of 0.3 Nm^{-2} was achieved using a turbo pump and the sample was cooled using liquid nitrogen. The sample is cooled in order to remove any thermal noise but it also lengthens the triplet and the polaron lifetimes so that they can be measured within the limits of the experimental set up. Prior to cooling, the sample chamber is flushed out with helium gas to aid the removal of oxygen and water from the chamber. This is essential to minimise any photo-degradation that may occur, as the sample is continuously exposed to the laser beam for up to two hours during the course of the PA scans. The PA spectrum, defined as the normalised change, ΔT, in the transmission of the probe beam, T, is proportional to the photoexcitation density, *n*. The lock-in amplifier simultaneously measures the in-phase (X) and quadrature (Y) signals, which can be compared to determine the excitation lifetime and correlate different PA bands. If the

phase difference between the driving signal and the output of the detector is set correctly then an instantaneous event will have no phase lag and will be recorded in X and not in Y. Any event with a lifetime could have a component in Y as it occurs out of phase with X and starts to come in phase with Y, where Y is delayed by 90 degrees with respect to X. The driving frequency plays an important part in this. If it is very low then the entire signal will occur in X. As the drive frequency is increased more and more of the signal will start to appear in Y. Photoluminescence can be considered as being an almost instantaneous event, relative to the lifetime of polaron and triplet states, that have lifetimes that are typically longer than 10^{-7} seconds. The choice of drive frequency is critical as the photoluminescence can obscure any high energy photoinduced states. The frequency was set so as the PL signal appeared in the X signal only. This meant that the Y signal wasn't contaminated by the PL. Due to the choice of frequency, components of the PA signal appeared in both the X and Y signals.

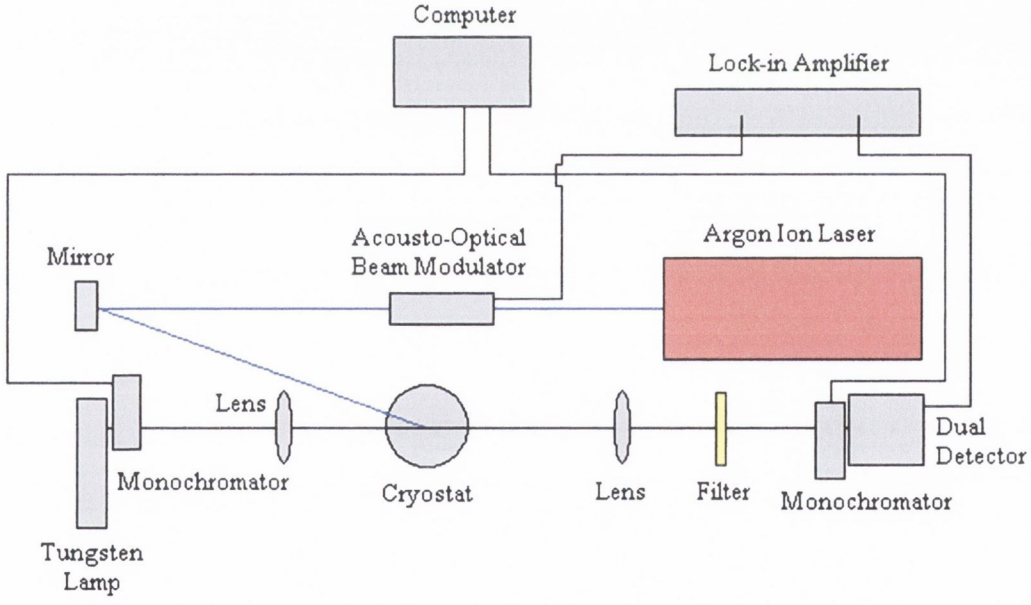

Figure 4. 1: Experimental set up for the Photoinduced absorption measurements.

The lifetimes of any PA bands observed can be measured by measuring their dependence on the pump modulation frequency. The probe wavelength is held constant at the maximum of the PA absorption band being studied while the frequency is scanned. For monomolecular recombination, the in-phase and

quadrature PA signals depend upon the modulation frequency, f, and the excitation lifetime, τ, as[15]

$$\Delta T_{IN} \propto 1/\left[1+(\omega\tau)^2\right]$$

$$\Delta T_{QUAD} \propto \omega\tau/\left[1+(\omega\tau)^2\right] \qquad \textit{Equation 4. 1}$$

where ω is the angular frequency.

By measuring the dependence of the PA signal on the laser power it is possible to identify the species responsible for the observed absorption. The probe wavelength is held constant at the maximum of the PA absorption band being studied while the power of the laser is scanned. The rate equation for photoexcitations is given by

$$\frac{dn}{dt} = G - Rn - Bn^2 \qquad \textit{Equation 4. 2}$$

where G is the generation rate (proportional to the laser flux), R is the monomolecular recombination rate and B is the bimolecular recombination rate. The steady state excitation density is proportional to the laser power ($n_{SS} = G/R$) for monomolecular recombination and proportional to the square root of the laser power ($n_{SS} = \sqrt{G/B}$) for bimolecular recombination. This can be used to distinguish excitations; as triplet excitons have monomolecular recombination (except at high excitation densities), whereas non-geminate polarons have bimolecular recombination. A power index between 0.5 and 1 indicates a combination of monomolecular and bimolecular recombination, as would be the case for a combination of non-geminate polarons and geminate polaron pairs.

All the above experiments were interfaced with a computer using Labview software.

Films of type Conventional and Treated were prepared from 25 g/l toluene solutions of PmPV. Additionally a further PmPV/polystyrene blend film, denoted as film type Matrix, was spun and baked in atmosphere from a non-degassed toluene solution containing PmPV at a concentration of 25 g/l and polystyrene (PS) at a concentration

of 15 g/l. All three film types were spun at 400 rpm on Spectrosil B substrates. Additionally after PA measurements had been performed on the treated film it was photo-degraded in air using the 457.9 nm beam of the argon ion laser until the integrated PL intensity had decreased to 40% of its initial value. PA measurements were then performed on the degraded film.

Additionally doping measurements were performed in solution using Iron tri-Chloride ($FeCl_3$) as an oxidising agent. $FeCl_3$ removes electrons from the polymer resulting in the formation of positive polarons on the polymer chain. The absorption caused by the presence of these polarons can be observed using an ultra violet - visible absorption spectrometer. At high concentrations of $FeCl_3$ it is possible to observe the formation of bi-polarons along with a simultaneous reduction in the polaron absorption, as at high polaron concentrations the formation of bi-polarons is favourable as discussed in chapter two. The absorption spectrum of polarons in PmPV was determined by doping a dilute solution of PmPV (1.25 g/l) in dichloromethane (CH_2Cl_2) with a solution containing $FeCl_3$ in dichloromethane at a concentration of 3.75 g/l. Drops of $FeCl_3$ were added to the PmPV solution and the absorption spectrum recorded.

4.2.4 Results and Analysis

The in-phase and quadrature PA spectra for each of the three film types, conventional, treated and matrix were recorded. An example of a PA spectrum is shown in Figure 4. 2. The example shown is for the treated film. Additionally the quadrature PA spectrum for the treated film after photo-degradation is also shown in Figure 4. 2.

A number of observations can be made from the sample PA spectra plotted in Figure 4. 2. Firstly the contamination of the in-phase spectrum due to the photoluminescence can be clearly seen above 1.85 eV. Heating of the sample by the probe beam modulates the magnitude of the fluorescence and thermochromic shifts can make it impossible to correct by simply scaling the PL intensity. The spectrum is very noisy and it is hard to know whether to attribute peaks to PA bands or poor PL correction.

The quadrature spectrum shows no such contamination. Secondly, the presence of several absorption peaks is evident in the quadrature spectrum. The assignment of these peaks isn't possible from the graph, but laser power dependence can be used to distinguish which absorbing species is associated with each peak. Thirdly, the overlap of the PA bands and the PL spectrum can be clearly seen. This indicates that the PL is being quenched by the presence of these sub gap absorption bands. This acts to reduce the PL efficiency of PmPV over certain wavelength ranges.

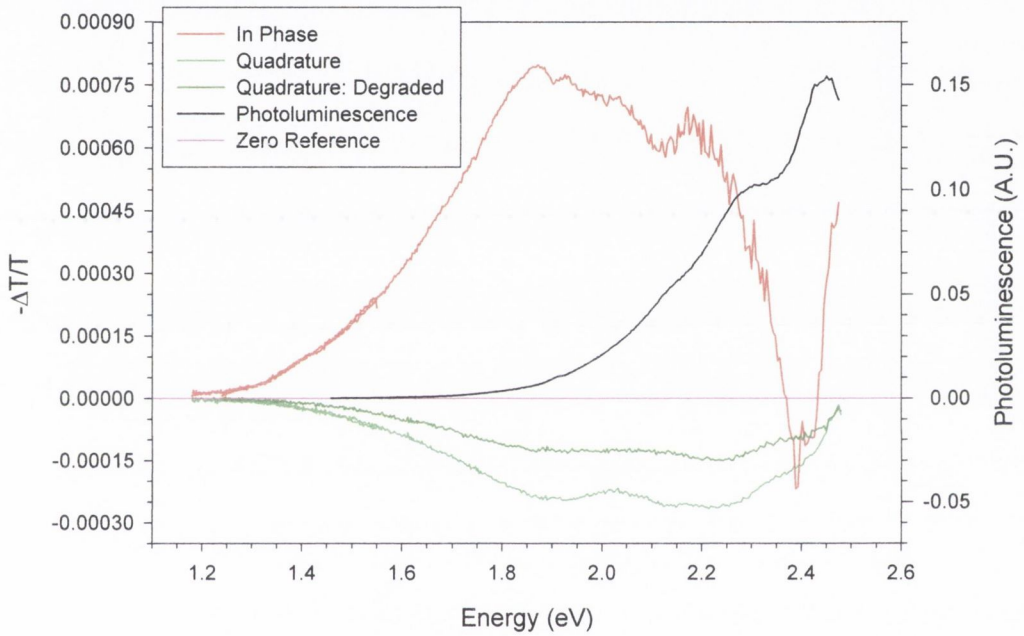

Figure 4. 2: In-phase (red) and quadrature (green) photoinduced absorption spectra for a treated film. The quadrature spectrum of the treated film after photo-degradation (dark green) and the photoluminescence (black) spectrum. The y-axis zero point reference (pink) is also shown.

There are two possible candidates for the PA bands observed. One is charged polarons and the other is neutral triplet excitons. The results of the doping experiment performed to determine the energy for polaron absorption in PmPV are shown in Figure 4. 3. It shows the absorption spectra for a PmPV solution as successive amounts of $FeCl_3$ solution are pipetted. The polymer is oxidised by the dopant and the absorption spectra show the formation of an absorption band with a peak at 2.28 eV (543 nm) due to positive polarons (cations) on the polymer chain. The

polarons being formed here are from charge transfer in solution, whereas the polarons being investigated by PA spectroscopy are formed by photoexcitation. The non-uniform increase with successive drops of $FeCl_3$ is attributed to non-uniform drop sizes. The lineshape of the doping induced absorption spectrum was independent of the dopant concentration and no second oxidation step was observed, which would have indicated the formation of positive bipolarons. The solution photoluminescence spectrum is also shown, to give a clear indication of the spectral overlap between the photoluminescence spectrum and the polaron absorption. A low energy shoulder is also visible around 1.9 eV (653 nm), indicating the possible presence of a second polaron absorption transition.

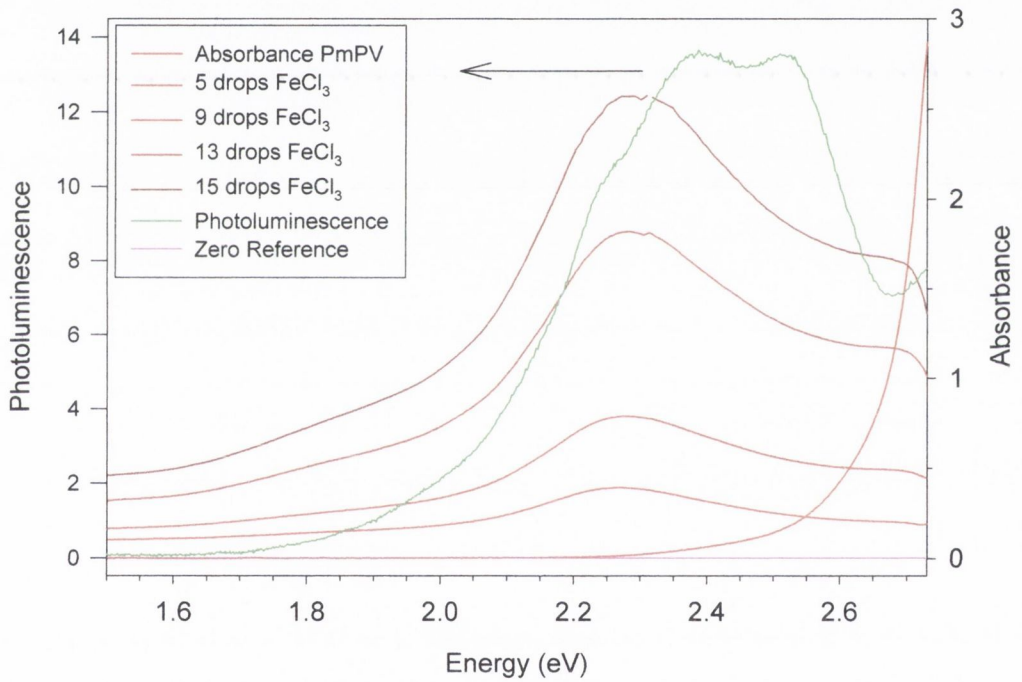

Figure 4. 3: Absorption edge of a 1.25 g/l PmPV solution in dichloromethane (red). Absorbance spectra of PmPV with increasing concentration of $FeCl_3$ (reddish-brown). Luminescence spectrum of the PmPV solution (green). The y-axis zero point reference (pink) is also shown.

The quadrature PA spectra for the conventional, the treated and the matrix film are shown in Figure 4. 4. The matrix film has a PA band with a maxima at 1.87 eV (663 nm). The conventional and treated films both possess a second PA band with a maximum at 2.25 eV (551 nm). This energy matches that of the polaron absorption in

Figure 4. 3 and this PA band is accordingly assigned to photogenerated polarons. The polaron absorption band is significantly stronger in the conventional film, which is consistent with a link between reduced photoluminescence efficiency and enhanced charge photogeneration. This is the case as the number of excitons created is the same in both film types for a given number of incident photons. The efficiency in the treated films is higher as fewer excitons decay by dissociation into charged species thus reducing the polaron yield in treated films. The peak at 1.87 eV is provisionally assigned to triplet excitons.

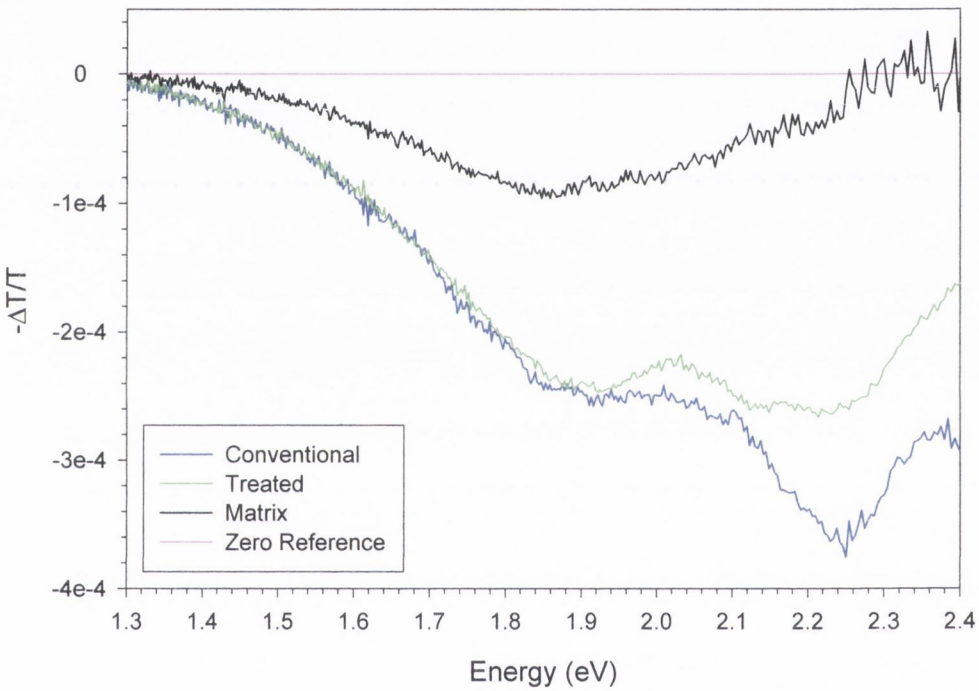

Figure 4. 4: Quadrature photoinduced absorption spectra for the conventional (blue), the treated (green) and the matrix (black) films. The absence of a peak at 2.25 eV in the matrix film is evident along with a reduction in the 2.25 eV peak in the treated film relative to the conventional film.

The dependence of the PA bands on pump power intensity was measured to verify the assignment of the PA bands at 1.87 eV and 2.25 eV to triplet excitons and polarons respectively. A representative graph is shown in Figure 4. 5 for the PA band at 1.87 eV. It should however be pointed out that the graphs were plotted against the In-Phase photoluminescence intensity as opposed to the laser beam intensity. This is

because the photoluminescence intensity is directly proportional to the laser power at low intensities and can be measured more accurately than the laser power.

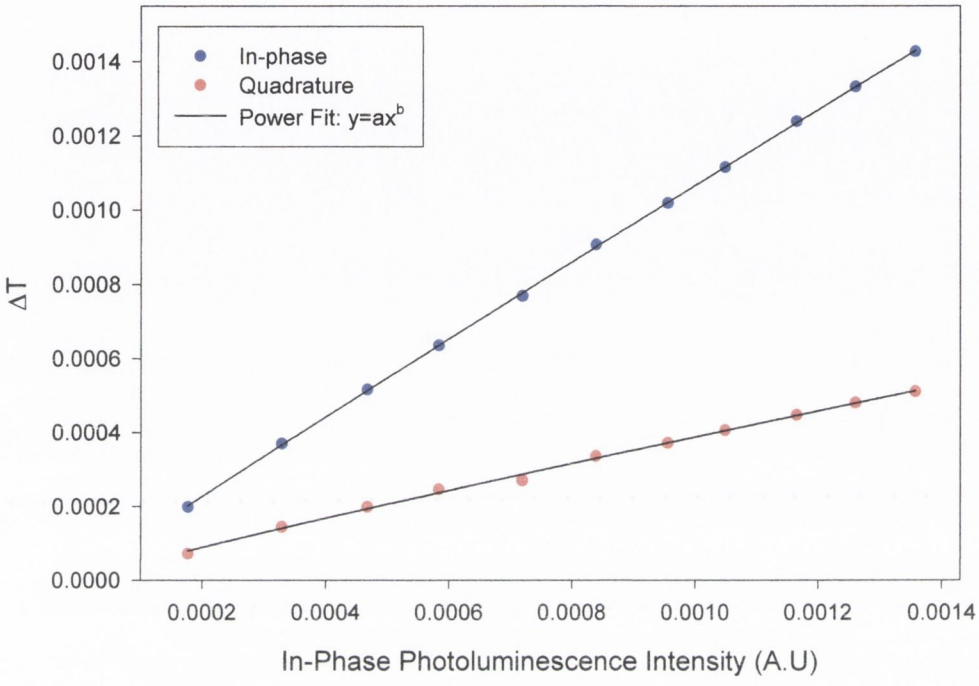

Figure 4. 5: Dependence of the photoinduced absorption band at 1.87 eV on laser power, for a conventional film. The in-phase (blue) and quadrature (red) signals are shown. The black lines are the power fits to the data.

The values measured for all the films are shown in Table 4. 1. The values measured for the 1.87 eV peak are close to unity indicating that this PA band is due to triplet excitons. Meanwhile the values for the 2.25 eV peak show a large deviation for the in-phase and quadrature signals. The in-phase signal for the 2.25 eV band is very noisy due to photoluminescence contamination, meaning that the quadrature value is more representative of the true power dependence of the 2.25 eV signal. The measured value of 0.88 for the conventional film is indicative of a combination of polarons and geminate polaron pairs as discussed previously. These results for the power dependence confirm the assignment of the PA bands at 1.87 eV and 2.25 eV to triplet excitons and polarons respectively.

Table 4. 1: Power dependence of the photoinduced absorption bands on pump beam intensity. In-phase and quadrature values are shown.

Power Dependence of the Photoinduced Absorption bands				
	1.87 eV		2.25 eV	
Film Type	In-Phase	Quadrature	In-Phase	Quadrature
Conventional	0.96	0.91	0.96	0.88
Treated	0.97	0.94	—	—

The fits to both the PA bands are approximately linear in laser power indicating that the recombination is monomolecular. The excitation lifetime can therefore be determined by measuring the dependence of the PA signals upon the modulation frequency. The results are modelled using Equation 4. 1. A representative graph is shown in Figure 4. 6.

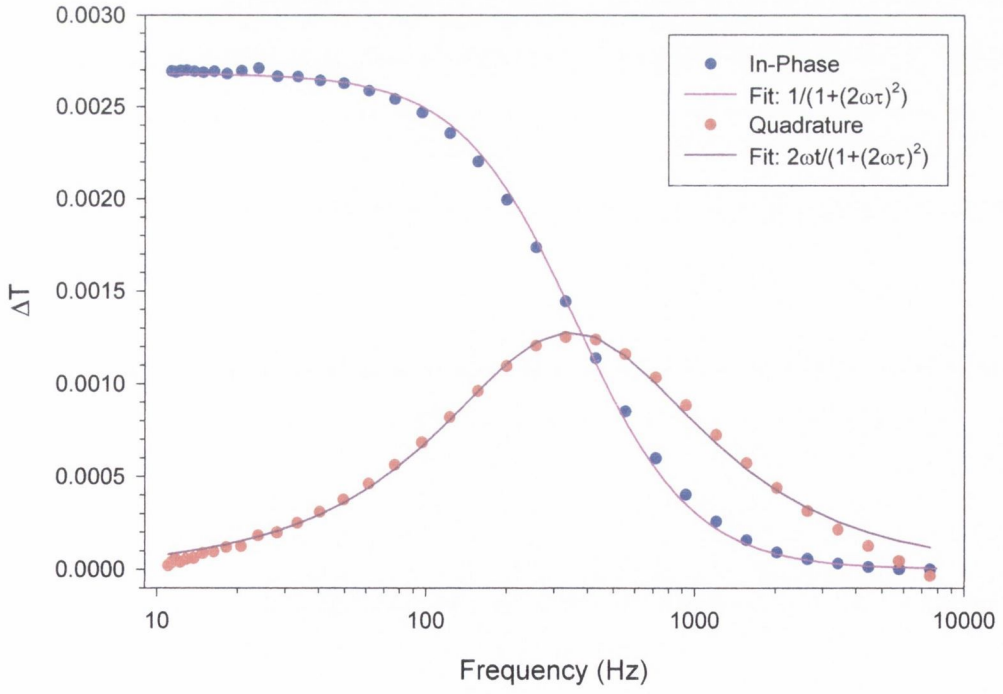

Figure 4. 6: Dependence of the in-phase (blue) and quadrature (red) photoinduced absorption signals upon the modulation frequency for the 1.87 eV band in the treated film. The solid lines are fits to the data.

*Table 4. 2: Frequency dependence of the photoinduced absorption bands. In-phase and quadrature lifetimes at 80 K are shown. The * indicates values after photo-degradation.*

Frequency Dependence of the Photoinduced Absorption bands				
	Lifetime (ms): 1.87 eV		Lifetime (ms): 2.25 eV	
Film Type	In-Phase	Quadrature	In-Phase	Quadrature
Conventional	0.44	0.46	0.46	0.41
Treated	0.44	0.45	—	—
Matrix	0.46	0.45	N/A	N/A
Treated*	0.44	0.43	0.43	0.45

Table 4. 2 shows the calculated values for the lifetime, τ, in milli seconds at 80 K for both polarons and triplet excitons. The lifetimes for both of the PA bands are the same within the calculated errors (±0.02ms). The similar lifetimes for the 1.87 eV and 2.25 eV PA band in all three film types indicates that any changes in the PA signal are due to different generation rates and not changes in polaron recombination rates. This enables direct comparisons to be made between the intensities of the various absorption bands in the recorded spectra.

4.2.5 Discussion

The assignment of the feature at 2.25 eV to polaron-pair formation is in clear agreement with the results using $FeCl_3$ as a dopant. Comparison of the PA spectrum of the matrix film with those of the conventional and the treated films provides further support of the assignment of these features. In the matrix film we continue to observe the triplet feature but no polaron peak. This indicates that polarons in PmPV are predominately formed through interchain coupling and that by disrupting aggregation by increasing the spacing between the polymer chains, through spinning films from polymer/polystyrene blends, reduces the polaron population. The reduced PL efficiency with increased charge photogeneration in the conventional and treated

films relative to the matrix film is consistent with quenching of luminescence by polarons through excited state absorption and direct quenching of singlet excitons.

The similar lifetimes for the 1.87 and 2.25eV PA bands in all three film types allows a direct comparison of the polaron peaks in the conventional and treated films. The PA results give important information about the properties of the three film types. Comparison of the PA signals shows that there is a significant reduction, about 30%, in the polaron population of the treated film relative to the conventional film. This would indicate that there is increased interchain separation in this film, agreeing with the previous measurements for the treated film which showed a thickness increase of ~30%. This reduction in polaron formation explains the increased PL efficiency measured in the treated film.

It is also noted that the intensity of the triplet peak in the matrix film is significantly reduced relative to the conventional and treated films. Since the measured lifetimes are the same in all three film types, the reduction can't be explained by a change in the excited state lifetime. An alternative explanation is that the triplet yield in the matrix film is significantly lower. This could be due to enhanced intersystem crossing or transformation of geminate polaron pairs from singlet to triplet spin configurations before recombination[16] in the conventional and treated films.

The PA spectrum for the photo-degraded treated film shows a reduction in intensity at all energies. The polaron band has increased relative to the triplet but it is difficult to make any direct comparison between the degraded and pristine film as the percentage triplet yield in the degraded film may not be the same as in the pristine film.

Matrix films have higher efficiencies than neat polymer films[10], due to reduced aggregate formation resulting from increased interchain separation and reduced crystallinity compared to neat PmPV films[17]. Waveguide loss measurements[18] showed that waveguides with reduced losses could be fabricated from PmPV through the incorporation of Polystyrene, which acts to break up the crystallinity of neat PmPV films.

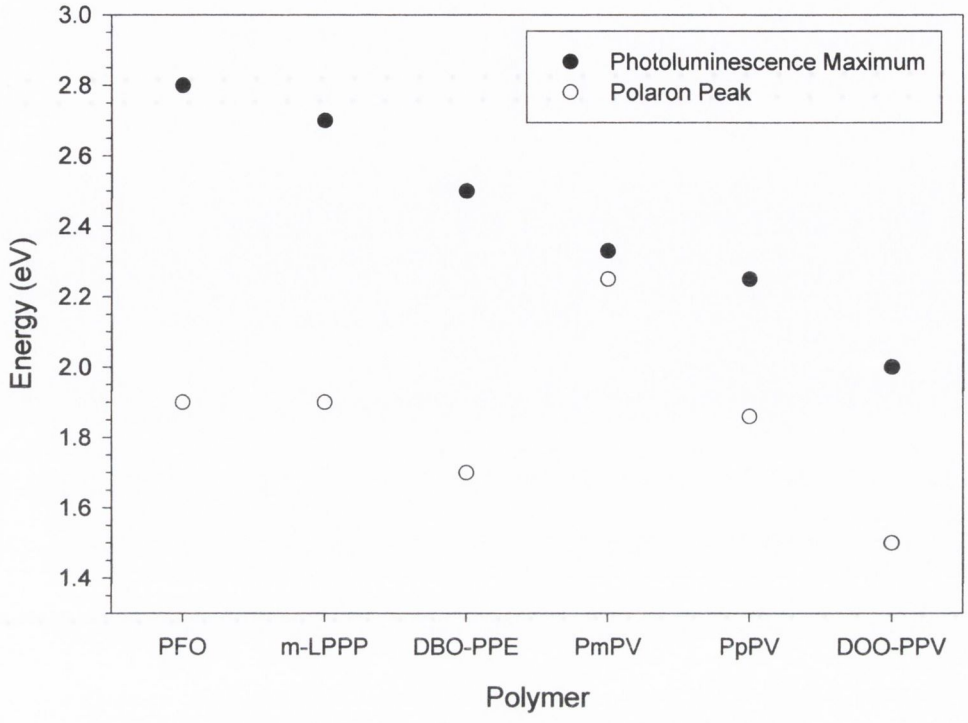

Figure 4. 7: The peaks of the PL spectra (solid circles) and high-energy polaron band (open circles) for a series of phenylene-based polymers. Every polymer shown with the exception of PmPV has C_{2h} symmetry.

The excited state triplet absorption peak occurs at a much higher energy for PmPV (1.87 eV) than in the PPV equivalent poly(2,5-dioctyloxy-*p*-phenylenevinylene) [DOO-PPV] (1.45 eV). This shows that slight changes in the backbone structure of a material can lead to dramatic changes in the energies of the excited states in polymers. As discussed previously the absorption and fluorescence of PmPV are blue shifted by 0.34 eV relative to DOO-PPV. The polaron excited state absorption band, as measured by doping and photogeneration, occurs at a relatively high energy for a phenylene polymer. Figure 4. 7 compares the PL and polaron peaks for a series of phenylene-based polymers: poly(9,9-dioctyl fluorene) [PFO][19], methyl-substituted ladder-type poly(*para*-phenylene) [m-LPPP][20], poly(2,5-dibutoxy phenylene ethynylene [DBO-PPE][21], poly(2,5-dioctyloxy-*para*-phenylene vinylene) [DOO-PPV][22], poly(*para*-phenylenevinylene-co-2,5-dioctyloxy-*para*-phenylene vinylene) [PpPV] and PmPV. Direct comparison with DOO-PPV shows that the absorption peak for polarons is blue shifted by 0.75 eV. This is significantly larger than the blue

shifts in absorption, fluorescence and triplet energy. This result can possibly be explained by the different symmetries possessed by DOO-PPV and PmPV. DOO-PPV possess C_{2h} symmetry with the parity of orbitals alternating between a_g and b_u. Optical transitions are only allowed between orbitals of opposite parity[23,24]. This doesn't appear to hold for the corresponding transitions in PmPV, resulting in a third allowed transition. This is shown schematically in Figure 4. 8. PpPV, the C_{2h} symmetric *para* equivalent of PmPV, doesn't show this third allowed transition.

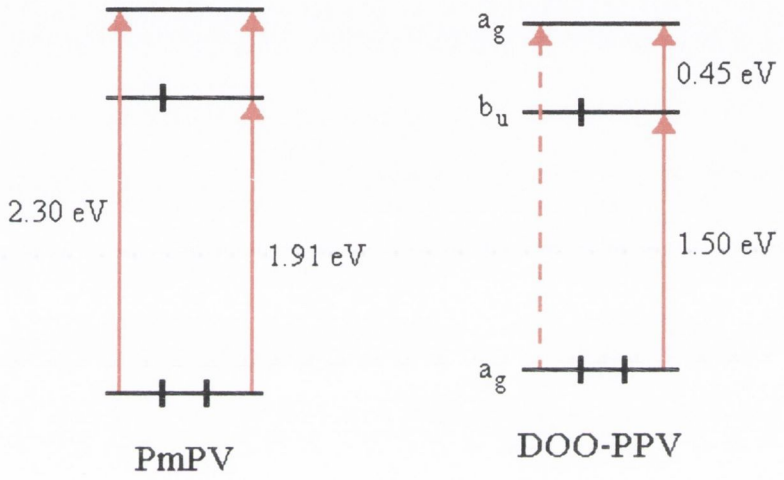

Figure 4. 8: Schematic diagram of the molecular orbitals of a negatively charged polaron in PmPV and DOO-PPV. The allowed transitions are shown by solid red lines and forbidden transitions by dashed red lines.

The doping spectra plotted in Figure 4. 3 show a weak absorption between 1.7 and 1.9 eV, the energy at which the polaron absorption would be expected. The doped absorption spectrum for PmPV can be resolved into two bands with maxima at 1.91 and 2.30 eV, as shown in Figure 4. 9, indicating that two transitions take place. The predominance of the high energy transition is unclear and warrants further study along with other possibilities for the observed changes.

Our results correlate reduced polaron photogeneration with enhanced quantum yield. Interchain aggregation can enhance polaron photogeneration[22], which in turn will reduce the PL quantum yield. Polarons quench singlet excitons[23] and, if the excited state absorption and PL spectra overlap, excited state absorption will also reduce the

PL quantum yield. These results also have important implications for the production of an electrically pumped polymer laser. The strong overlap of the excited state absorption of polarons and the fluorescence in PmPV makes such an application unlikely for this material. This is highly evident in Amplified Spontaneous Emission (ASE) experiments. Laser action has been demonstrated in solutions of PmPV[25] but spectral narrowing under high intensity laser illumination in ASE waveguiding geometries has not been observed in PmPV despite having been observed in other PPV derivatives[26]. This has been attributed to the quenching of fluorescence due to polaron absorption and high waveguide losses due to scattering caused by the highly crystalline nature of PmPV.

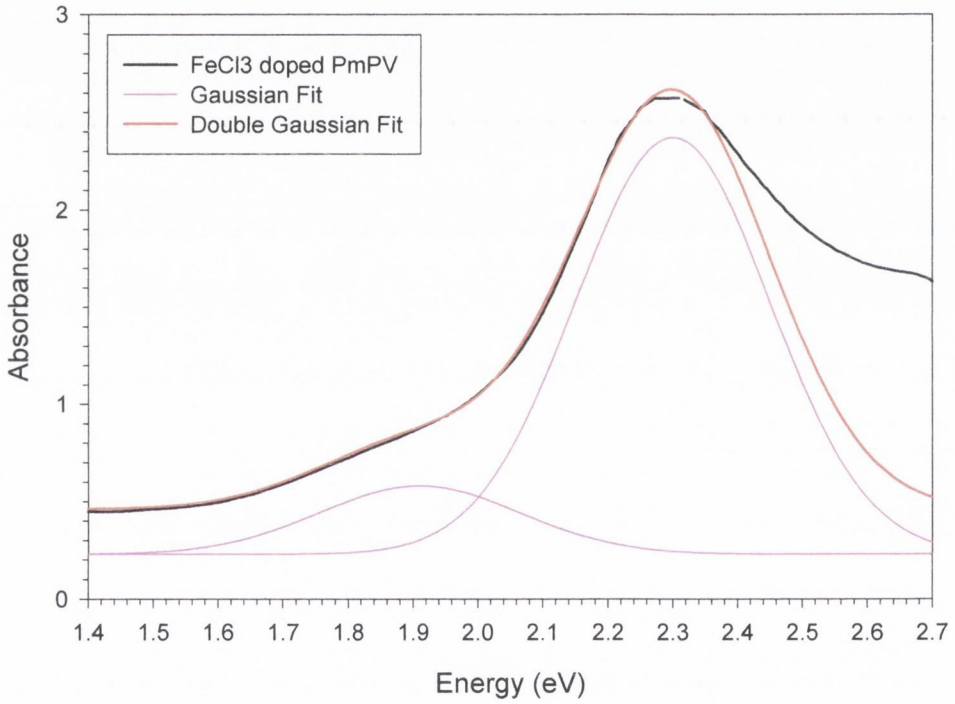

Figure 4. 9: The absorption spectrum (black) of PmPV doped with $FeCl_3$, in solution. The pink lines show the deconvolution of the polaron absorption into two bands with peaks at 1.91 and 2.30 eV. The red line is the combined fit to the spectrum.

As detailed above the spectral overlap of the photoluminescence and the polaron absorption doesn't occur in every luminescent polymer. By studying the differences between the structures of these polymers it is possible to acquire the information necessary to design polymeric materials suitable for solid state lasing applications. Candidate polymers would have to form solid state thin film structures with sufficient

interchain separation to prevent polaron formation. Bulky sidechains have been used but they tend to give rise to scattering which decreases output light coupling from devices. Symmetry considerations may have to be taken into account for the reasons outlined. Polymeric design can only achieve so much and if combined with the correct choice of solvent and thin film preparation technique significant steps can be taken towards the fabrication of solid state polymer lasers. Small molecules have been used to exhibit high gain in waveguide structures[27]. The nature of small molecules restricts exciton and interchain exciton diffusion resulting in the formation of very few polarons. This has lead to extensive research with small molecules over the last decade.

4.3 Conclusions

In conclusion, the excited state absorbing species have been fully characterised for conventional, treated and matrix PmPV films. Doping and photoinduced absorption studies have shown that there are excited state absorption bands at 2.25 eV for polarons and 1.87 eV for triplet excitons. The energy of the polaron absorption was found to be at a higher energy that expected. A possible explanation was provided by the breaking of symmetry on the polymer backbone due to the incorporation of the meta linkage. Other explanations such as the reduced conjugation length cannot however be ruled out. The absence of the polaron absorption in the matrix film and its reduction in the treated film shows that by controlling thin film processing the photophysical properties of thin films can be controlled. In this work increasing interchain separation can significantly reduce the number of polarons formed in thin films of PmPV. This decrease in polaron formation results in increased photoluminescence efficiency. This work has important implications for understanding further the photophysics of luminescent polymers and more immediately in developing a successful polymer for use as an emissive layer in an electrically pumped organic laser.

4.4 References

1 R. H. Friend, R. W. Gymer, A. B. Holmes, J. H. Burroughes, R. N. Marks, C. Taliani, D. D. C. Bradley, D. A. Dos Santos, J. L. Bredas, M. Logdlund and W. R. Salaneck, 'Electroluminescence in conjugated polymers.' Nature 397 (1999) 121-128.

2 J. R. Sheats, H. Antoniadis, M. Hueschen, W. Leonard, J. Miller, R. Moon, D. Roitman and A. Stocking, 'Organic electroluminescent devices.' Science 273 (1996) 884-888.

3 A. Dodabalapur, 'Organic light emitting diodes.' Solid State Communications, 102 (1997) 259-267.

4 P. L. Burn, A. B. Holmes, A. Kraft, D. D. C. Bradley, A. R. Brown, R. H. Friend and R. W. Gymer, 'Chemical tuning of electroluminescent copolymers to improve emission efficiencies and allow patterning.' Nature 356 (1992) 47-49.

5 N. Tessler, G. J. Denton and R. H. Friend, 'Lasing from conjugated-polymer microcavities.' Nature 382 (1996) 695-697.

6 F. Hide, M. A. Diaz-Garcia, B. J. Schwartz, M. R. Andersson, Q. B. Pei and A. J. Heeger, 'Semiconducting polymers: a new class of solid-state laser materials.' Science 273 (1996) 1833-1836.

7 N. Tessler, 'Lasers based on semiconducting organic materials.' Adv. Materials 11 (1999) 363-370.

8. N. Tessler, N. T. Harrison, D. S. Thomas and R. H. Friend, 'Current heating in polymer light emitting diodes,' Appl. Phys. Lett. 73 (1998) 732-734.

9. G. Kranzelbinder and G. Lising, 'Organic solid-state lasers,' Reports on Progress in Physics 63 (2000) 729-762.

10 M. Yan, L. J. Rothberg, E. W. Kwock, T. M. Miller, 'Interchain excitations in conjugated polymers.' Phys. Rev. Lett. 75 (1995) 1992-1995.

11 T. Q. Nguyen, V. Doan, B. J. Schwartz, 'Conjugated polymer aggregates in solution: Control of interchain interactions.'J. Chem. Phys. 110 (1999) 4068-4078.

12. Esprit Project 28580 LUPO, 'A novel approach to solid state short wavelength laser generation using luminescent polymers,' Project Report.

13 B. J. Schwartz, F. Hide, M. R. Andersson and A. J. Heeger, 'Ultrafast studies of stimulated emission and gain in solid films of conjugated polymers.' Chem. Phys. Lett. 265 (1997) 327-333.

14 L. J. Rothberg, M. Yan, F. Papadimitrakopoulos, M. E. Galvin, E. W. Kwock and T. M. Miller, 'Photophysics of phenylenevinylene polymers.' Synth. Met. 80 (1996) 41-58.

15 C. Botta, S. Luzzati, R. Tubino, D. D. C. Bradley and R. H. Friend, 'Photoinduced absorption of polymer solutions.' Phys. Rev. B. 48 (1993) 14809-14817.

16 E. L. Frankevich, A. A. Lymarev, I. Sokollik, F. E. Kasasz, S. Blumstengel, R. H. Baughman and H. H. Hörhold, 'Polaron-pair generation in poly(phenylene vinylenes).' Phys. Rev. B. 46 (1992) 9320-9324.

17 B. McCarthy, 'Substrate mediated ordering in PmPV thin films', Proceedings of Materials Research Society, Boston, December 1999.

18 K. P. Kretsch, (unpublished work)

19 A. J. Cadby, P. A. Lane, S. Martin, D. D. C. Bradley, M. Wohlgenannt, C. An and Z. V. Vardeny, Optical studies of photoexcitations of poly(9,9-dioctyl fluorine) Synth. Met. 111 (2000) 515-518.

20 W. Graupner, M. Mauri, J. Stampfl, G. Leising, U. Scherf and K. Müllen, 'Photo-excited and doping-induced electronic states in a poly(para-phenylene)-type ladder polymer.' Solid State Communications. 91 (1994) 7-12.

21 P. A. Lane, X. Wei, and Z. V. Vardeny, 'Spin and spectral signatures of polaron pairs in pi-conjugated polymers.' Physical Review B 56 (1997) 4626-4637.

22 T. Q. Nguyen, I. B. Martini, J. Liu, B. J. Schwartz, 'Controling interchain interactions in conjugated polymers: The effect of chain morphology on exciton-exciton annihilation and aggregation in MEH-PPV films.'J. Phys. Chem. B 104 (2000) 237-255.

23 P. A. Lane, X. Wei, and Z. V. Vardeny, 'Studies of charged excitations in pi-conjugated oligomers and polymers by optical modulation.' Phys. Rev. Lett. 77 (1996) 1544-1547.

24 J. Cornil and J. L. Bredas, 'Nature of the optical-transitions in charged oligothiophenes.' Adv. Mater. 7 (1995) 295-297.

25 W. Holzer, A. Penzkofer, S-H Gong, A. Bleyer and D. D. C. Bradley, 'Laser action in poly(m-phenylenevinylene-co-2,5-dioctoxy-p-phenlyenevinylene.' Adv. Mater. 8 (1996) 974-978.

26 M. D. McGehee, R. Gupta, S. Veenstra, E. K. Miller, M. A. Diaz-Garcia and A. J. Heeger, 'Amplified Spontaneous Emission and Distributed Feedback Lasing from Photopumped films of a Conjugated Polymer.' Phys. Rev.B – Cond. Matt. 58 (1998) 7035-7039.

27 K. P. Kretsch, C. Belton, S. Lipson, W. J. Blau, F. Z. Henari, H. Rost, S. Pfeiffer, A. Teuschel, H. Tillman and H-H Hörhold, 'Amplified Spontaneous Emission and Optical Gain spectra from Stilbenoid and PPV Model Compounds.' J. Appl. Phys. 86 (1999) 6155-6159.

Chapter 5

Electrical Analysis and Properties of PmPV

5.1 Outline

This chapter is divided into three main sections, in addition to the outline and conclusions, the first of which deals with the current-voltage (I-V) characteristics of conventional and treated films for both electron only and hole only devices. The I-V characteristics are used to study differences in the electrical transport properties between the two film types. Detailed tables of all the calculated properties are presented and analysed. The second section uses impedance spectroscopy to enable additional electrical properties to be analysed and others to be re-measured using a different experimental technique. The use of alternating voltage measurements allows a more in-depth study of fundamental material properties to be performed. The third section applies what has been learnt in the first two sections and the previous two chapters into fabricating and analysing the performance of an LED prepared using a treated film relative to one prepared from a conventional film. The chapter concludes with a detailed conclusions section for the chapter.

5.2 Charge Carrier Injection from Contacts

5.2.1 Introduction

An electrical contact is generally defined as the junction between a metal and a non-metal, the purpose of which is to either enable or block the injection of charge carriers through the junction. The non-metallic material is usually an insulator or a semiconductor. Metal–electrolyte, semiconductor–electrolyte and insulator–electrolyte contacts also exist, but for the purpose of this discussion the

possible combination of electrical contacts that exist shall be limited to metal-insulator and metal-semiconductor contacts.

5.2.2 Electrical Contacts

In the solid state model when two materials are brought together to form a contact their Fermi levels (E_F) must be aligned. This is achieved by the flow of free charge carriers from one material to the other, resulting in the formation of positive and negative space charge regions on opposite sides of the contact, which act as a potential barrier. The potential across this barrier is known as the contact potential and acts to set up an electric field to prevent the further net flow of free charge across the interface between the two materials.

Charge carriers produced by optical or thermal excitation within a solid don't usually result in an alteration of the overall charge in the solid, whereas charge carriers injected from a contact produce a net space charge resulting in *space charge limited current* under the application of an electric field. This build up of excess space charge in a material can alter its electrical properties as outlined in the following sections.

The work function (ϕ_m) of a metal is the potential barrier between the Fermi level of the metal and the lowest energy level of an electron in vacuum, called the vacuum level. Due to the fact that the Fermi level of a semiconductor is in the band gap the work function (ϕ_s) is defined as

$$\phi_s = \chi_s + (E_C - E_F) \qquad \textit{Equation 5. 1}$$

where χ_s is the electron affinity of the semiconductor and E_c is the energy at the bottom of the conduction band. As can be seen from Equation 5. 1 the work function of a semiconductor is dependant on the position of the Fermi level, which is a function of dopant and impurity concentration. The electron affinity is defined as the energy released when an electron in the vacuum level goes into a state at the bottom of the conduction band. The band diagrams for the work function of a metal and an intrinsic semiconductor are shown in Figure 5. 1.

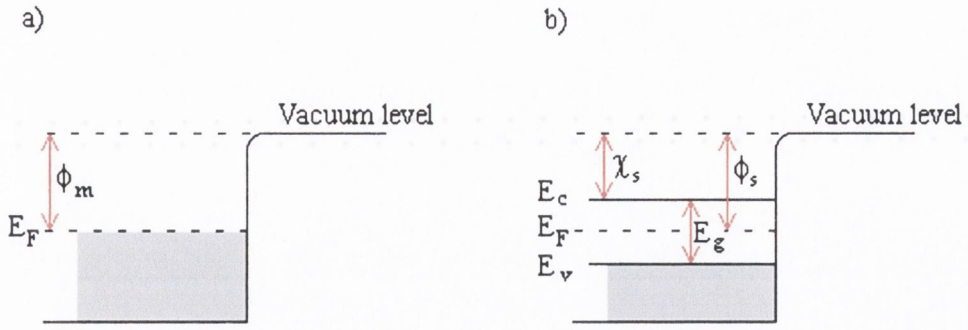

Figure 5. 1: Energy band diagram showing the work function of a) a metal, ϕ_m and b) an intrinsic semiconductor, ϕ_s, where χ_s is the electron affinity of the semiconductor.

The contact potential can clearly be defined as the difference between the work functions of the two materials forming the contact. For a metal–*n*-type semiconductor contact, where $\phi_m > \phi_s$, the contact potential (V_d) is given by

$$V_d = \frac{1}{q}(\phi_m - \phi_s) = \frac{1}{q}\left[\phi_m - \chi_s - (E_c - E_F)\right] \qquad \textit{Equation 5. 2}$$

where q is the charge of an electron. For charge to be injected from the bottom of the conduction band of the semiconductor into the metal the electrons must have an energy equal to or greater than the potential barrier qV_d, while for charge to be injected from the metal into the semiconductor the electrons at the fermi level in the metal must have an energy equal to, or greater than the potential barrier ϕ_m-χ_s, as shown in Figure 5. 2. Potential barriers formed by a space charge region whose width

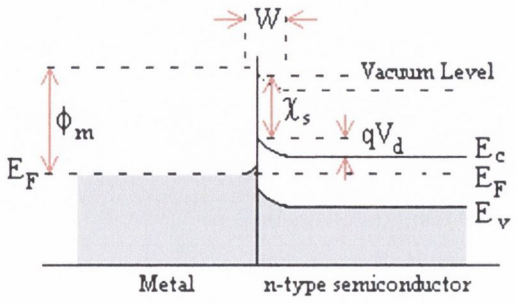

Figure 5. 2: Energy level diagram for a metal – n-type semiconductor contact.

(W) and height depend on applied voltage are known as Schottky barriers. The lowering of a potential barrier due to the application of an electric field is known as the Schottky Effect.

5.2.2.1 Neutral Contacts

A neutral contact[1,2] is one at which the carrier concentration is neutral on both sides of the point of contact. Hence there is no space charge or band bending at the metal - semiconductor interface. This condition occurs when $\phi_m = \phi_s$ although it can also occur when $\phi_m \neq \phi_s$ due to electron (hole) trapping levels sufficiently above (below) the fermi level in wide band gap semiconductors.

5.2.2.2 Blocking Contacts

The Schottky barrier shown in Figure 5. 2 is an electron blocking contact as viewed by electrons in the metal, in which $\phi_m > \phi_s$. Under forward bias electrons can easily flow from the semiconductor to the metal but under reverse bias the flow of electrons from the metal is limited by the electrons available over the Schottky barrier, the density of which is significantly lower than in the bulk of the semiconductor. This type of conduction is known as *electrode limited.* Electron emission from a metal, across a blocking contact, maybe due to either thermionic emission or high field tunnelling. The corresponding condition for a contact to be a blocking contact for holes is $\phi_m < \phi_s$, as seen by holes on the metal side, of a metal-p-type-semiconductor junction.

5.2.2.3 Ohmic Contacts

An ohmic contact has negligible contact resistance relative to the semiconductor bulk and hence doesn't degrade device performance due to the small voltage drop across it relative to the voltage drop across the bulk. The free carrier density in the contact is significantly greater than in the bulk of the semiconductor, resulting in the contact acting as a reservoir of carriers. Charge injection from an ohmic contact is said to be bulk limited seeing as the contact acts as a reservoir of free

charge carriers, meaning the carrier conduction is controlled by the impedance of the semiconductor bulk. It should be pointed out that the current-voltage characteristics of an ohmic contact are only linear when the conduction is ohmic. When the conduction is space charge limited the current-voltage characteristics are not linear. An example of such a contact would be between the semiconductor Gallium Arsenide and metal Gold alloyed with Indium, Germanium and Silicon.

5.2.3 Electrode Limited Conduction

A blocking contact, as described previously, is known as an electrode limiting contact because the electrodes and not the semiconductor bulk control the current-voltage characteristics. There are two possible ways for charge carriers to inject from electrodes into a semiconductor and they are by Field Enhanced Thermionic Emission and by Field Assisted Quantum Mechanical Tunnelling.

5.2.3.1 Field Enhanced Thermionic Emission

In a conducting material, the electrons are governed by Fermi-Dirac statistics. As the temperature is increased some electrons have sufficient energy to pass over the surface potential barrier separating the two materials. This process of increasing the temperature of a bulk material to increase the number of electrons that can leave the material is called thermionic emission. This is invariably aided by the Schottky effect[3], which acts to reduce the value and width of the potential barrier, thus increasing the number of electrons able to surmount the barrier.

If all the electrons emitted from the cathode are carried away in the conduction band and collected at the anode the field enhanced thermionic emission current density is given by

$$J = A^{*}T^{2}\,\mathbf{exp}\left(\frac{B\sqrt{E}}{kT}\right) \qquad \textit{Equation 5. 3}$$

where A^{*} is the effective Richardson constant, T is the temperature in Kelvin and B is a function of both the work function and the image force. It also depends on whether the contact is neutral or blocking. The reduction in the value of the work

function is known as the *Schottky effect*. At a constant temperature the natural log of the thermionic emitted current density is proportional to the square root of the applied field. When considering field enhanced thermionic emission we assume that the width of the depletion region is greater than the electron wavelength so as field assisted quantum mechanical tunnelling can be neglected. Additionally it should be pointed out that this scenario assumes an Ohmic contact at the other electrode hence it is not valid for symmetrical devices.

5.2.3.2 Field Assisted Quantum Mechanical Tunnelling

Field emission is the quantum mechanical tunnelling of electrons through a potential barrier from a metal to a semiconductor or an insulator in the presence of a strong electric field. Fowler and Nordheim[4] proposed that at high applied fields or at low temperatures that conduction by field assisted quantum mechanical tunnelling through the contact potential barrier was dominant. The presence of an electric field can significantly lower and narrow the potential barrier thus increasing the probability of quantum mechanical tunnelling through the barrier. Due to the largely temperature independent nature of the current-voltage characteristics at high fields, the low temperature–high field expression holds in most situations for electrode limited conduction. The Fowler–Nordheim expression is

$$J = \left(\frac{q^3}{8\pi\ h\phi_B}\right)\left(\frac{V}{d}\right)^2 \exp\left(\frac{-8\pi\left(2m^*\right)^{1/2}\phi_B^{3/2}}{3hq}\Big/\frac{V}{d}\right) \qquad \textit{Equation 5. 4}$$

where q is the charge of an electron, h is Plank's constant, ϕ_B is the barrier height, m^* is the effective carrier mass, V is the applied voltage and d is the semiconductor/insulator thickness. Equation 5. 4 simplifies to

$$\ln\left(J/E^2\right) = A + B/E \qquad \textit{Equation 5. 5}$$

where A and B are proportional to the barrier height and E is the electric field defined as V/d.

5.2.4 Bulk Limited Conduction

The ohmic contact detailed above leads to bulk limited conduction due to the build up of a reservoir of free charge carriers at the electrode. When the carrier-injecting electrode provides an excess of charge carriers the current is controlled by the bulk properties of the material into which the charge is being injected. The build up of space charge creates an electric field that acts to reduce the rate of charge injection from the electrode. Thus the current is controlled by the mobility of the charge carriers in the bulk. The presence of impurities can act to trap injected charge carriers, thus controlling the current-voltage characteristics of the material. This will be discussed in detail later, but for the moment we will concentrate on unipolar charge carrier injection into trap free organic materials.

5.2.4.1 Unipolar Charge Carrier Injection: Trap Free Current-Voltage Characteristics

Due to the complex nature of charge carrier injection, the following assumptions are made prior to deriving the current-voltage characteristics. 1) The injecting ohmic contact is perfect. 2) Charge carrier mobility is field independent. 3) The drift component of the current is dominant over the diffusion component, which we ignore. This is true when the applied voltage is greater that kT/e, where e is the elementary charge. 4) There are shallow traps present which contribute a thermally generated free charge carrier density of p_0.

At low applied voltages the free carriers will start to drift with an average drift velocity, v_d, which is proportional to the applied field, E.

$$v_d = \mu E \qquad \textit{Equation 5. 6}$$

where μ is the charge carrier mobility. This is governed by Ohm's Law:

$$J = \sigma E \qquad \textit{Equation 5. 7}$$

where J is the current density and σ is the conductivity. The conductivity is related to the mobility by

$$\sigma = p_0 e \mu \qquad \textit{Equation 5. 8}$$

where p_0 is the free carrier density and e is the elementary charge.

5.2.4.1.1 Dielectric Relaxation Time

The ability of a material to redistribute excess injected charge in order to maintain charge neutrality is governed by the dielectric relaxation time, τ_d. This is the time taken for a material to restore charge neutrality after the injection of a small excess of charge. It is defined as follows

$$\tau_d = \varepsilon/\sigma = \varepsilon/p e \mu \qquad \textit{Equation 5. 9}$$

Where ε is the permittivity of the material, which is related to the strength of the Coulomb interaction within the material. When the injected charge carrier density, p, is low, the carrier transit time, τ_t, is greater than τ_d implying that the material can redistribute excess charge to maintain charge neutrality. τ_t is defined as the time taken for a carrier to travel from the cathode to the anode and is given by

$$\tau_t = d/v_d \qquad \textit{Equation 5. 10}$$

where d is the thickness of the organic layer. However organic materials tend to have extremely low free carrier densities meaning that with increasing applied voltage, p becomes greater than p_0, the transit time becomes less than the dielectric relaxation time (from Equation 5. 6) and the free carriers cannot compensate for the injected charge carriers. The current then becomes space charge limited.

When p equals p_0, τ_t equals τ_d. By combining Equation 5. 6 with Equation 5. 10 the expression for τ_t becomes

$$\tau_t = d^2/\mu V \qquad \textit{Equation 5. 11}$$

where V is the applied voltage. The voltage at which these two times are equal is called V_Ω.

The current density in the material may be written in terms of the total injected free charge per unit area, Q, and the transit time

$$J = Q/\tau_t \qquad \textit{Equation 5. 12}$$

A given voltage between a cathode and an anode a distance d apart can only support a total charge Q per unit area. Hence Q is proportional to V with the proportionality constant C defined by

$$C = Q/V = \varepsilon A/d \qquad \textit{Equation 5. 13}$$

where A is the cross sectional area and the proportionality constant C is called the capacitance. C_0 is the geometric capacitance and $C = 2C_0$ if the charge is distributed evenly between cathode and anode and approaches C_0 due to a non-uniform distribution of charge, since the charge is injected at one electrode. Ignoring this factor-of-two and combining Equation 5. 6, 5. 11, 5. 12 and 5. 13 the current density can be written as

$$J \approx \varepsilon \mu V^2 / d^3 \qquad \textit{Equation 5. 14}$$

This equation describes the current-voltage characteristics of unipolar space charge limited currents in organic materials. The result derived analytically by Mott and Gurney in 1940[5] differs only through the presence of a numerical factor 9/8

$$J = 9\varepsilon \mu V^2 / 8\, d^3 \qquad \textit{Equation 5. 15}$$

This equation is the solid state equivalent of Childs law for space charge limited (SCL) current in a vacuum[6].

In the absence of any traps the current-voltage characteristics of organic materials obey Equation 5. 15. However, this is unrealistic as polymeric materials always contain impurities, which give rise to a free carrier density. Also if there are very shallow traps present in the material that can be thermally excited, then there will be thermally generated charge carriers present which, along with any impurity carriers, dominate the I - V characteristics at low voltages if $p_0 >> p$, meaning the I - V characteristic will be ohmic. As discussed previously there is a transition

voltage, V_Ω, at which $\tau_t \approx \tau_d$. When V_Ω is reached $p = p_0$ and the ohmic current equals the SCL current as shown in Equation 5. 16

$$e\, p_0\, \mu\, V / d = 9\, \varepsilon\, \mu V^2 / 8\, d^3 \qquad \textit{Equation 5. 16}$$

giving the following at $V = V_\Omega$.

$$V_\Omega = 8 e p_0 d^2 / 9\varepsilon \qquad \textit{Equation 5. 17}$$

It should be pointed out that the two currents can flow simultaneously but that when $V < V_\Omega$, ohmic processes dominate and when $V > V_\Omega$, SCL processes dominate. Due to the fact that both currents can flow simultaneously, the transition from ohmic to SCL at V_Ω is not abrupt, but is gradual, as will be seen later.

5.2.4.1.2 Impurities in Organic Materials Leading to Charge Carrier Trapping

Organic materials aren't the perfectly pure materials as assumed in the above derivation. They contain energy levels in the forbidden energy gap, which act to trap charge carriers, thus affecting I-V characteristics. These sites result from imperfections in the polymer chain and the presence of impurities in the polymer film. Impurities on the polymer chain include the functional groups at the end of every chain that are left over from the polymerisation reaction. Polarons on the polymer chain, as discussed in chapter 2, form energy levels in the band gap. Interchain coupling between polymer chains in the solid state leads to the formation of sub gap recombination sites as discussed in chapter 4. Any chemical impurities present can also act to create energy levels in the band gap. Electron traps are defined as shallow if they are above the quasi-Fermi level and deep if they are below the quasi-Fermi level respectively, where as hole traps are defined as shallow if they are below the quasi-fermi level and deep if they are above the quasi-fermi level. The probability of deep traps being occupied approaches unity as the energy difference between the trap level and the quasi-fermi level is usually greater than kT.

5.2.4.2 Unipolar Charge Carrier Injection: Current-Voltage Characteristics in the Presence of Single or Multiple Discrete Traps

A few assumptions are made in the following discussion, the most important being that the spatial distribution of traps is uniform. This means that we can take the thickness of the semiconductor layer to be thickness d instead of an effective thickness, d_{eff}.

At low bias these traps reduce the number of injected carriers that are free to conduct. For a given voltage the current is reduced by a factor of θ, defined as the ratio of the free carrier density to the total carrier density and is given by

$$\theta = p/(p+p_t) \qquad \textit{Equation 5. 18}$$

where p_t is the trapped carrier density and free carrier density includes both thermally generated and injected carriers. Equation 5. 15 changes to

$$J = 9\varepsilon\mu\theta V^2/8d^3 \qquad \textit{Equation 5. 19}$$

It can be clearly seen that as p_t approaches zero, that θ approaches unity and the I–V characteristics approach the trap free case. In the presence of traps θ is always less than unity and can be as small[7] as 10^{-7}.

The transition voltage, V_Ω, from ohmic to SCL current is now defined as

$$V_\Omega = 8ep_0 d^2/9\theta\varepsilon \qquad \textit{Equation 5. 20}$$

indicating that V_Ω increases with the trap density. It should also be pointed out that V_Ω increases with the thermally generated carrier density. The mobility of the charge carriers becomes the effective mobility μ_{eff} defined by

$$\mu_{eff} = (p/p+p_t)\mu = \theta\mu \qquad \textit{Equation 5. 21}$$

A direct result of the filling of trapping sites is that the quasi-fermi level moves closer to the bottom of the conduction band for electron injection and closer to the top of the valence band for hole injection. At some point during charge injection the quasi-fermi level will pass through the trapping energy level. This voltage is

known as the *trap filled limit* and is denoted by V_{TFL}. This voltage marks the transition from the low current trapping I-V characteristics to the high current trap free I-V characteristics. There are two cases depending on whether the traps are shallow or deep.

5.2.4.2.1 Trap Filled Limit: Shallow Traps

In this case the energy of the trap lies above (below) the quasi-fermi level for electrons (holes). The value of V_{TFL} depends on the value of θ. The larger the trap density, the smaller the value of θ and hence the larger the value of V_{Ω} and V_{TFL}. At V_{TFL} all traps are filled and there is a very dramatic increase in current as μ_{eff} returns to μ. If the material contains two or more discrete trap levels, this dramatic increase in current will be observed two or more times with the value of μ_{eff} increasing at each transition until it reaches μ after the final transition.

5.2.4.2.2 Trap Filled Limit: Deep Traps

In the case of deep traps the energy of the trap lies below (above) the quasi-fermi level for electrons (holes). All injected carriers will initially be used to fill the traps. The transition from ohmic conduction to SCL conduction will take place at V_{Ω}, which will be equal to V_{TFL}. In this case the transition is from ohmic to trap free SCL conduction as all the traps are filled and the traps are too deep to be thermally excited.

5.2.4.3 Unipolar Charge Carrier Injection: Current-Voltage Characteristics in the Presence of Exponentially and Gaussianly Distributed Traps

Not all organic systems have discrete trap energy levels. The trap energy levels can have an exponential or gaussian distribution within the energy gap. Mark and Helfrich[8] showed the I-V characteristics for traps distributed exponentially to be given by

$$J = e^{1-m}\mu N\left(\frac{2m+1}{m+1}\right)^{m+1}\left(\frac{m}{m+1}\frac{\varepsilon}{N_t}\right)^{m}\frac{V^{m+1}}{d^{2m+1}} \qquad \textit{Equation 5. 22}$$

where N is the density of states in the conduction or valence band, N_t is the trap density for exponentially distributed traps, μ is the electron or hole mobility and m is the ratio of T_c:T, where T is the temperature and T_c is the characteristic temperature for the exponential distribution of traps.

The I-V characteristics for Gaussianly distributed deep traps[9] is the same as for exponentially distributed traps (Equation 5. 22) except that N_t is the trap density for gaussianly distributed traps and m is a function of the square root of the standard deviation of the gaussian distribution and temperature. For shallow traps the I-V characteristics are the same as for single discrete trap levels (Equation 5. 19) except that θ has been replaced by θ_g and d by d_{eff}, where θ_g depends on several factors including the density of states in the conduction or valance band, the density of gaussianly distributed traps, the standard deviation of the gaussian distribution and temperature. d_{eff} is due to the inhomogeneous spatial distribution of free and trapped carriers.

For a complete study on the topics discussed in Sections 5.2.2, 5.2.3 and 5.2.4 the reader is referred to references[7,10].

5.2.5 Experimental Methods and Procedures

Unipolar sandwich structure devices were prepared and tested under an applied Direct Current (D.C.) Voltage in order to determine some of the electrical properties of PmPV, such as D.C. conductivity, charge carrier mobility and the free carrier density. These values were measured for hole only and electron only currents. Comparisons were made between PmPV devices prepared by the conventional and the treated techniques.

All films were prepared from a filtered (0.8μm pore diameter) 25g/l toluene solution, at 400rpm for 60 seconds. The bottom contacts were deposited by Sputtering 75 nm

thick layers of the required contact metal on to 50 mm square glass substrates. PmPV films were then spun on top of the bottom contact using the required spinning technique. Finally the top contacts were deposited, by thermal evaporation or sputtering, depending on the metal being deposited, to a thickness of 75 nm, using the same metal as for the bottom contact. Additionally a number of films were prepared at 1000rpm. The device structure is shown in Figure 5. 3.

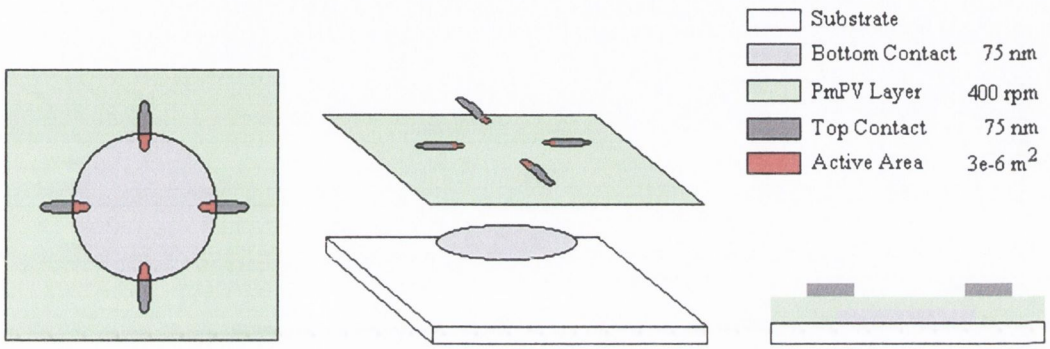

Figure 5. 3: Device architecture for devices used to measure the electrical properties of PmPV. The sandwich structure shows four top electrodes for clarity. In total fifteen top electrodes were deposited onto the PmPV layer.

Electron and hole only currents were obtained using Aluminium (Al) and Platinum (Pt) contacts respectively, the work functions of which are 4.28 eV and 5.65 eV respectively. Hole and electron injection in PPV type polymers is best achieved using Gold (Au) (5.10 eV) and Calcium (Ca) (2.87 eV) electrodes respectively. Gold electrodes were used but difficulties arose during the deposition of the top contacts that didn't arise with Pt. Ca electrodes oxidise rapidly in air and thus require glovebox technology, which wasn't available.

The devices were tested in a purpose built test rig. They were contacted using conductive silver paint and pressure probes. The probes were connected to a Keithley 2400 source measure unit via coaxial cable. The open circuitry in the test rig was shielded from any electromagnetic radiation that may have interfered with the measurements by placing the rig in a purpose made metal cover. An argon feed meant that the devices were tested in an inert atmosphere, as a vacuum attachment wasn't possible. The source meter was interfaced to a computer using National

Instruments protocols in visual basic. The Current-Voltage (I-V) characteristics were displayed on screen in real time.

Devices were initially forward biased from 0-10V to check for any shorting that sometimes occurred. Subsequent runs were taken in 0.5 V steps up to 20 V and in 1 V steps there after. The initial small voltage increment was so as to enable a large number of data points to be obtained in the ohmic region of the I-V data. Devices were also reverse biased to check for symmetrical I-V behaviour, which is to be expected from unipolar devices. Film thicknesses were measured using optical profilometry.

5.2.5.1 Sputtering

Developed in 1852[11] the process wasn't explained correctly until 1909[12]. Sputtering involves the deposition of almost any material from a target, on to almost any substrate material. A plasma is formed over the target by ionising an inert gas, usually argon, using a radio-frequency power supply. The target is negatively charged causing the argon ions to accelerate towards it. Due to the agron ion bombardment, target atoms are ejected from the target surface and move towards the substrate, where they are deposited to form thin films. Magnetron cathodes allow for lower operating voltages and higher current densities giving rise to higher deposition efficiencies. The process is performed under high vacuum. Sputtering is widely used in the deposition of bottom contacts directly onto a substrate. Due to the high ejection velocities of metal particles from the target, the sputtering of top contacts directly onto polymer thin films requires careful control of all sputtering parameters.

5.2.6 Results and Analysis

The aim of this experimental section is to fully characterise the Current-Voltage (I-V) characteristics of PmPV in both the Conventional and Treated thin film formats and to study the effects, if any, of the changes in film morphology on the I-V characteristics. As previously discussed it had been noted that films of type T

prepared at 400 rpm showed a thickness increase of ~30% over films of type C, whereas at 600 rpm there was a negligible thickness increase. Films were prepared at 400 and 1000 rpm to enable further comparisons to be made between the I-V characteristics. The films prepared are detailed in Table 5. 1. The fabrication of hole only devices at 1000 rpm from platinum electrodes was unsuccessful, as was the fabrication of hole only devices using gold electrodes. This was because it was only possible to sputter these materials. This resulted in only one set of hole only devices being fabricated at 400 rpm using platinum.

Table 5. 1: Specifics of PmPV films used for current-voltage analysis. The spin speed is measured in rpm.

Specifics of PmPV Films Used For D.C. Current-Voltage Analysis

Film Type	Spin Speed	Bottom Contact	Deposition Method	Top Contact	Deposition Method	Film Thickness		% Increase
						Mean	Std. Dev.	
C	400	Al	Sputtering	Al	Evaporation	410	5 nm	
T	400	Al	Sputtering	Al	Evaporation	553	19 nm	+35
C	1000	Al	Sputtering	Al	Evaporation	247	7 nm	
T	1000	Al	Sputtering	Al	Evaporation	247	6 nm	0
C	400	Pt	Sputtering	Pt	Sputtering	355	23 nm	
T	400	Pt	Sputtering	Pt	Sputtering	406	5 nm	+14

There are a number of observations that can be made from the results presented in Table 5. 1. The first is that thickness increases have been measured in the treated films prepared at 400 rpm compared to their conventional counterparts, while in the 1000 rpm films there is no increase observed. The differences in film thickness for the conventional films prepared at 400 rpm for electron only and hole only devices can be explained by the fact that different solutions were used in preparing these films. All films were prepared in pairs, (i.e. conventional and corresponding treated), but the solution used to prepare one pair of films wasn't always the same as that used

to prepare another pair of films. Differences in concentration could have arisen due to a number of factors, during the preparation of the solutions. The percentage increase in film thickness for the hole only treated film at 400 rpm is less that that for the corresponding electron only device and the percentage increase measured previously. The reasons for this are discussed in Chapter 3, section 3.3.5. A minimum of four points were used to calculate the mean and standard deviation for the film thicknesses presented.

I-V curves, for the six films detailed in Table 5. 1 were recorded. The electron only and hole only data will be presented separately for clarity as different trends were observed. The fabrication of hole only devices at 1000 rpm were unsuccessful due to the difficulties of sputtering top platinum contacts onto thin polymer films. The nature of sputtering lead to the implantation of platinum atoms deep into the polymer film, resulting in direct current paths between the bottom and top platinum electrodes, capable of conducting currents of two amperes, the maximum that could be sourced. (The heat generated at these currents resulted in the cracking of the glass substrate, and the destruction of the device electrode).

5.2.6.1 Electron Only Current-Voltage Characteristics

The analysis of the electron only data was hampered at very low voltages, as the noise was comparable with the current being produced by the applied voltage. This tended to occur in the ohmic region of device operation, were operating currents of 10^{-11} Amperes or less were the norm. At currents above 10^{-11}A the signal to noise ratio increased significantly allowing meaningful data to be recorded. The voltage at which this transition normally occurred usually coincided with the transition form ohmic to space charge limited (SCL) current characteristics. This made the fitting of a straight line to the ohmic region difficult, resulting in slopes significantly less than one. The conductance is required to calculate the conductivity, as given by

$$\sigma = \frac{Gd}{A} \qquad \textit{Equation 5. 23}$$

where G is conductance (G=1/R) and A is the device active area. In order to obtain approximate values for the conductivity, a straight line of slope one was force fitted to the data. This resulted in two values for the voltage dependence in the ohmic region resulting in two estimates of the conductivity. It also gives rise to two values for V_Ω. Both values of V_Ω were used to calculate values for the free carrier density, p_o, and the effective mobility, $\theta\mu_{Ohmic}$, which was calculated from Equation 5. 8. The data in the SCL current region, which is proportional to the voltage squared, could be easily fitted to. This enabled the effective mobility, $\theta\mu_{SCL}$, to be calculated using Equation 5. 19, which is dependant on film thickness, device area, the permittivity of the polymer and the intercept of the linear fit to the SCL region of the data and the current axis. Due to the good fit to the data the intercept could be accurately calculated. The remaining values could be accurately measured, except for the permittivity of the polymer, which was calculated using a value of 3 for the relative permittivity, which is generally accepted as the recognised value for PPV type polymers[13,14]. The value of $\theta\mu_{SCL}$ was the only value that could be accurately determined from the I-V characteristics of the electron only devices, the other values were all interdependent on each other and the values obtained from the forced fit, although the values for $\theta\mu_{Ohmic}$ calculated using the forced fit agreed very favourably with $\theta\mu_{SCL}$. Values for the effective dielectric relaxation time, $\theta\tau_d$, were calculated using $\theta\mu_{Ohmic}$, $\theta\mu_{SCL}$, and the two values for V_Ω. As the voltage continued to sweep through the SCL region it reached a point where the current increased dramatically and became proportional to V^β, where $\beta > \sim 8$ in all four devices. This high slope region is indicative of the transition from trap limited SCL current to trap free SCL current. There is a small transition region both before and after the high slope region, but unfortunately all the devices broke down before reaching trap free SCL currents.

A representative I-V curve and its Log-Log plot are shown in Figure 5. 4 - Figure 5. 11, for the four electron only devices detailed in Table 5. 1. Table 5. 2 and Table 5. 3 detail the average values of all the parameters obtained from the I-V data for these devices.

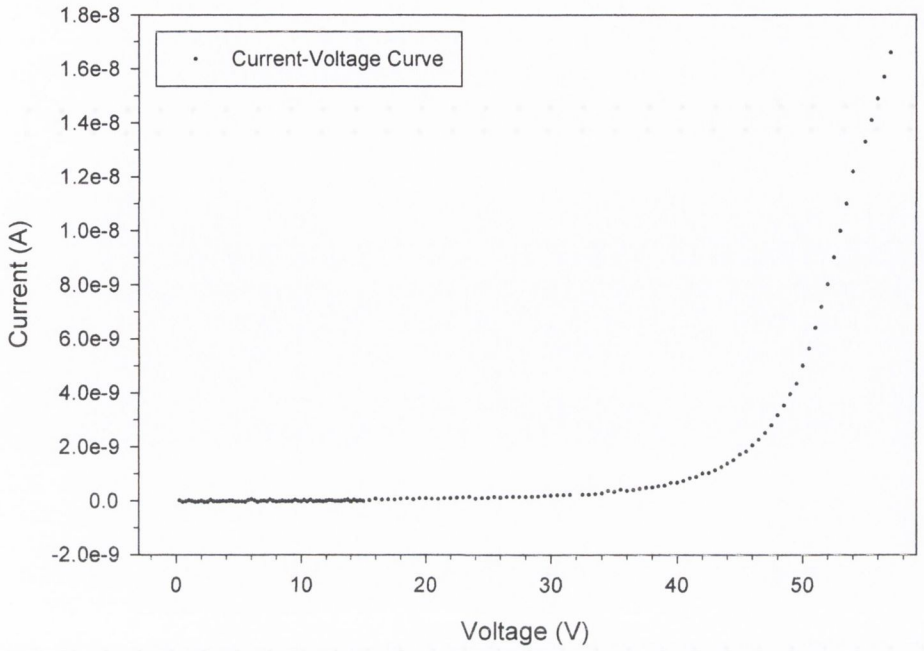

Figure 5. 4: Current-Voltage plot for a Conventional film of PmPV spun at 400 rpm, for a trap limited electron only current.

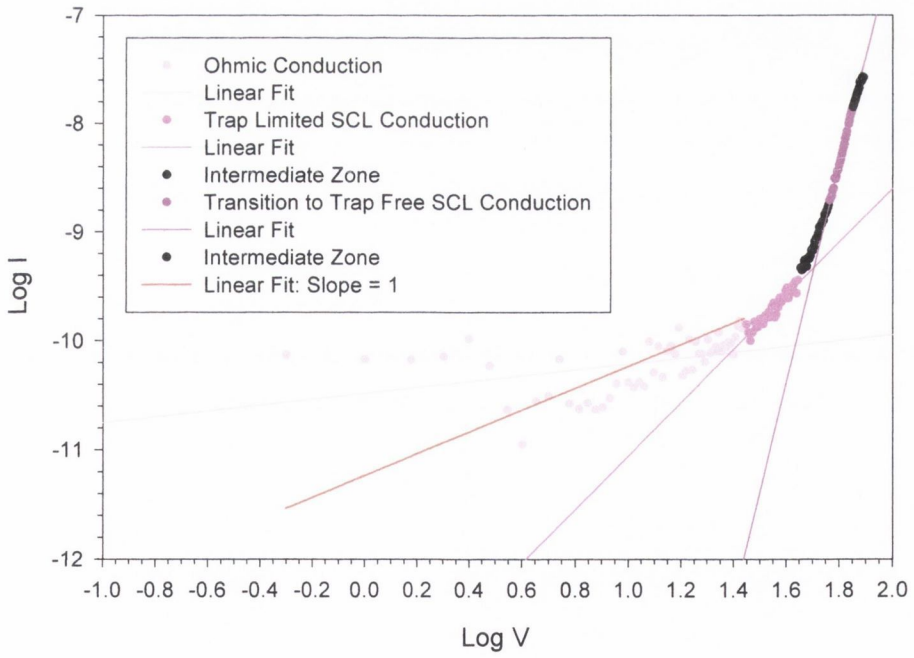

Figure 5. 5: Log V vs Log I plot for a Conventional film of PmPV spun at 400 rpm, for a trap limited electron only current. The various conduction regions are clearly indicated. The red line is a forced fit to the ohmic region.

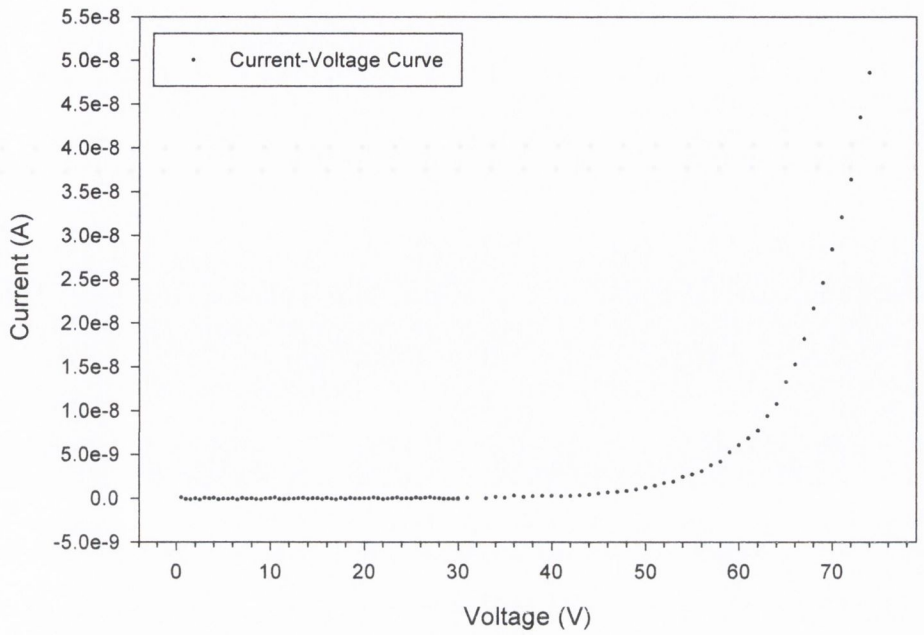

Figure 5. 6: Current-Voltage plot for a Treated film of PmPV spun at 400 rpm, for a trap limited electron only current.

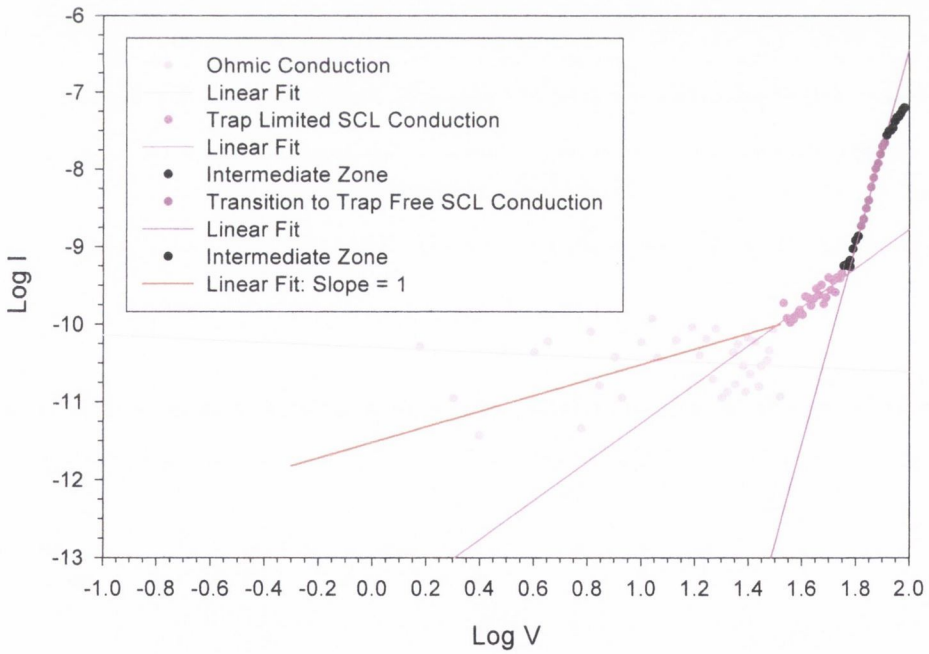

Figure 5. 7: Log V vs Log I plot for a Treated film of PmPV spun at 400 rpm, for a trap limited electron only current. The various conduction regions are clearly indicated. The red line is a forced fit to the ohmic region.

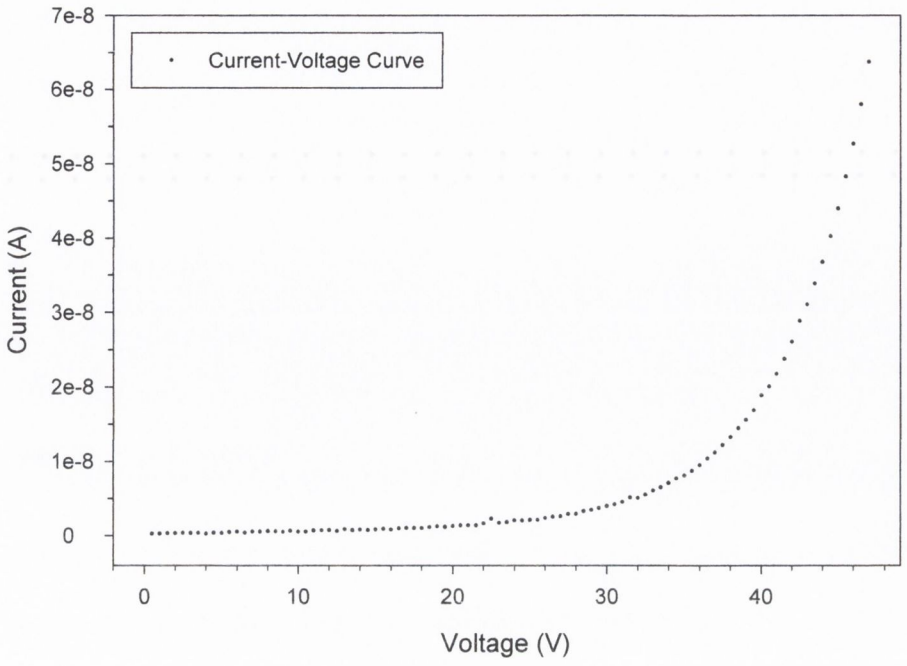

Figure 5. 8: Current-Voltage plot for a Conventional film of PmPV spun at 1000 rpm, for a trap limited electron only current.

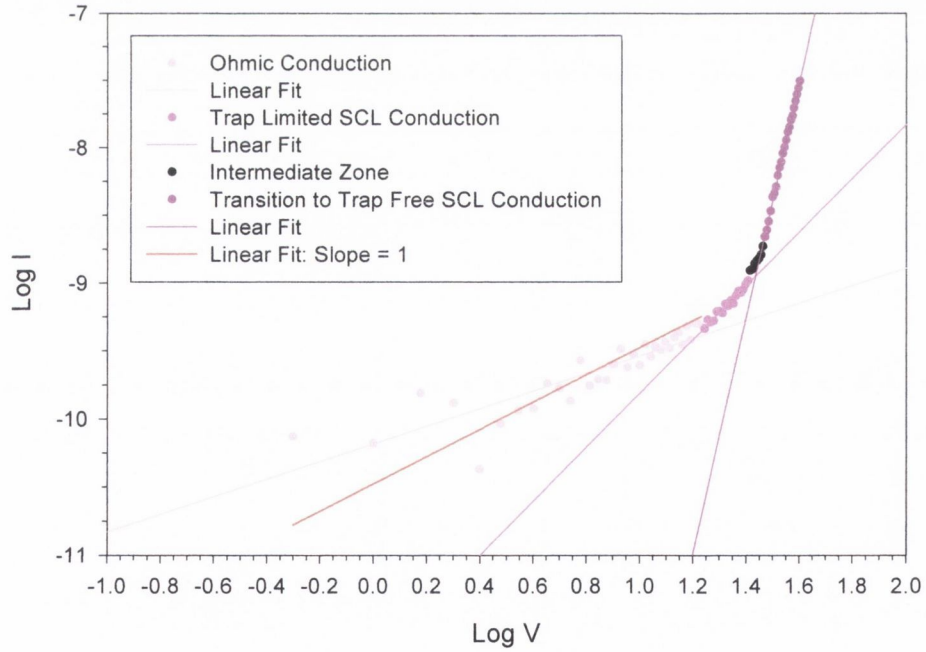

Figure 5. 9: Log V vs Log I plot for a Conventional film of PmPV spun at 1000 rpm, for a trap limited electron only current. The various conduction regions are clearly indicated. The red line is a forced fit to the ohmic region.

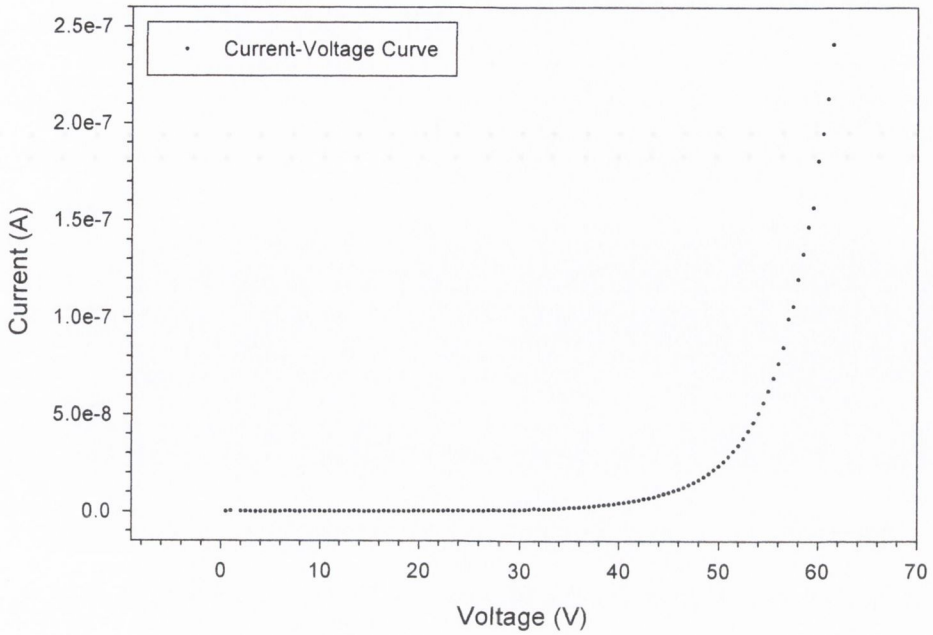

Figure 5. 10: Current-Voltage plot for a Treated film of PmPV spun at 1000 rpm, for a trap limited electron only current.

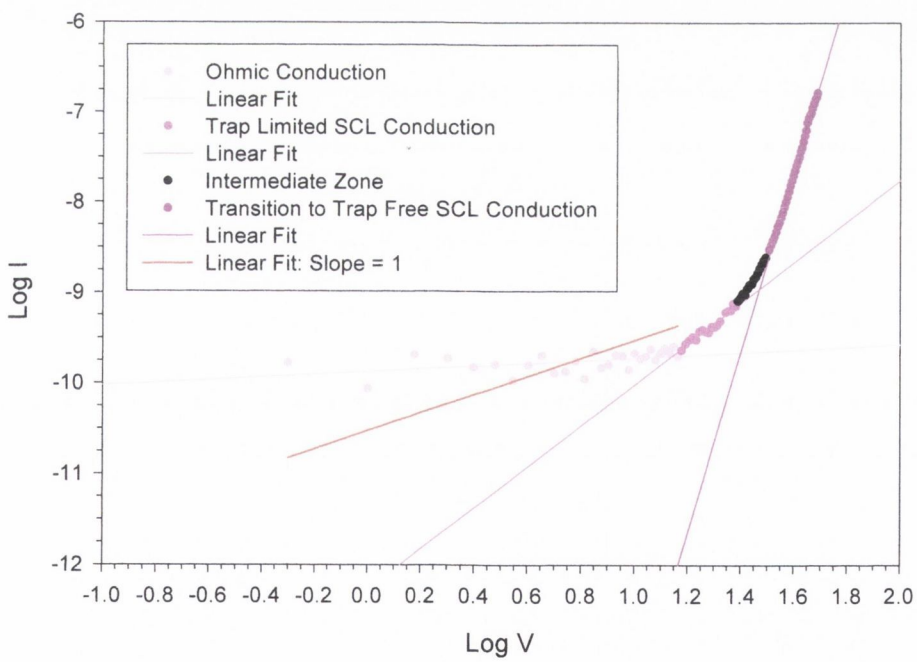

Figure 5. 11: Log V vs Log I plot for a Treated film of PmPV spun at 1000 rpm, for a trap limited electron only current. The various conduction regions are clearly indicated. The red line is a forced fit to the ohmic region.

*Table 5. 2: Current-Voltage parameters for trap limited electron only currents in PmPV films prepared at 400 rpm. An * indicates results derived from force fitting a line of slope one to the ohmic region of the Log V vs Log I graph. NE is the number of electrodes tested and NP is the total number of points used to obtain the average values presented.*

Current-Voltage Parameters for Electron Only Currents in PmPV at 400 rpm						
	TRAP LIMITED CHARACTERISTICS					
	CONVENTIONAL		NE:13/15 NP:29	TREATED		NE:7/15 NP:19:
	Mean	Std. Dev.		Mean	Std. Dev.	
Slope 1	0.29	0.31		0.17	0.47	
Slope 1*	1.00	0.00		1.00	0.00	
Slope 2	2.06	0.14		2.19	0.15	
Slope 3	9.39	2.29		11.45	2.46	
V_{Ω}	17.56	6.55		20.26	9.28	V
V_{Ω}*	27.41	14.05		26.53	10.93	V
V_{TFL}	47.64	6.34		49.84	11.57	V
E_{TFL}	1.16e+08	0.16e+08		0.90e+08	0.21e+08	Vm^{-1}
σ	32.30e-13	22.50e-13		79.00e-13	63.60e-13	Sm^{-1}
σ*	6.07e-13	3.56e-13		6.79e-13	2.72e-13	Sm^{-1}
p_o	1.95e+22	0.73e+22		1.24e+22	0.57e+22	m^{-3}
p_o*	3.05e+22	1.56e+22		1.62e+22	0.67e+22	m^{-3}
$\theta\mu_{Ohmic}$	10.70e-16	6.54e-16		47.00e-16	35.71e-16	$m^2V^{-1}s^{-1}$
$\theta\mu_{Ohmic}$*	1.26e-16	0.37e-16		3.09e-16	1.97e-16	$m^2V^{-1}s^{-1}$
$\theta\mu_{SCL}$	1.17e-16	0.66e-16		1.92e-16	1.50e-16	$m^2V^{-1}s^{-1}$
$\theta\tau_{d\text{-}Ohmic}$	18.20	21.29		13.82	25.97	s
$\theta\tau_{d\text{-}Ohmic}$*	63.01	40.06		44.47	15.21	s
$\theta\tau_{d\text{-}SCL}$	112.57	85.00		123.03	96.33	s
$\theta\tau_{d\text{-}SCL}$*	82.36	71.77		92.87	65.48	s

The average values presented in Table 5. 2 were obtained from a total of 29 and 19 I-Vs for the conventional and treated films respectively. 13 of the 15 electrodes on the conventional film and 7 of the 15 electrodes on the treated film were usable.

*Table 5. 3: Current-Voltage parameters for trap limited electron only currents in PmPV films prepared at 1000 rpm. An * indicates results derived from force fitting a line of slope one to the ohmic region of the Log V vs Log I graph. NE is the number of electrodes tested and NP is the total number of points used to obtain the average values presented.*

Current-Voltage Parameters for Electron Only Currents in PmPV at 1000 rpm						
	TRAP LIMITED CHARACTERISTICS					
	CONVENTIONAL		NE:10/15 NP:22	TREATED		NE:11/15 NP:16
	Mean	Std. Dev.		Mean	Std. Dev.	
Slope 1	0.29	0.18		0.30	0.18	
Slope 1*	1.00	0.00		1.00	0.00	
Slope 2	2.12	0.19		2.15	0.18	
Slope 3	8.83	2.09		9.75	1.90	
V_{Ω}	15.36	2.59		14.13	2.44	V
V_{Ω}*	26.06	3.83		23.25	6.47	V
V_{TFL}	30.21	5.12		31.76	6.71	V
E_{TFL}	1.22e+08	0.21e+08		1.29e+08	0.27e+08	Vm^{-1}
σ	14.70e-12	5.88e-12		9.62e-12	6.16e-12	Sm^{-1}
σ*	3.70e-12	1.27e-12		2.36e-12	1.28e-12	Sm^{-1}
p_o	4.48e+22	0.75e+22		4.29e+22	0.74e+22	m^{-3}
p_o*	7.59e+22	1.12e+22		7.07e+22	1.97e+22	m^{-3}
$\theta\mu_{Ohmic}$	21.30e-16	9.84e-16		13.90e-16	7.78e-16	$m^2V^{-1}s^{-1}$
$\theta\mu_{Ohmic}$*	3.10e-16	1.06e-16		2.20e-16	1.53e-16	$m^2V^{-1}s^{-1}$
$\theta\mu_{SCL}$	2.57e-16	1.88e-16		1.55e-16	1.13e-16	$m^2V^{-1}s^{-1}$
$\theta\tau_{d\text{-}Ohmic}$	2.20	1.14		4.22	4.26	s
$\theta\tau_{d\text{-}Ohmic}$*	8.34	4.37		13.89	6.75	s
$\theta\tau_{d\text{-}SCL}$	24.00	19.57		39.51	28.54	s
$\theta\tau_{d\text{-}SCL}$*	14.69	12.70		26.66	22.17	s

The average values presented in Table 5. 3 were obtained from a total of 22 and 16 I-Vs for the conventional and treated films respectively. 10 of the 11 electrodes that were tested on the conventional film were usable and 7 of the 15 electrodes on the treated film were usable.

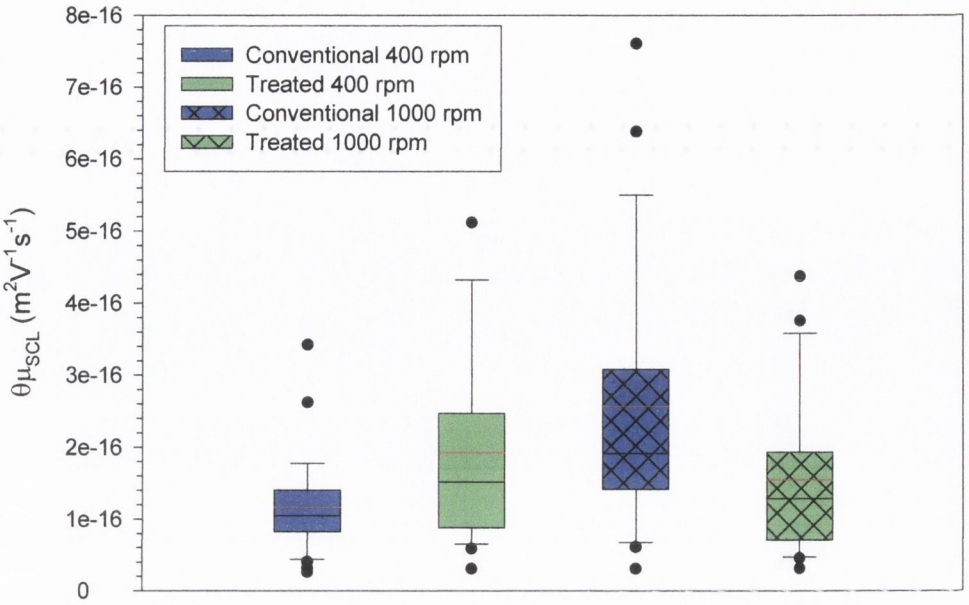

Figure 5. 12: Box plot of $\theta\mu_{SCL}$ for electron only currents in conventional and treated films prepared at 400 and 1000 rpm. The plot shows the median (black), mean (red) 10th, 25th, 75th, and 90th percentiles as horizontal boxes with error bars. All outlying points are also plotted.

It is immediately clear from Table 5. 2 and Table 5. 3 that the effective mobility, $\theta\mu_{SCL}$, calculated from the SCL current region of the Log V vs Log I graphs, is equal within the error scales presented for all four films This is shown graphically in Figure 5. 12 and indicates that the treated films do not show any reduction in electron trapping sites, through either the removal of air from the films or through increased interchain separation. In Table 5. 2 and Table 5. 3 an * (asterisk) indicates results derived from force fitting a line of slope one to the ohmic region of the Log V vs Log I graph. It is evident that the values for $\theta\mu_{Ohmic}$* are the same as $\theta\mu_{SCL}$ in all four films, indicating that the force fit to the ohmic region is a very good approximation. The value for conductivity arrived at using the forced fit, σ*, are equal for the films prepared at the same spin speed, but smaller in the 400 rpm films compared to the 1000 rpm films. Since the effective mobilities are equal in all films, this implies from Equation 5. 8 that the free carrier density, p_o, is smaller in the 400 rpm films. The calculated values of p_o and p_o* in the 400 rpm films are smaller. The only difference between the conventional films prepared at 400 and

1000 rpm, is the thickness of the resulting film. The value of p_o shouldn't differ with film thickness, as the value is presented as a quantity per unit volume. This implies that the values for p_o and those for p_o*, across all four films, are equal and that the apparent discrepancies help define the limitations of this type of measurement. This implies that that the values of σ* are equal, within the limitations of this kind of measurement, for all four films. Additionally the value of V_Ω and V_Ω* should be larger in the 400 rpm films and if calculated in terms of the electric field, E, (E = V/d) they should be equal in all four films, provided the mobility is equal. The values calculated for V_Ω and V_Ω* in terms of the electric field show a similar spread to the voltage dependant values. Considering the uncertainties in calculating V_Ω and V_Ω* due to the fits to the ohmic region, comparisons are difficult. This however is not the case for V_{TFL}, which could be measured accurately. It is noted that V_{TFL} is similar for the films prepared at the same spin speed, but that it occurs at a higher applied voltage in the 400 rpm films compared to the 1000 rpm films. There should however be no difference between the four film types due to the mobilities being equal. Taking the film thickness differences into account and expressing V_{TFL} in terms of the electric field, E_{TFL}, the values are equal as expected. The standard deviation of the slope of the Log V vs Log I graph in the SCL region is very small, indicative of the good fit to the data that was obtained and the consistency of the I-V characteristics of the devices. The slope of the transition region from trap limited SCL conduction to trap free SCL conduction is similar in all four films, although it does increase slightly in the 400 rpm treated film, whilst still remaining equal within the standard deviation. The presence of these high slope regions could indicate the presence of an exponential distribution of traps or deep gaussianly distributed traps. The clearly defined slope two regions observed in these PmPV films shows the presence of shallow, but discrete traps, or shallow gaussianly distributed traps. The high slope transition region could be due to an exponential trap distribution or deep gaussianly distributed traps. In this case the observed shallow but discrete traps and/or the shallow gaussianly distributed traps are superimposed on an exponential or deep gaussianly distributed traps distribution.

Due to the high workfunction of aluminium (4.2eV) relative to the electron affinity of PmPV, there is the possibility that the conduction of electron only currents in PmPV may be electrode limited as detailed in Section 5.2.3. The electron affinity of most PPV derivatives has been measured to lie between 2.4-3.0eV[15] and the value for PmPV is expected to be similar. The experimental data was plotted to both the Field Enhanced Thermionic Emission and the Field Assisted Quantum Mechanical Tunnelling equations. The Field Enhanced Thermionic plot shows a remarkable similarity to the SCL conduction plots. Any dependence of ln J on $E^{1/2}$ that may be present is limited to very high fields. The Field Assisted Quantum Mechanical Tunnelling plot does show a definite dependence of ln (J/E^2) on 1/E at very high fields. The fields at which this dependence occurs are significantly greater than the trap filled limit voltage in the SCL conduction plots. Additionally, the high field fit shown predicts a barrier height of $\sim 10^{11}$ eV. These two plots indicate that electrode limited conduction cannot provide an explanation for the I-V behaviour observed in these devices. This supports the findings of the fits to space charge limited conduction already presented.

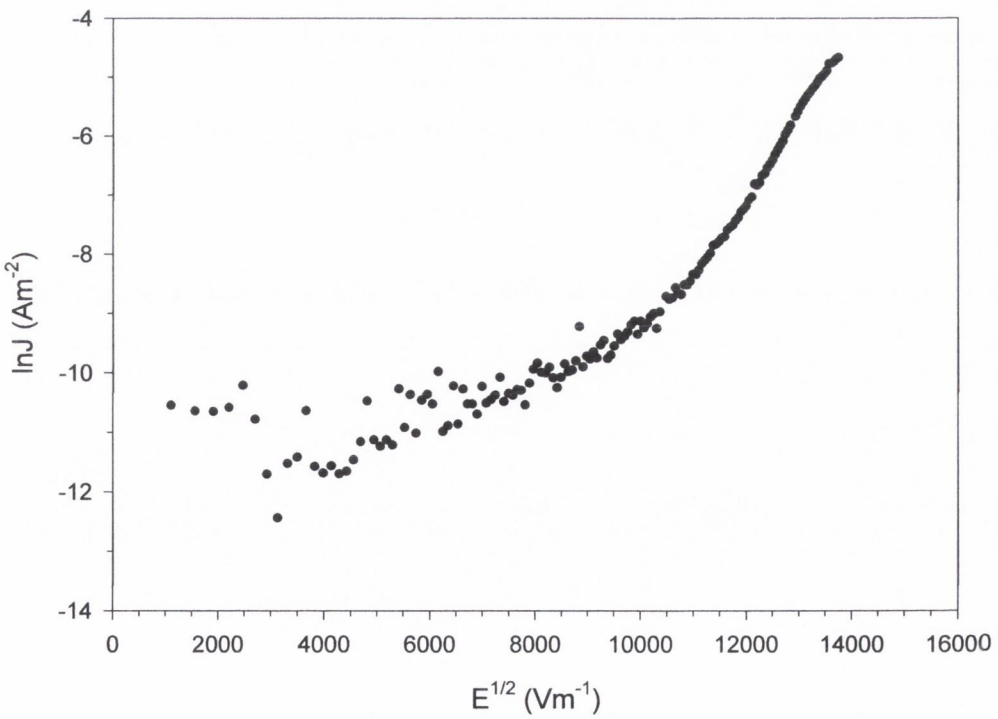

Figure 5. 13: Field Enhanced Thermionic Emission plot for electron only currents in a 400 rpm conventional film.

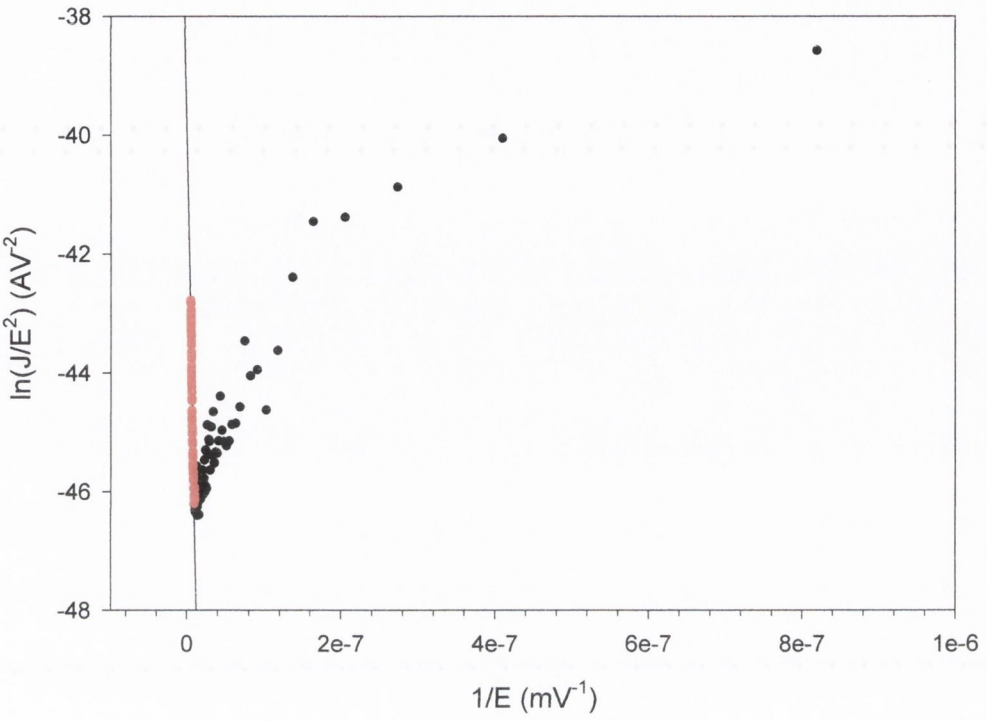

Figure 5. 14: Field Assisted Quantum Mechanical Tunnelling plot for electron only currents in a 400 rpm conventional film. Tunnelling can be seen at very high fields (red region). The linear fit to the high field region is also shown.

5.2.6.2 Hole Only Current-Voltage Characteristics

Due to the higher currents associated with holes the problems associated with the low electron only currents didn't arise. Clearly defined ohmic regions with a slope of one could be easily fitted to. The points in the linear region of the I-V plots were fitted to in the Log V vs Log I plots enabling very accurate values for the conductance to be calculated. The values for the conductance calculated from both plots were equal within error, although the values obtained from the Log-Log plots were used in all calculations.

A representative I-V curve and its Log-Log plot are shown in Figure 5. 15 - Figure 5. 18, for the two hole only devices detailed in Table 5. 1. Table 5. 4 details the average values of all the parameters obtained from the I-V data for these devices.

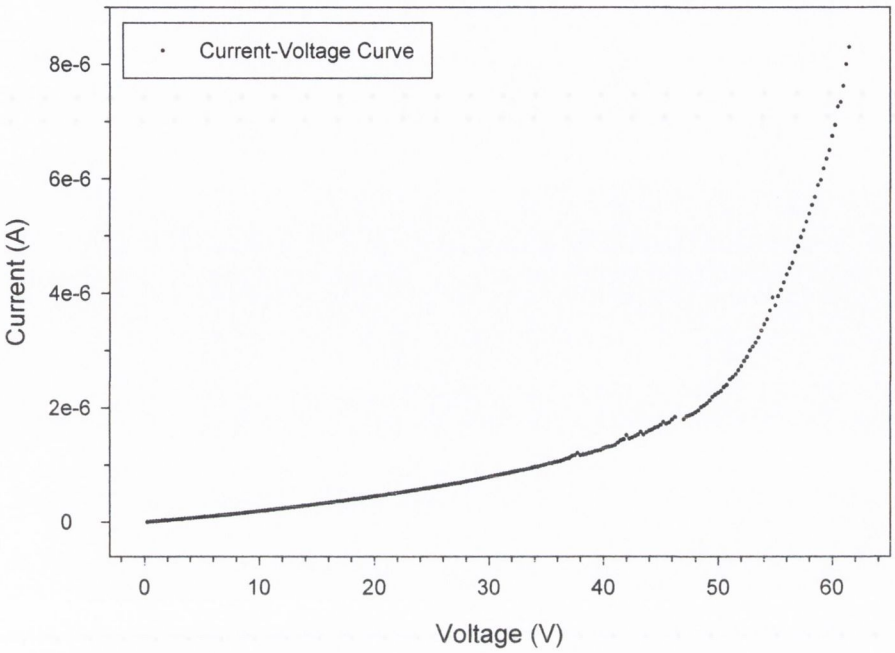

Figure 5. 15: Current-Voltage plot for a Conventional film of PmPV spun at 400 rpm, for a trap limited hole only current.

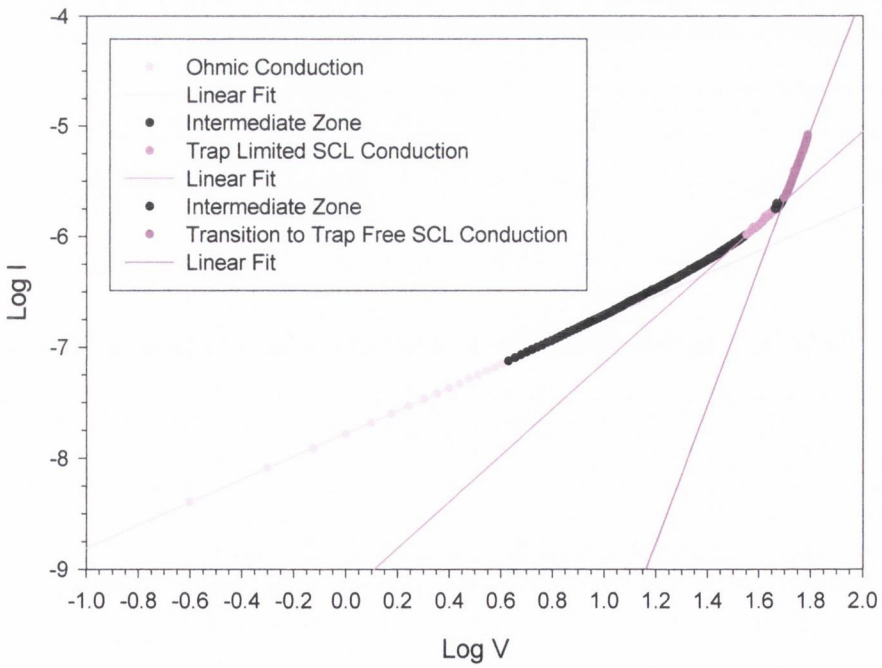

Figure 5. 16: Log V vs Log I plot for a Conventional film of PmPV spun at 400 rpm, for a trap limited hole only current. The various conduction regions are clearly indicated.

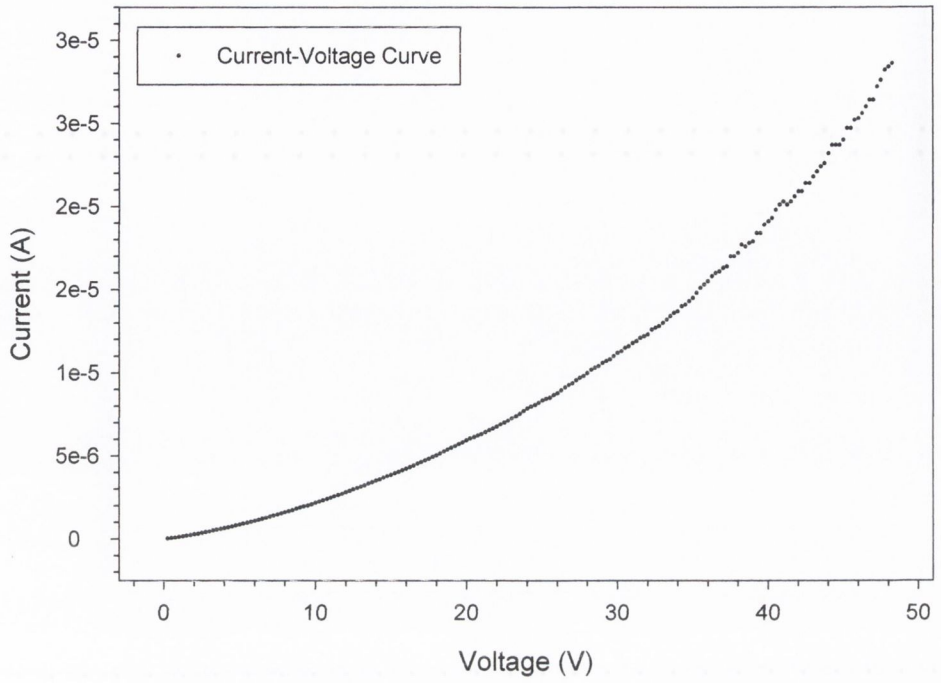

Figure 5. 17: Current-Voltage plot for a Treated film of PmPV spun at 400 rpm, for a trap free hole only current.

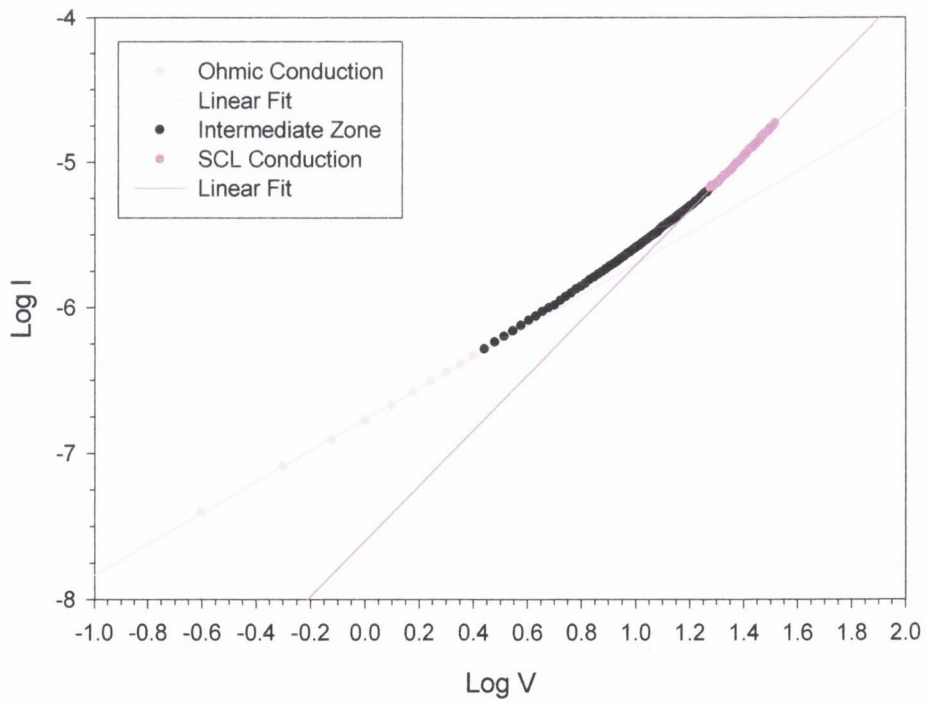

Figure 5. 18: Log V vs Log I plot for a Treated film of PmPV spun at 400 rpm, for a trap free hole only current. The various conduction regions are clearly indicated.

Some immediate differences are noticeable between the conventional and treated films and between the hole only and electron only devices. Between the conventional and treated film it is noted that the treated film displays the characteristics of trap free SCL conduction, whereas the conventional film displays the characteristics of trap limited SCL conduction. This indicates that hole trapping sites are either removed through the removal of air from the PmPV films and/or through the increased interchain separation observed in the treated film. Fabrication of films at 1000 rpm is need to establish which mechanism is responsible for the removal of hole trapping sites in treated films. Unfortunately this isn't possible for reasons outlined previously. It is also noted that the slope of the transition region from trap limited to trap free currents is half that observed in electron only devices.

The absence of the high slope transition region from trap limited to trap free conduction in the treated film combined with the higher mobilities measured in the treated film compared to the conventional film indicate that the conduction observed in the treated film is trap free, while that observed in the conventional film is trap limited. The higher conductivity values measured in the treated film, using Equation 5. 23, clearly show that there are differences between the types of conduction in the two film types. The values for the mobility calculated using fits to the ohmic and SCL regions of the Log V vs Log I are almost identical, indicating that the fits to the data are good. The presence of trap free SCL conduction in the treated film allows the value of θ in the conventional film to be calculated. The value shown in Table 5. 4 is close to unity, which is very big compared to some organic materials, indicating that the density of hole traps is very low in PmPV. The standard deviation of the slope of the Log V vs Log I graph in both the Ohmic and the SCL regions for both films is very small, indicative of the good fits to the data that were obtained and the consistency of the I-V characteristics of the devices. Due to the differences in hole mobility between the two film types the dielectric relaxation time is approximately an order of magnitude lower in the treated film. It is also noted that the transition voltage V_Ω is slightly higher in the treated film. This is to be expected due to the increased film thickness, since p_o is equal in both film types. When calculated in terms of the

electric field they are still similar. In both cases the errors are too big to allow any discernible difference to be observed.

Table 5. 4: Current-Voltage parameters for trap limited and trap free hole only currents in PmPV films prepared at 400 rpm. NE is the number of electrodes tested and NP is the total number of points used to obtain the average values presented.

Current-Voltage Parameters for Hole Only Currents in PmPV at 400 rpm						
	TRAP LIMITED			TRAP FREE		
	CONVENTIONAL		NE:9/15 NP:16	TREATED		NE:7/12 NP:10
	Mean	Std. Dev.		Mean	Std. Dev.	
Slope 1	1.09	0.10		1.08	0.05	
Slope 2	2.01	0.13		2.01	0.08	
Slope 3	4.34	1.15		N/A	N/A	
V_{Ω}	12.12	6.49		14.62	5.94	V
V_{TFL}	33.05	9.57		N/A	N/A	V
σ	6.57e-9	7.46e-9		3.55e-08	2.83e-08	Sm^{-1}
p_o	1.79e+22	0.96e+22		1.66e+22	0.67e+22	m^{-3}
$\theta\mu_{Ohmic}$	2.09e-12	1.70e-12	μ_{Ohmic}	1.26e-11	0.74e-11	$m^2V^{-1}s^{-1}$
$\theta\mu_{SCL}$	2.26e-12	1.76e-12	μ_{SCL}	1.47e-11	0.97e-11	$m^2V^{-1}s^{-1}$
$\theta\tau_{d\text{-}Ohmic}$	0.014	0.016	$\tau_{d\text{-}Ohmic}$	0.0013	0.0010	s
$\theta\tau_{d\text{-}SCL}$	0.012	0.014	$\tau_{d\text{-}SCL}$	0.0011	0.0007	s
θ_{Ohmic}	0.17			N/A		
θ_{SCL}	0.15			N/A		

The average values presented in Table 5. 4 were obtained from a total of 16 and 10 I-Vs for the conventional and treated films respectively. 9 of the 15 electrodes on the conventional film were usable and 7 of the 12 electrodes on the treated film that were tested, were usable.

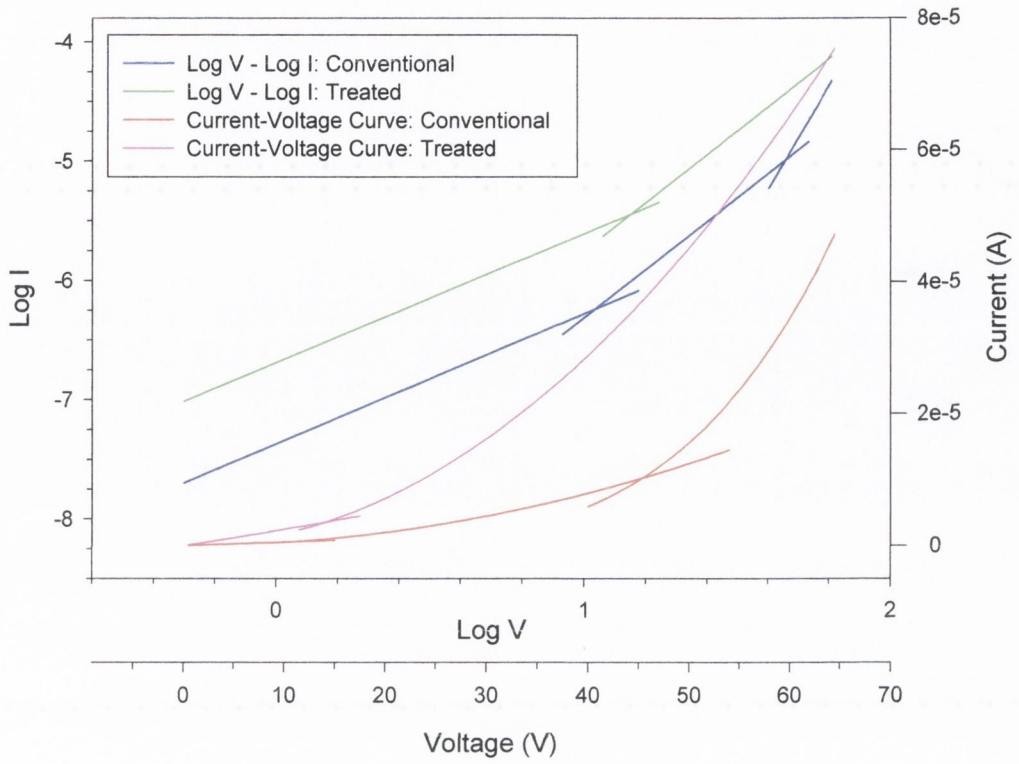

Figure 5. 19: Current-Voltage Curves and their Log-Log plots for Conventional and Treated films. The curves were generated using the values in Table 5. 4.

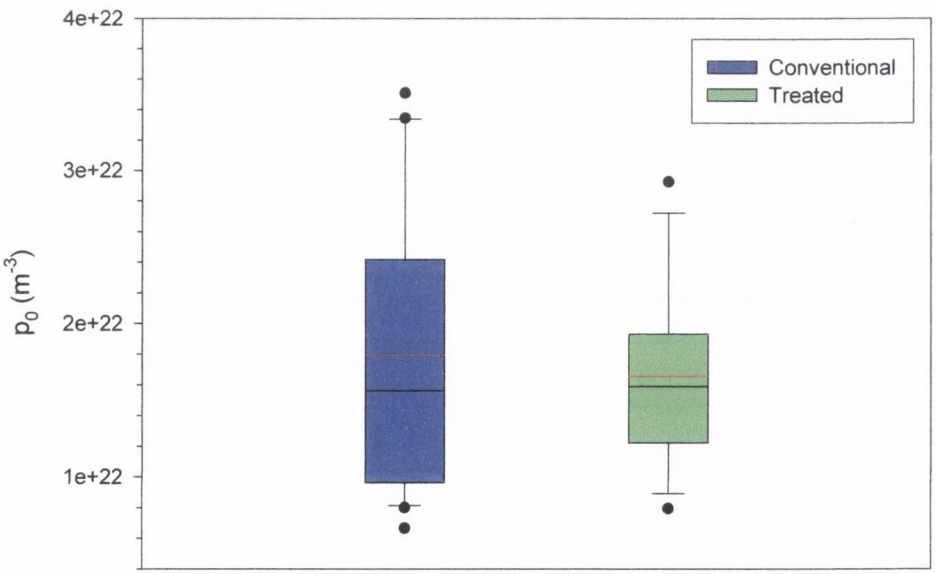

Figure 5. 20: Box plot of the free carrier density for hole only currents in conventional (blue) and treated (green) films prepared at 400 rpm. The plot shows the median (black), mean (red) 10th, 25th, 75th, and 90th percentiles as horizontal boxes with error bars. All outlying points are also plotted.

The slopes and intercepts of the I-V characteristics calculated for the conventional and treated film were used to generate I-V curves. The differences can be clearly seen in Figure 5. 19. The currents in the treated film are larger for a given voltage. The influence of traps on the magnitude of the current flowing in the conventional film is very evident.

5.2.7 Discussion

The I-V curves generated in Figure 5. 19, from the values shown in Table 5. 4, show clear differences between trap limited and trap free hole currents in PmPV films. The increased current density in the treated film results in lower applied voltages to achieve a given current density. This has the potential to reduce the drive voltage for light emission in Light Emitting Diodes (LEDs). Unfortunately similar results weren't seen for electron only currents. An LED made from a treated PmPV film would show an increase in current density and possibly light emission compared to an LED made from a conventional PmPV film, but it wouldn't show the maximum performance possible for a single layer device that would be achieved in the absence of electron trapping sites. LEDs are discussed in more detail in Section 5.4.

It can be clearly seen that the magnitude of the standard deviation is large for the parameters presented in tables Table 5. 2, Table 5. 3, Table 5. 4, indicating that this type of analysis does have its limitations. This is clearly shown in Figure 5. 20, where a clear overlap is evident between both data sets over a large range of values for p_0. Before any clear differences can be distinguished, differences of one order of magnitude must exist between values. This is the case for the mobility in the hole only devices.

The clearly defined slope two SCL regions in both the electron only and hole only devices imply the presence of either shallow single or multiple discrete trapping levels or shallow gaussianly distributed traps. The presence of an exponential trap distribution or a deep gaussianly distributed trap distribution is inferred by the high slope transition regions, where the current is proportional to V^{m+1} where $m > 2$. (m also depends on the type of trap distribution). When these traps are filled the current

then becomes SCL with slope two. The high slope regions in the electron only data for the 400 rpm films show that at high applied voltages the slope is beginning to level out, possibly to the trap free value of two, but unfortunately the devices break down before the characteristics become clear. In summary these results show the clear presence of shallow single or multiple discrete trapping levels or shallow gaussianly distributed trapping levels. These levels may be superimposed on an exponential or deep gaussianly distributed trap distribution extending from the bottom of the conduction band. This is inferred by the high slope transition region, which is indicative of this type of trap distribution and the transition from trap limited SCL conduction to trap free SCL conduction. Exponentially distributed traps do exist in PPV's. The exponential distribution of traps in pure PPV LED's has been shown and fully analysed in reference[16].

The mobility of holes in PPV and it derivatives has previously been measured[17] between 10^{-7}-10^{-11} $m^2V^{-1}s^{-1}$ at room temperature, with values as low as 10^{-13} being measured by some groups[18,19]. Blom et al[20] has measured the hole trap density of pure PPV to be zero. The apparent removal of hole trapping sites in the treated film at 400 rpm is a very favourable result. The values measured in this work compare very favourably with other PPV derivatives[21].

The number of electrodes used on each film type is shown in the tables. Each device had fifteen electrodes, but sometimes due to a piece of dust on the film, a number of the electrodes could be unusable, thus reducing the number of available electrodes. Additionally some electrodes would contain electrical shorts that gave rise to large currents or resulted in the electrode being destroyed.

In the next section impedance spectroscopy is used to further study the electrical properties of the two film types for electron only and hole only currents. Direct comparisons can be made between some of the parameters measured using the two techniques, while impedance spectroscopy can be used to measure some new parameters which may give a deeper understanding of PmPV treated films.

5.3 Impedance Spectroscopy

5.3.1 Introduction

Impedance spectroscopy is a very important experimental method for characterising many of the electrical properties of materials and their interface with electrodes. The dynamics of bound or mobile charge in the bulk and interface regions of any kind of solid or liquid can be studied. The significant difference between resistance and impedance measurements is the fact that the latter incorporates the phase difference between the applied alternating voltage and the resulting current, allowing fundamental material constants, such as the dielectric constant, to be studied. The technique was initially used in electro-chemistry before the first work on ionic solids in 1969[22]. It is now widely used in organic solid-state physics for characterising the electrical properties of polymers and their interfaces in Organic Light Emitting Diodes (OLEDs)[23,24].

5.3.2 Theory

'The apparent opposition in an electrical circuit to the flow of an alternating current through it[25].' The application of an alternating voltage, v(t), with amplitude V at angular frequency ω

$$v(t) = V\sin(\omega t) \qquad \textit{Equation 5. 24}$$

results is a phase shifted current, i(t),

$$i(t) = I\sin(\omega t + \phi) \qquad \textit{Equation 5. 25}$$

where I is the amplitude of the current and ϕ is the phase shift due to the capacitive nature of the dielectric. For purely resistive behaviour, ϕ is zero[26] and the impedance is frequency independent. The impedance as a function of frequency, Z(ω), can be defined as

$$Z(\omega) = v(t)/i(t) \qquad \textit{Equation 5. 26}$$

with magnitude

$$|Z(\omega)| = V/I(\omega) \qquad \textit{Equation 5. 27}$$

Due to the phase shift associated with impedance, $Z(\omega)$ is best represented as a complex quantity

$$Z(\omega) = \mathbf{Re}\, Z + \iota\, \mathbf{Im}\, Z \qquad \textit{Equation 5. 28}$$

where $\iota = \sqrt{-1}$. Thus in rectangular coordinates ReZ = |Z|cos(ϕ) and ImZ = |Z|sin(ϕ).

The resistive and capacitive nature of dielectrics, resulting in the observed current-voltage phase lag, means that these two parameters can be used to describe the impedance of the dielectric. The real and imaginary Z components represent the resistance, R, and the capacitive reactance, X_c, respectively. C is the capacitance.

$$Z(\omega) = R(\omega) + \iota X_c = R(\omega) + \iota \frac{1}{\omega C(\omega)} \qquad \textit{Equation 5. 29}$$

5.3.2.1 Impedance Related Functions

The impedance $Z(\omega)$ can be expressed in several other forms, which can prove very useful in obtaining important material parameters. The first and possibly the most useful of these is the Admittance, $Y(\omega)$, which is defined as the inverse of the impedance.

$$Y(\omega) = Z(\omega)^{-1} = G(\omega) + \iota\, B(\omega) = G(\omega) + \iota\omega C(\omega) \qquad \textit{Equation 5. 30}$$

Where G is the conductance and B is the susceptance.

The Modulus function, $M(\omega)$, is the other form that $Z(\omega)$ is sometimes expressed in terms of.

$$M(\omega) = \iota\omega Z(\omega) \qquad \textit{Equation 5. 31}$$

Cole-Cole plots[27] of all three quantities, $Z(\omega)$, $Y(\omega)$ and $M(\omega)$, along with the real and imaginary components versus angular frequency, can prove very useful in determining device parameters, as will be outlined later.

It is usual, with modern instrumentation, to scan the applied voltage over a frequency range and measure Z as a function of ω. The frequency range scanned is usually between 0.1 Hz–1 MHz as the dielectric relaxation time, τ_d, for most polymeric materials falls within this frequency range[28,29]. The response of the system can be modelled using an equivalent circuit containing a network of resistors and capacitors in parallel. Assuming the simplest case with one R-C in parallel, τ_d is equal to the product of the resistor and capacitor.

5.3.2.2 Equivalent Circuits

An equivalent circuit made up of capacitors and resistors can approximate experimental impedance data. Resistors represent conductive pathways through the material, thus representing the conductivity of the region they are modelling. The capacitors on the other hand represent space charge polarisation regions. An example of the two simplest equivalent circuits is shown in Figure 5. 21, where the shunt resistance, R_s, can be thought of as a representing a contact resistance.

Each R-C component represents a region of the polymer layer between two electrodes. A depletion region at an electrode and the semiconductor bulk are two such regions. If two or more such regions exist, they combine together in series and can be modelled by adding additional R-C component in series with the components shown in Figure 5. 21.

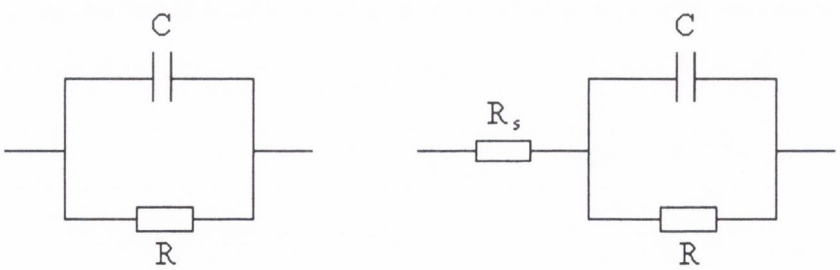

Figure 5. 21: Equivalent circuits, representing the conductive and space charge polarisation regions within a material experiencing an applied alternating voltage. A contact resistance is also shown in the right hand diagram.

The addition of an R-C component produces an additional region in the data. Each region can be fitted separately meaning that we can represent the admittance of each region by Equation 5. 30. Taking the inverse of this, Z(ω) can be written as

$$Z(\omega) = R_s + \frac{R - \imath\omega CR^2}{1 + (\omega CR)^2} \qquad \textit{Equation 5. 32}$$

where R_s has been added in series and can be omitted if no shunt resistance is visible in the recorded data. Written separately we have

$$\mathbf{Re}\, Z(\omega) = R_s + \frac{R}{1 + (\omega CR)^2} \qquad \textit{Equation 5. 33}$$

$$\mathbf{Im}\, Z(\omega) = \frac{-\omega CR^2}{1 + (\omega CR)^2}$$

Equation 5. 33 holds for an equivalent circuit of the type shown in Figure 5. 21.

5.3.2.3 Bipolar Measurements

The extraction of electron and hole mobility values from bipolar impedance spectroscopy of polymer films wasn't possible until quite recently[30]. The extraction of other parameters such as capacitance from bipolar devices has been commonplace for the last decade[31,32,33], but the recent addition of charge carrier mobilities to the list of extractable parameters from bipolar devices has increased the already high value of impedance spectroscopy to this area of physics. The differential susceptance, defined as

$$-\Delta B(\omega) = -\omega[C(\omega) - C_o] \qquad \textit{Equation 5. 34}$$

where C_o is the geometric capacitance, plotted against frequency separates out the electron and hole relaxation peaks enabling charge carrier mobilities to be calculated. This is only possibly due to electrons and holes having different dielectric relaxation times and hence different mobilities.

5.3.2.4 Dielectric Polarisation

The relative movement of positive and negative charges in a dielectric material is known as polarisation. The application of an electric field induces polarisations in a material through both the orientation of permanent dipoles that may exist within the material and through the induced polarisation of individual atoms or ions. The general relationship between the polarisation, P, and the electric field, E, is

$$P = \varepsilon_0 \chi E + \text{Higher Order Terms in E} \qquad \textit{Equation 5. 35}$$

where χ is the linear susceptibility, which is related to the polarisability of the material. The higher order terms only come into play at high electric fields.

The insertion of a dielectric material between two parallel electrodes acts to reduce the potential difference between the electrodes, leading to an increased capacitance for the same amount of charge on the electrodes. The ratio between the original capacitance without the dielectric present, C_0, and the increased capacitance with the dielectric present, C, is called the dielectric constant or the relative permittivity, ε_r of the material. The presence of a polarisable material between the two electrodes acts to reduce the electric field between the electrodes due to the induction of surface charges in the dielectric. The presence of dipoles in a dielectric acts to increase its polarisability in the presence of an electric field, if the dipoles can realign. The dipole moment, p, is equal to ql, where q is the magnitude of one of the charges and l is the separation between the charges. The greater the separation between the two charges in a dipole the greater the polarisability of the material and hence the greater the permittivity of the material. In polymeric materials delocalisation of electrons in the π molecular orbitals relative to the positively charged atoms, act as dipoles and the separation is related to their delocalisation length along the polymer backbone. Longer delocalisation lengths thus allow for a greater polarisability of the material.

5.3.3 Experimental Methods and Procedures

Unipolar sandwich structure devices were prepared as described in section 5.2.5, although both the top and the bottom contacts were deposited to a thickness of 50 nm

as opposed to 75 nm and all top contacts were deposited by sputtering as opposed to thermal evaporation. They were tested under an applied Alternating Voltage in order to determine the capacitance and resistance of PmPV in the solid state. Other properties such as the dielectric relaxation time, τ_d, were also calculated. These values were measured for hole only and electron only currents. Comparisons were made between PmPV devices prepared by the conventional and the treated techniques.

The devices were tested in the same purpose built test rig as detailed previously. The probes were connected to a Zahner Electric IM6e Impedance Spectrum Analyzer via coaxial cable. The IM6e was interfaced to a computer using software provided with the IM6e. The impedance characteristics were displayed on screen in real time.

Devices were initially forward biased from 0-10V to check for any shorting that sometimes occurred. A 5 mV alternating voltage was applied in all the measurements recorded in this thesis. The initial run was recorded at 0 V D.C. bias, while subsequent runs were recorded with either positive or negative D.C. bias incrementing in 1 V steps to ±4 V. The final run was recorded at 0 V D.C. bias and compared with the initial run for completeness. Data was recorded between 0.1 Hz and 1 MHz for all measurements. D.C. biased I-V characteristics were then recorded up to 15V so as to establish the extent of the ohmic conduction region and to enable values for the D.C. conductivity to be compared between the I-V and the impedance data, where possible. Devices were also reverse biased to check for symmetrical I-V behaviour, which is to be expected from unipolar devices. Film thicknesses were measured using optical profilometry.

It should be pointed out that the applied alternating voltage should be less than 25mV at 25^0C. This is the thermal voltage, V_T=kT/e=25mV. At alternating voltages greater than V_T the response of the system will not be linear, due to the generation of additional charge carriers, which can lead to problems in accurately determining $Z(\omega)$.

It should also be pointed out that the values obtained from the model (equivalent circuit) fits to the raw impedance data are frequency independent and that depending on the polymeric material being tested the frequency dependant values can differ from the model values over the entire frequency range being measured or just at the extremities of the frequency range being measured. This can be seen in the graphs, as the frequency dependant and model values are both plotted for comparison.

5.3.4 Results and Analysis

The aim of this experimental section is to fully characterise the alternating voltage characteristics of PmPV in both the Conventional and Treated thin film formats and to study the effects, if any, of the changes in film morphology on the alternating voltage characteristics. The films prepared are detailed in Table 5. 5.

There are a number of observations that can be made from the results presented in Table 5. 5. As previously discussed it had been noted that films of type treated prepared at 400 rpm showed a thickness increase of ~30% over films of type conventional. The values of the film thickness increase measured for these devices are comparable with earlier measurements. However there is a noticeable difference in thickness between the conventional films prepared at 400 rpm for electron only and hole only devices. The thickness for the hole only device is comparable with earlier measurements. The significant thickness increase in the conventional film, for the electron only device, compared to earlier measurements has been put down to the use of a solution that had been made up several weeks prior to being used, leading to possible solvent evaporation. The films were prepared in pairs, (i.e. conventional and corresponding treated), but different solutions were used to prepare the hole only and the electron only films. Additionally, differences in concentration could have arisen due to a number of factors, during the preparation of the solutions, such as concentration changes caused by filtering the solution. A minimum of four points were used to calculate the mean and standard deviation for the film thicknesses presented.

Table 5. 5: : Specifics of PmPV films used for impedance analysis. The spin speed is measured in rpm.

Specifics of PmPV Films Used For Impedance Analysis

Film Type	Spin Speed	Bottom Contact	Deposition Method	Top Contact	Deposition Method	Film Thickness		% Increase
						Mean	Std. Dev.	
C	400	Al	Sputtering	Al	Sputtering	497	41 nm	
T	400	Al	Sputtering	Al	Sputtering	625	32 nm	+26
C	400	Pt	Sputtering	Pt	Sputtering	306	14 nm	
T	400	Pt	Sputtering	Pt	Sputtering	391	13 nm	+28

Impedance spectroscopy was performed on the four films detailed in Table 5. 5. The electron only and hole only data will be presented separately for clarity. Before presenting specific electron and hole only data, comparisons will be made between results obtained using the frequency independent equivalent circuit model and the frequency dependant equations. The fabrication of hole only devices at 1000 rpm was not attempted for reasons discussed previously and it was decided not to prepare electron only devices at 1000 rpm as there would be no corresponding hole only devices for comparison.

5.3.4.1 Model and Frequency Dependant Data Comparisons

Before presenting the electron and hole only data it is important to show the excellent agreement between results obtained using the frequency independent equivalent circuit model (Equation 5. 32) and the frequency dependant equations presented in Equation 5. 29, Equation 5. 30 and Equation 5. 31.

A representative graph is shown in each case for hole only data.

5.3.4.1.1 Capacitance:

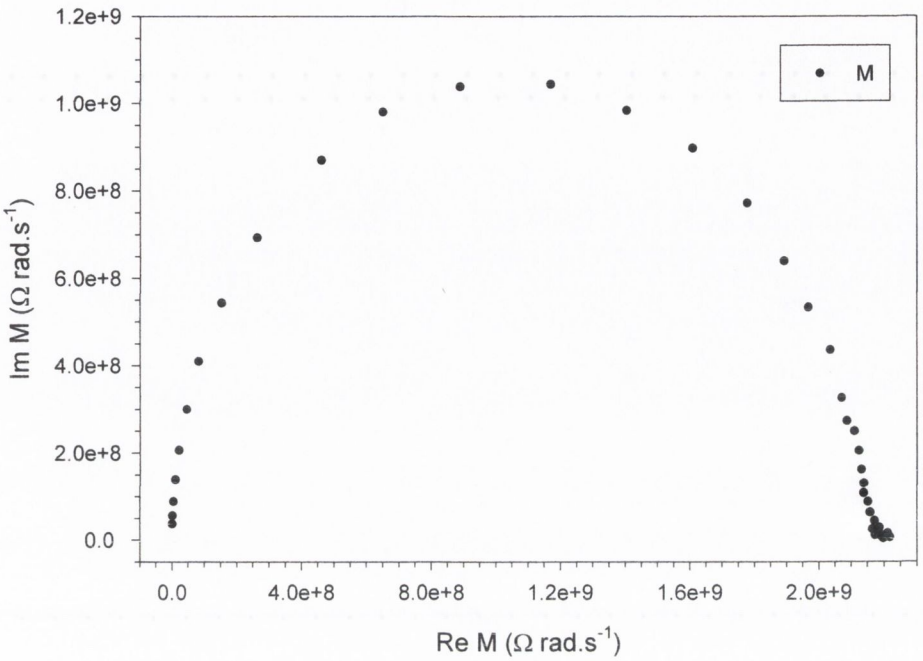

*Figure 5. 22: Cole-Cole plot of **Re**M vs **Im**M.*

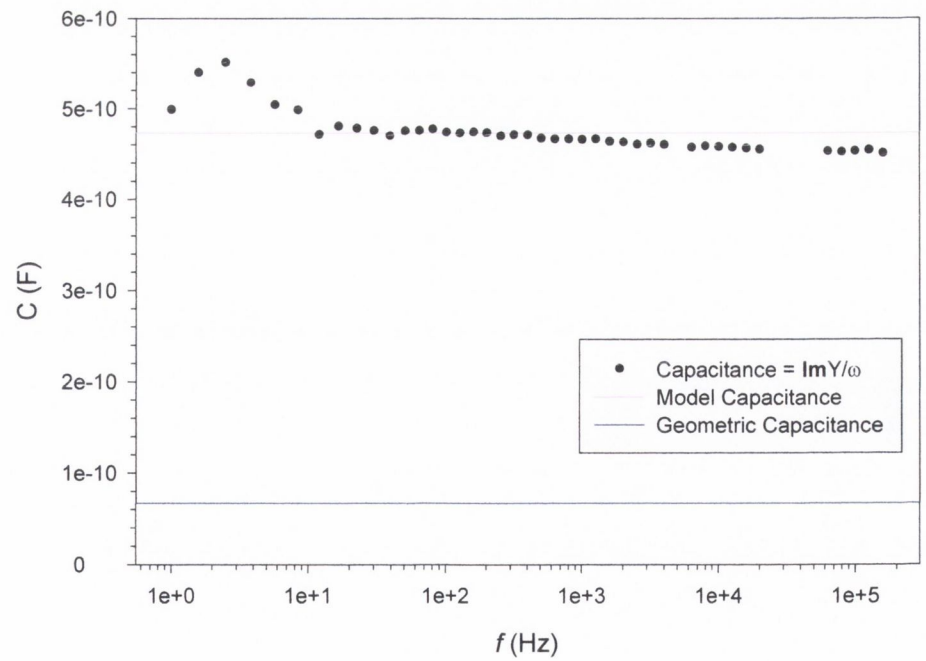

Figure 5. 23: Frequency dependant Capacitance (black circles), Model Capacitance (pink line) and Geometric Capacitance (blue line).

The value of the capacitance calculated from the inverse of the x-axis intercept on the Cole-Cole plot in Figure 5. 22, agrees with the model value calculated using Equation 5. 33 for equivalent circuits. It should be pointed out that this graph does not go through the origin. Additionally the frequency dependent values for the capacitance for PmPV are largely frequency independent except for frequencies below 10 Hz as shown in Figure 5. 23.

5.3.4.1.2 Resistance

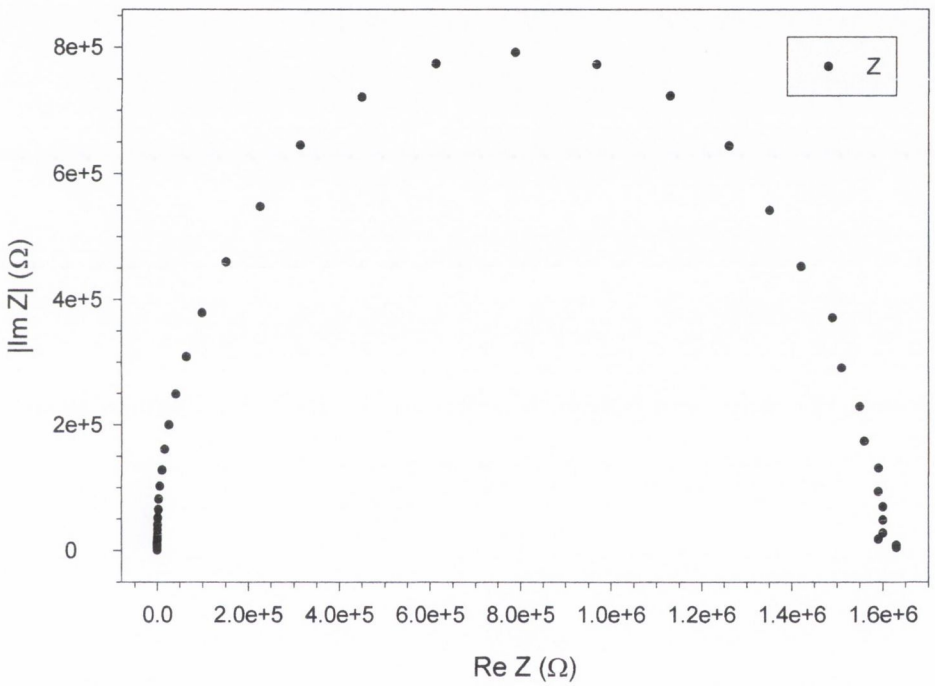

*Figure 5. 24: Cole-Cole plot of **ReZ** vs **ImZ**.*

The value of the resistance calculated from the x-axis intercept on the Cole-Cole plot in Figure 5. 24, agrees with the model value calculated using Equation 5. 33. Additionally the frequency dependant values for the resistance for PmPV are largely frequency independent except for frequencies above 2e+4 Hz as shown in Figure 5. 25.

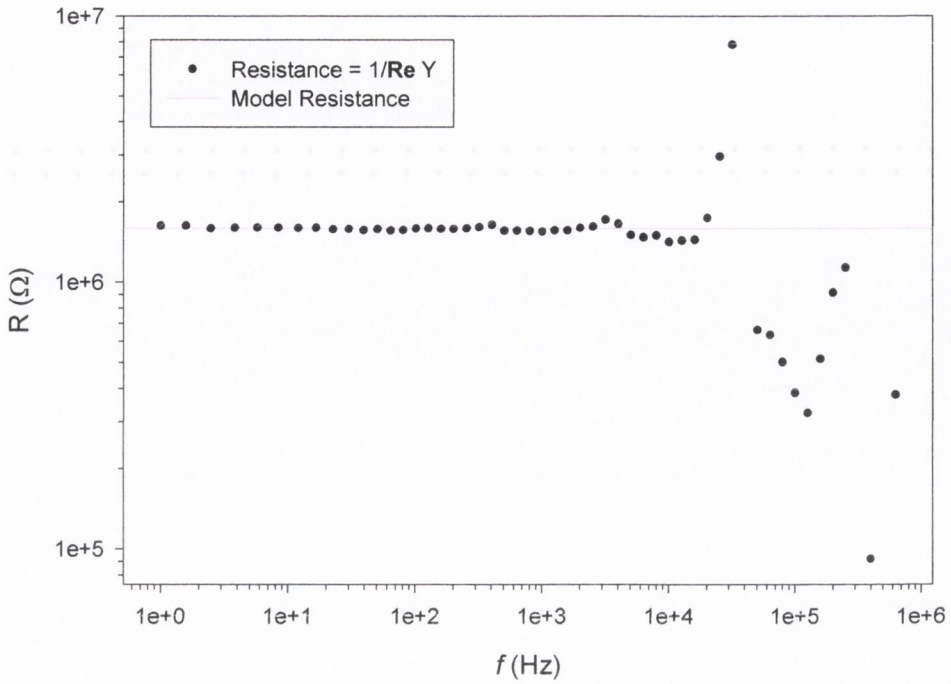

Figure 5. 25: Frequency dependant Resistance (black circles), Model Resistance (pink line).

These representative graphs show that accurate values can be obtained from the equivalent circuit model for both resistance and capacitance, for hole only data.

5.3.4.2 Hole Only Impedance Spectroscopy Characteristics

The frequency dependant real and imaginary impedance values were fitted to Equation 5. 33, using a Levenberg-Marquardt non-linear least squares fitting routine[34,35] with R and C as free parameters. **Re**Z and **Im**Z were fitted individually and simultaneously, resulting in three solutions for R and C. An example of a **Re**Z and **Im**Z vs angular frequency plot and the least squares fit is shown in Figure 5. 26 and Figure 5. 27 for a conventional and treated film respectively. In both graphs the D.C. bias is 0V and the alternating voltage is 5 mV. The insets in these two graphs show the linear fit to the high frequency side of the resonance frequency (i.e. $\omega >> RC$). The slope of the **Re**Z and **Im**Z in this region should be –2 and –1 respectively. This can be shown by taking the common log of Equation 5. 33.

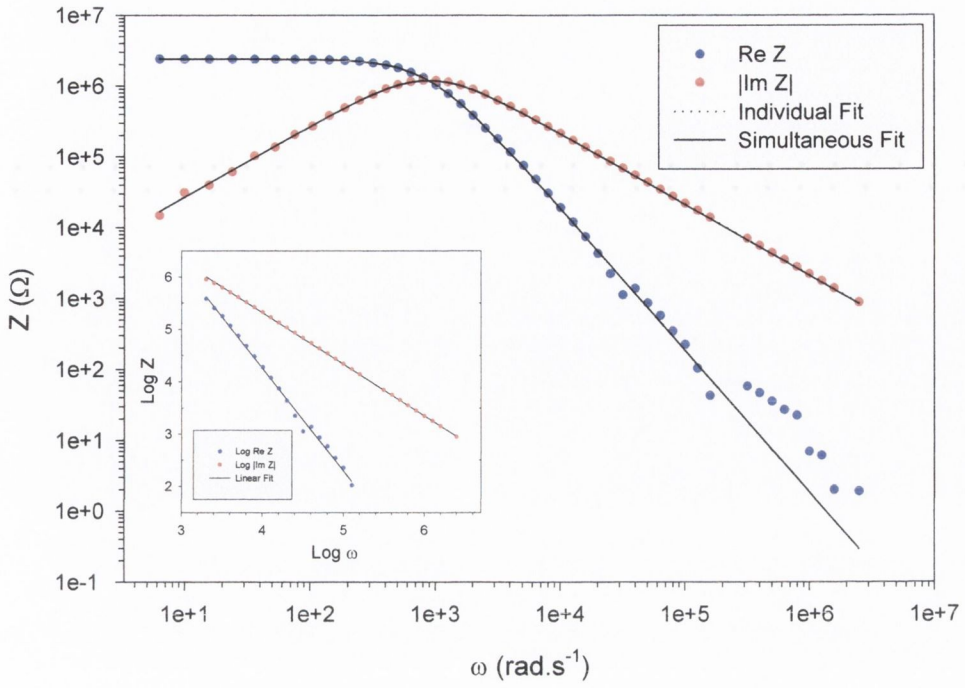

Figure 5. 26: ***Re****Z and* ***Im****Z vs angular frequency, for a conventional film at 400 rpm. The individual and simultaneous fits are also shown. The inset shows the linear fit to the high frequency side of the resonance frequency, where* $\omega >> RC$.

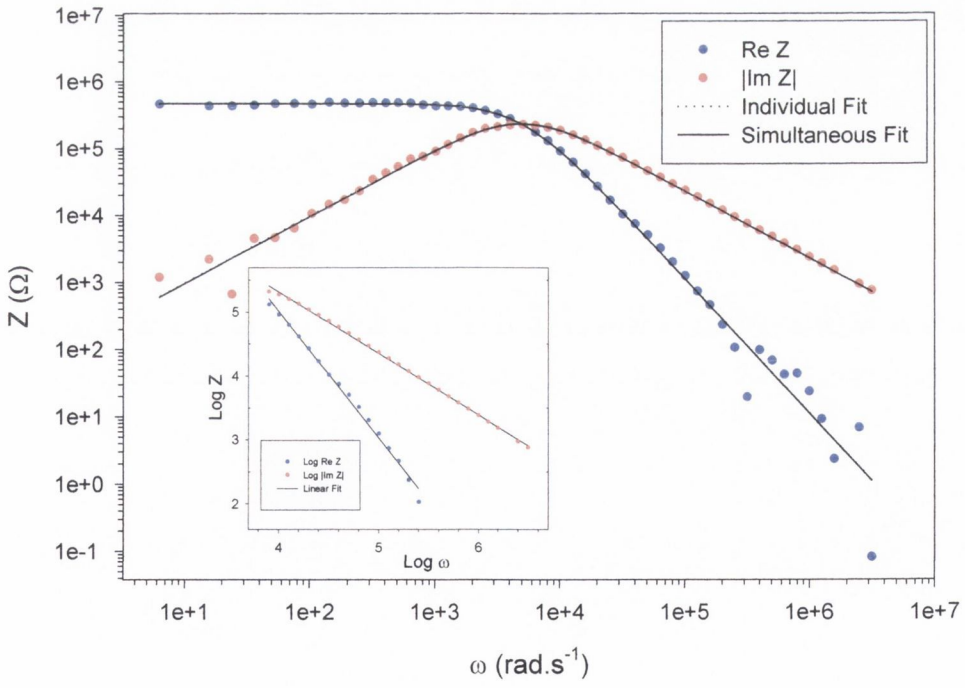

Figure 5. 27: ***Re****Z and* ***Im****Z vs angular frequency, for a treated film at 400 rpm. The individual and simultaneous fits are also shown. The inset shows the linear fit to the high frequency side of the resonance frequency where* $\omega >> RC$.

A number of observations can be made from these two representative graphs, prior to fitting to them. The first is that the resonance frequency in the treated film is higher than in the conventional film, indicating that the dielectric relaxation time is shorter in the treated film. Secondly there is no obvious shunt resistance visible at the high frequency end of **Re**Z, meaning that R_s should not be included in the fit to the real date. Thirdly the resistance of the treated film is lower than that of the conventional film. This can be gauged by the value of **Re**Z at low frequency. It is also noted that the simultaneous fits to **Re**Z and **Im**Z match the individual fits to **Re**Z and **Im**Z.

The average values of the capacitance obtained from the fits to the real and imaginary impedance for zero and positive D.C. bias voltages up to 4 volts are shown in Figure 5. 28 and in Table 5. 6. It is clear that the capacitance of both film types is constant, within experimental error, over the range of D. C. voltages applied. It is also noted that the capacitance values for both film types are equal.

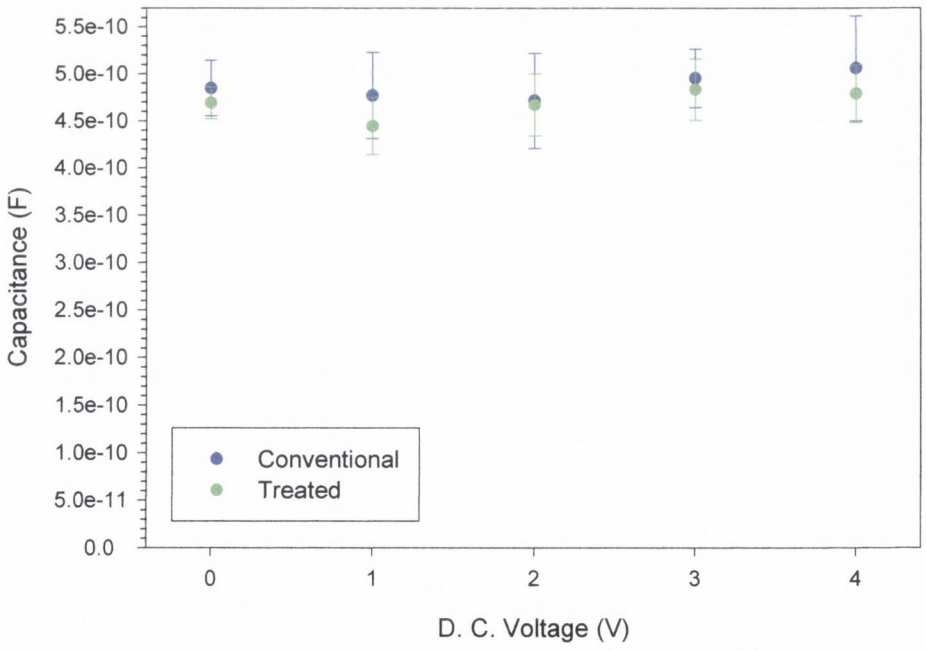

Figure 5. 28: Capacitance values from 0 – 4 V D.C. for 400 rpm conventional (blue) and treated (green) films measured using impedance spectroscopy with 5 mV alternating voltage.

With a difference in film thickness between the two film types, differences in the measured capacitance values were expected due to Equation 5. 13.

Table 5. 6: Capacitance values from 0 – 4 V D.C. for 400 rpm conventional and treated films measured using impedance spectroscopy with 5 mV alternating voltage. NE is the number of electrodes tested and NP is the total number of points used to obtain the average values presented.

CAPACITANCE (F) HOLE CURRENTS						
	CONVENTIONAL		NE:7/8	TREATED		NE:5/15
DC V	Mean	Std. Dev.	NP	Mean	Std. Dev.	NP
0	4.85e-10	0.30e-10	7	4.69e-10	0.17e-10	6
1	4.77e-10	0.46e-10	7	4.45e-10	0.30e-10	5
2	4.71e-10	0.50e-10	7	4.67e-10	0.33e-10	5
3	4.95e-10	0.31e-10	6	4.83e-10	0.33e-10	3
4	5.06e-10	0.56e-10	7	4.79e-10	0.31e-10	5
Overall	4.87e-10	0.43e-10	34	4.67e-10	0.29e-10	24

The plot of V vs $1/C^2$ yields some additional and important information. This plot is shown in Figure 5. 29 and clearly shows that the values are independent of voltage. The interface between an electrode and a dielectric results in the formation of a depletion region, due to the presence of impurities and the matching of the Fermi levels. As the D.C. applied voltage is increased the width of this depletion region will decrease, resulting in changes in the capacitance. If the depletion region is smaller than the thickness of the film then a second region should be evident in Figure 5. 26 and Figure 5. 27 as the depletion region and the dielectric bulk will have different values for resistance and capacitance. If only one region is present, then the depletion region is wider than the thickness of the dielectric. As the D.C. voltage is increased it is possible for the width of the depletion region to become narrower than that of the dielectric giving rise to a second region as described above. This would be observed in the plots of impedance against angular frequency as detailed above and as a decrease in the value of $1/C^2$ with increasing D.C. voltage in the plot of V vs $1/C^2$. This isn't

evident in either plot meaning that the depletion region created by the contacts is greater than the film thickness.

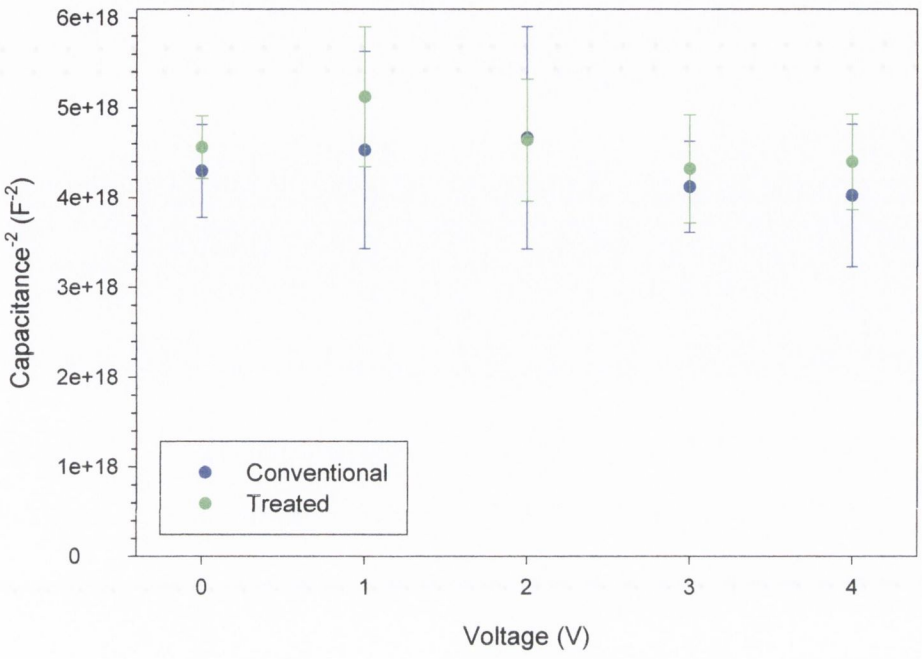

Figure 5. 29: The inverse of the square of the Capacitance, from 0 - 4V D.C. for 400 rpm conventional (blue) and treated (green) films measured using impedance spectroscopy with 5 mV alternating voltage.

The resistance values obtained from the fits to the real and imaginary impedance for zero and positive D.C. bias voltages up to 4 volts, were converted into resistivity using the device area and thickness. Resistivity is a meaningful quantity as it is measured in ohm metres. The values obtained are shown in Figure 5. 30 and Table 5. 7.

The D.C. applied bias of up to 4V is not sufficient to move from the ohmic conduction region to the SCL conduction region. This is verified by the I-V curves recorded after the impedance scans. Within the ohmic region the resistivity remains constant. The resistivity values measured for the conventional and treated films are constant within experimental error, as expected over the applied voltage range. However a difference of one order of magnitude exists between their means. This implies that the conductivity of the treated film is higher than the conventional film, indicating a higher mobility in the treated film. The conductivity was calculated from the value of the resistance obtained from the fits

to the impedance data. These values were compared to the values calculated using the I-V curves.

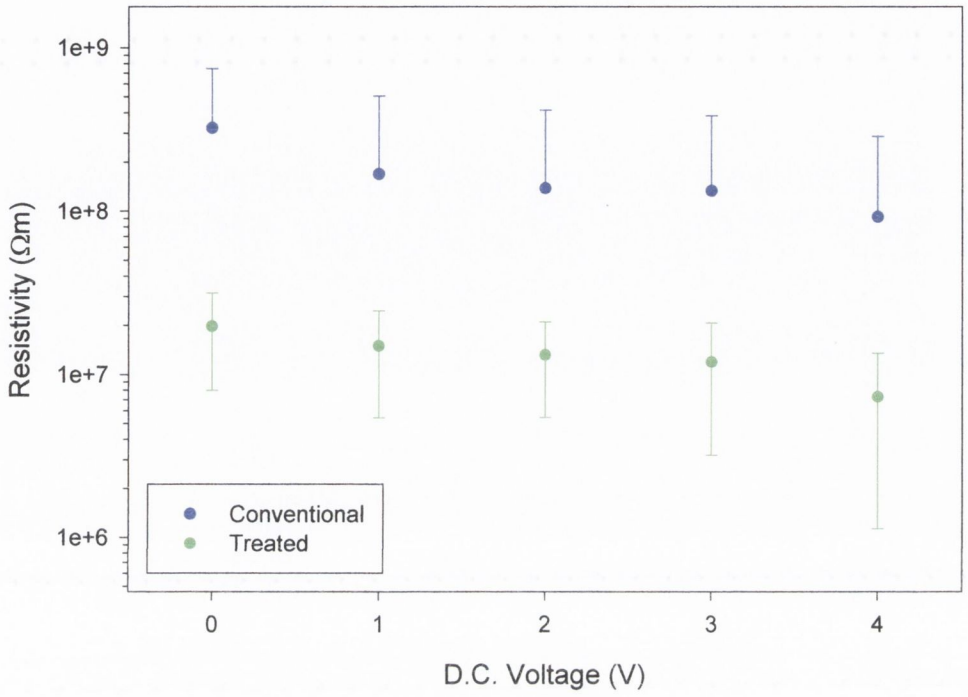

Figure 5. 30: Resistivity values from 0 - 4V D.C. for 400 rpm conventional and treated films measured using impedance spectroscopy with 5 mV alternating voltage. The resistivity axis is plotted on a logarithmic scale.

Table 5. 7: Resistivity values from 0 - 4V D.C. for 400 rpm conventional and treated films measured using impedance spectroscopy with 5 mV alternating voltage. NE is the number of electrodes tested and NP is the total number of points used to obtain the average values presented.

RESISTIVITY (Ωm) HOLE CURRENTS						
	CONVENTIONAL		NE: 7/8	TREATED		NE:5/15
DC V	Mean	Std. Dev.	NP	Mean	Std. Dev.	NP
0	3.23e+08	4.22e+08	7	1.97e+07	1.18e+07	6
1	1.69e+08	3.39e+08	7	1.50e+07	0.96e+07	5
2	1.38e+08	2.77e+08	7	1.32e+07	0.78e+07	5
3	1.33e+08	2.50e+08	6	1.19e+07	0.87e+07	3
4	0.92e+08	1.94e+08	7	0.73e+07	0.62e+07	5
Overall	1.72e+08	3.00e+08	34	1.38e+07	0.94e+07	24

The results are presented in Table 5. 8. The values obtained by the two different experimental methods are almost identical. The conductivity of the treated film is one order of magnitude larger than the conventional film in both instances. It should also be pointed out that the values presented in Table 5. 8, are presented for each electrode, and thus include values recorded at different D.C. bias voltages. This is only possible if all measurements take place within the ohmic conduction region, as stated previously.

Table 5. 8: Conductivity values for conventional and treated films prepared at 400 rpm, calculated using impedance spectroscopy. The results are presented for each electrode. The average value, $Overall_{I-V}$, calculated from I-V curves is also presented. NE is the number of electrodes tested and NP is the total number of points used to obtain the average values presented.

CONDUCTIVITY (Sm^{-1}) HOLE CURRENTS						
	CONVENTIONAL		NE:7/8	TREATED		NE:5/15
Electrode	Mean	Std. Dev.	NP	Mean	Std. Dev.	NP
1	0.13e-08	0.04e-08	5			
2	2.16e-08	1.36e-08	4			
3	3.44e-08	3.58e-08	5			
5	4.58e-08	0.37e-08	5			
6	3.59e-08	2.96e-08	5	7.50e-07	4.20e-07	5
7	6.87e-08	0.85e-08	5	4.40e-07	6.94e-07	4
8	2.87e-08	2.50e-08	5	0.70e-07	0.34e-07	5
9				0.50e-07	0.19e-07	5
11				0.57e-07	0.11e-07	5
Overall	3.41e-08	2.74e-08	34	2.66e-07	2.22e-07	24
$Overall_{I-V}$	2.89e-08	5.66e-08	15	1.81e-07	2.46e-07	25

The value of the relative permittivity allows fundamental differences between dielectric materials to be observed. Due to the very good agreement between values obtained using the frequency independent equivalent circuit model and values calculated using the frequency dependent equations, it was possible to calculate the relative permittivity, ε_r, of the two film types by dividing the measured capacitance by the geometric capacitance. The values obtained are

shown in Table 5. 9. The values have been recorded for D.C. bias voltages ranging from 0 – 4 Volts, with 5 mV alternating voltage. The results show a clear distinction between the conventional and the treated film. The higher value in the treated film indicates a higher polarisability, indicative of possibly film morphology changes.

Table 5. 9: Relative Permittivity values for conventional and treated films prepared at 400 rpm, calculated using impedance spectroscopy. The results are presented for each electrode. NE is the number of electrodes tested and NP is the total number of points used to obtain the average values presented.

RELATIVE PERMITTIVITY (ε_r) HOLE CURRENTS						
	CONVENTIONAL		NE:7/8	TREATED		NE:5/15
Electrode	Mean	Std. Dev.	NP	Mean	Std. Dev.	NP
1	6.12	0.45	5			
2	4.94	0.54	4			
3	5.27	0.13	5			
5	5.26	0.05	5			
6	5.49	0.21	5	6.35	0.11	5
7	5.23	0.09	5	6.17	0.22	4
8	5.24	0.47	5	7.10	0.46	5
9				7.09	0.72	5
11				7.31	0.17	5
Overall	5.38	0.45	34	6.83	0.59	24

Table 5. 10: Dielectric Relaxation time for conventional and treated films prepared at 400 rpm, calculated using impedance spectroscopy. NE is the number of electrodes tested and NP is the total number of points used to obtain the average values presented.

DIELECTRIC RELAXATION (τ_d) HOLE CURRENTS						
	CONVENTIONAL		NE:7/8	TREATED		NE:5/15
	Mean	Std. Dev.	NP	Mean	Std. Dev.	NP
Overall	0.011	0.020	34	0.00098	0.00081	24

The dielectric relaxation time was also calculated for both film types. The results are shown in Table 5. 10. The values have been recorded for D.C. bias voltages

ranging from 0 – 4 Volts, with 5 mV alternating voltage. These values are identical with the values recorded previously in section 5.2.6.2, using I-V curves.

5.3.4.3 Electron Only Impedance Spectroscopy Characteristics

It should be pointed out that no meaningful **Re**Z data was recorded for electron only devices. The reason for this is unknown. This limited our analysis of the electron only data to model fits to **Im**Z.

ImZ was fitted as described previously for holes. It is immediately evident from the graphs of angular frequency vs **Im**Z that the resonance frequency occurs at a significantly lower frequency to that for hole only devices, indicating a larger dielectric relaxation time. The average values of the capacitance obtained from the fits to **Im**Z for zero, positive and negative D.C bias voltages up to ±4 volts are shown in Figure 5. 31 and in Table 5. 11. As with the hole only devices it is clear that the capacitance of both film types is constant, within experimental error, over the range of D. C. voltages applied.

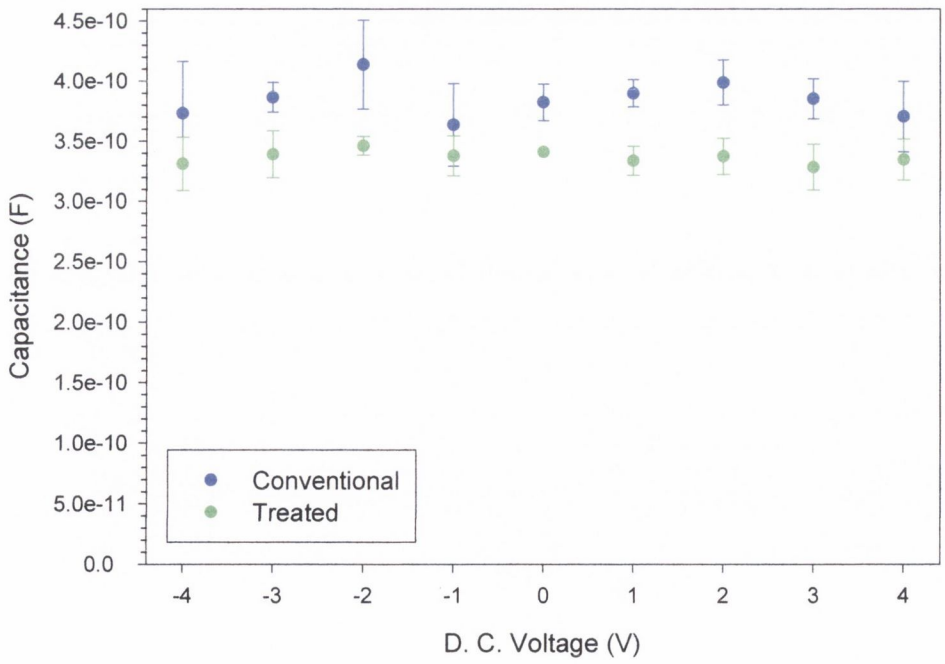

Figure 5. 31: Capacitance values from –4 V - +4V D.C. for 400 rpm conventional (blue) and treated (green) films measured using impedance spectroscopy with 5 mV alternating voltage.

It is also noted that the capacitance values for the treated film are slightly lower than that for the conventional film. With a difference in film thickness between the two film types, differences in the measured capacitance values were expected. The decrease measured however is not as big as expected from the measured thickness increase. It is also noted that the measured capacitance values are slightly lower than that measured for holes, which is to be expected due to the larger film thicknesses measured in the electron only films.

Table 5. 11: Capacitance values from –4 V - +4V D.C. for 400 rpm conventional and treated films measured using impedance spectroscopy with 5 mV alternating voltage. NE is the number of electrodes tested and NP is the total number of points used to obtain the average values presented.

CAPACITANCE (F) ELECTRON CURRENTS						
	CONVENTIONAL		NE:10/15	TREATED		NE:10/11
DC V	Mean	Std. Dev.	NP	Mean	Std. Dev.	NP
-4	3.73e-10	0.43e-10	7	3.31e-10	0.22e-10	6
-3	3.86e-10	0.12e-10	3	3.39e-10	0.19e-10	5
-2	4.13e-10	0.37e-10	4	3.46e-10	0.08e-10	6
-1	3.64e-10	0.34e-10	2	3.38e-10	0.17e-10	6
0	3.82e-10	0.15e-10	7	3.41e-10	0.00	1
1	3.90e-10	0.11e-10	5	3.34e-10	0.12e-10	4
2	3.99e-10	0.19e-10	3	3.37e-10	0.15e-10	3
3	3.85e-10	0.17e-10	3	3.29e-10	0.19e-10	7
4	3.70e-10	0.29e-10	4	3.35e-10	0.17e-10	4
Overall	3.84e-10	0.28e-10	38	3.37e-10	0.16e-10	42

The plot of V vs $1/C^2$ is shown in Figure 5. 32. It is clear from the graph that the width of the depletion region is greater than the sample thickness, even at D.C. applied voltages of ±4 volts.

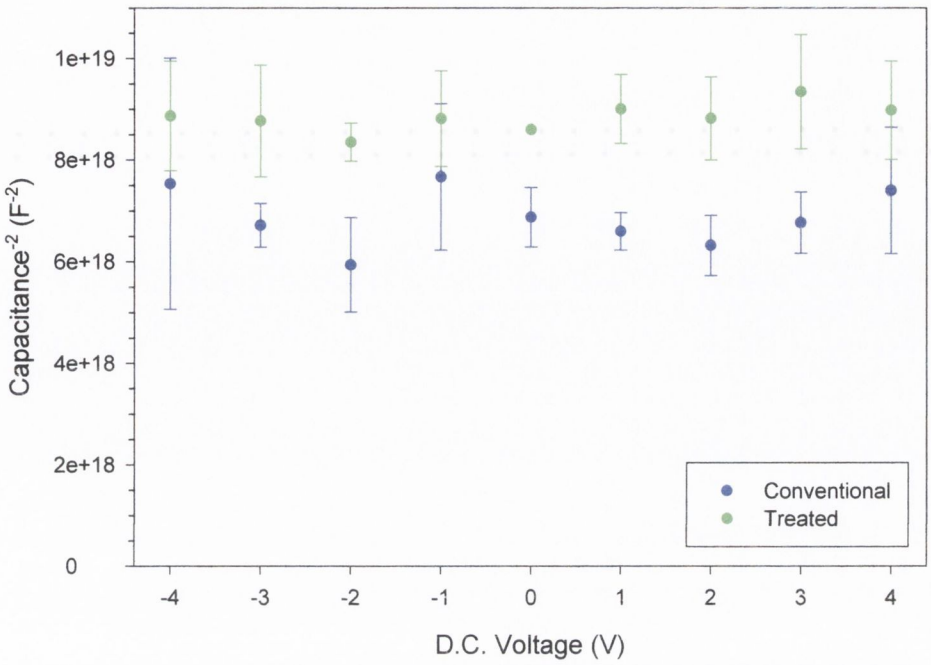

Figure 5. 32: The inverse of the square of the Capacitance, from –4 V - +4V D.C. for 400 rpm conventional (blue) and treated (green) films measured using impedance spectroscopy with 5 mV alternating voltage.

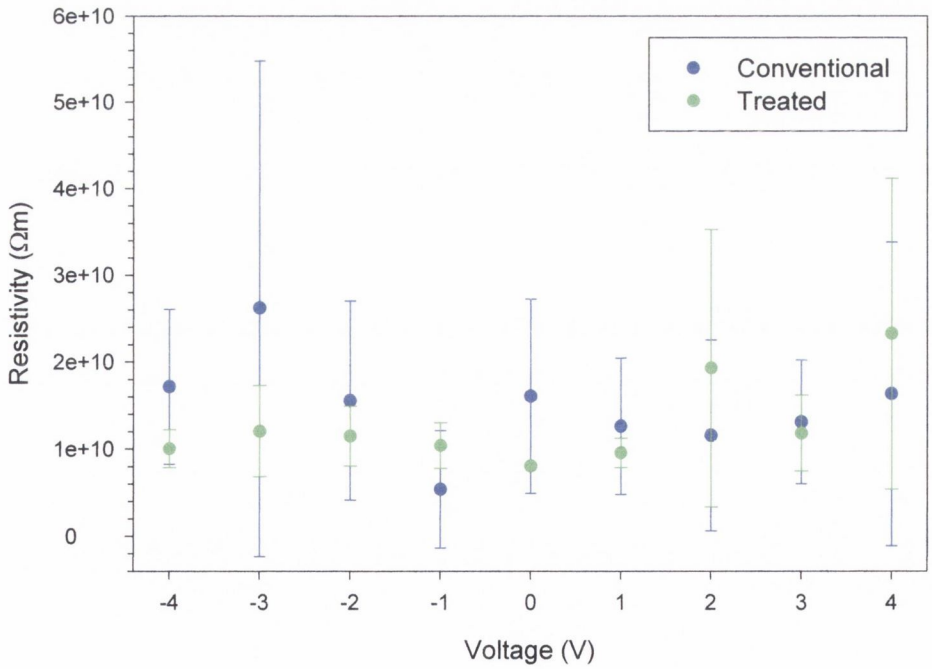

Figure 5. 33: Resistivity values from –4 V - +4V D.C. for 400 rpm conventional and treated films measured using impedance spectroscopy with 5 mV alternating voltage.

The resistance values obtained from the fits to the imaginary impedance for zero, positive and negative D.C bias voltages up to ±4 volts, were converted into resistivity using the device area and thickness. The values obtained are shown in Figure 5. 33 and Table 5. 12. It is clear from Figure 5. 33 that the resistivity of the two film types is the same. This agrees with the I-V measurements performed in Section 5.2.6.1. As with the hole only devices, the application of up to ±4 volts is not sufficient to move out of the ohmic conduction region. This implies that the resistivity should be constant over this voltage range, which can be clearly seen from the data presented.

Table 5. 12: Resistivity values from –4 V - +4V D.C. for 400 rpm conventional and treated films measured using impedance spectroscopy with 5 mV alternating voltage. NE is the number of electrodes tested and NP is the total number of points used to obtain the average values presented.

RESISTIVITY (Ωm) ELECTRON CURRENTS						
	CONVENTIONAL		NE:10/15	TREATED		NE:10/11
DC V	Mean	Std. Dev.	NP	Mean	Std. Dev.	NP
-4	1.72e+10	0.89e+10	7	1.01e+10	0.23e+10	6
-3	2.62e+10	2.86e+10	3	1.21e+10	0.52e+10	5
-2	1.56e+10	1.14e+10	4	1.15e+10	0.34e+10	6
-1	0.54e+10	0.67e+10	2	1.04e+10	0.26e+10	6
0	1.61e+10	1.12e+10	7	0.81e+10	0.00e+00	1
1	1.26e+10	0.78e+10	5	0.96e+10	0.17e+10	4
2	1.16e+10	1.10e+10	3	1.93e+10	1.60e+10	3
3	1.31e+10	0.71e+10	3	1.18e+10	0.44e+10	7
4	1.64e+10	1.75e+10	4	2.33e+10	1.79e+10	4
Overall	1.55e+10	1.21e+10	38	1.42e+10	1.06e+10	42

The conductivity was calculated from the value of the resistance obtained from the fit to the imaginary impedance data. These values were not compared to values calculated using the I-V curves recorded after the impedance scans, as similar problems to those that occurred in section 5.2.6.1 with noise at low voltages made accurate calculation of the conductivity impossible. The results are presented in Table 5. 13. The conductivity of both film types is equal. It should also be pointed

out that the values presented in Table 5. 13, are presented for each electrode, and thus include values recorded at different D.C. bias voltages. This is only possible if all measurements take place within the ohmic conduction region, as stated previously.

Table 5. 13: Conductivity values for conventional and treated films prepared at 400 rpm, calculated using impedance spectroscopy. The results are presented for each electrode. NE is the number of electrodes tested and NP is the total number of points used to obtain the average values presented.

CONDUCTIVITY (Sm^{-1}) ELECTRON CURRENTS						
	CONVENTIONAL		NE:10/15	TREATED		NE:10/11
Electrode	Mean	Std. Dev.	NP	Mean	Std. Dev.	NP
1				9.93e-11	5.07e-11	4
2	6.15e-11	2.46e-11	4	8.59e-11	4.73e-11	5
3	5.30e-11	2.80e-11	4	9.01e-11	1.96e-11	5
4	6.33e-11	2.71e-11	5	9.75e-11	4.47e-11	4
5	8.77e-11	2.55e-11	3	10.6e-11	3.90e-11	5
6				8.04e-11	5.12e-11	4
7				9.50e-11	5.60e-11	4
8	3.76e-11	2.93e-11	2	9.12e-11	3.97e-11	5
9	14.14e-11	10.03e-11	3	8.14e-11	1.26e-11	2
10	4.05e-11	1.83e-11	2	9.62e-11	3.06e-11	4
13	13.22e-11	11.52e-11	4			
14	6.47e-11	3.20e-11	5			
15	9.66e-11	4.63e-11	6			
Overall	8.03e-11	5.74e-11	38	9.19e-11	3.89e-11	42

It was possible to calculate the relative permittivity, ε_r, of the two film types by dividing the measured capacitance by the geometric capacitance. The values obtained are shown in Table 5. 14. The values have been recorded for D.C. bias voltages ranging from –4 V – +4 Volts, with 5 mV alternating voltage. The results show a clear distinction between the conventional and the treated film. The higher value in the treated film indicates a higher polarisability, indicative of possibly film morphology changes.

Table 5. 14: Relative Permittivity values for conventional and treated films prepared at 400 rpm, calculated using impedance spectroscopy. The results are presented for each electrode. NE is the number of electrodes tested and NP is the total number of points used to obtain the average values presented.

RELATIVE PERMITTIVITY (ε_r) ELECTRON CURRENTS

	CONVENTIONAL		NE:10/15	TREATED		NE:10/11
Electrode	Mean	Std. Dev.	NP	Mean	Std. Dev.	NP
1				8.398	0.095	4
2	6.537	0.058	4	8.393	0.167	5
3	7.105	0.089	4	8.270	0.091	5
4	6.658	0.079	5	8.776	0.082	4
5	7.028	0.098	3	8.753	0.081	5
6				8.742	0.203	4
7				8.393	0.223	4
8	6.753	0.061	2	7.376	0.084	5
9	7.054	0.202	3	6.824	0.094	2
10	7.245	0.045	2	7.219	0.035	4
13	6.991	0.060	4			
14	7.039	0.105	5			
15	7.222	0.153	6			
Overall	6.961	0.252	38	8.221	0.603	42

Table 5. 15: Dielectric Relaxation time for conventional and treated films prepared at 400 rpm, calculated using impedance spectroscopy. NE is the number of electrodes tested and NP is the total number of points used to obtain the average values presented.

DIELECTRIC RELAXATION (τ_d) ELECTRON CURRENTS

	CONVENTIONAL		NE:10/15	TREATED		NE:10/11
	Mean	Std. Dev.	NP	Mean	Std. Dev.	NP
Overall	1.07	0.67	38	1.09	0.86	42

The dielectric relaxation time was also calculated for both film types. The results are shown in Table 5. 15. The values have been recorded for D.C. bias voltages ranging from –4 V – +4 Volts, with 5 mV alternating voltage. These values are smaller than those measured in section 5.2.6.1, although direct comparisons are difficult due to the difficulties discussed previously.

5.3.5 Discussion

The results obtained using the equivalent circuit model represent the values of a resistor-capacitor in parallel network and are frequency independent. The frequency dependant results measure the actual values of the resistance and capacitance at a given frequency. If the frequency dependant results are largely frequency independence then the results can be accurately modelled using the equivalent circuit model. The hole results detailed above are frequency independent over the bulk of the frequency range measured, enabling accurate values to be obtained from the equivalent circuit model. Due to the absence of **Re**Z data for the electron only devices the results could only be obtained using the equivalent circuit model. The frequency dependence of the electron only data is unknown. The similarities between the electron and hole only data presented and the good agreement with results obtained previously from I-V measurements, indicates that the electron only data can be accurately modelled using equivalent circuits.

One of the main aims of this thesis is to study the properties of PmPV films prepared using the treated technique, relative to conventional films. Impedance spectroscopy has provided an ideal opportunity for studying several important material properties, including resistivity, conductivity, dielectric relaxation time and permittivity. The capacitance and resistance values are calculated by fitting to the measured impedance values or by transforming the impedance to the admittance and separating into real and imaginary components. Both methods give the same values over most of the frequency range measured. As a result of this the model values were used for calculating the material parameters listed above.

The resistance of a material changes with film thickness, hence must be converted to resistivity before any comparisons are made between the two film types. The same is true for the conductance, which must be converted to conductivity. Seeing as resistivity and conductivity are the inverse of each other we will limit our discussion to the conductivity as we can compare these results with the previous I-V curve results in Section 5.2. The calculated values for the hole conductivity show a clear difference for conventional and treated films. The conductivity of the treated film is one order of magnitude bigger that for the conventional film. The I-V measurements taken on the same devices as the impedance measurements show the same order of magnitude difference and remarkably good agreement with the values calculated using impedance spectroscopy. This not only shows that the two different experimental techniques give the same values but it also acts to verify the clear difference between the conductivity values in the conventional and treated films that we measured in Section 5.2. The electron only devices also verified the trends shown in the measurements of Section 5.2, where the measured values for the conductivity were the same for conventional and treated films. It should however be pointed out that while the trends between treated and conventional films were the same between the I-V and impedance measurements on the films prepared in this section and the I-V measurements on films prepared in Section 5.2, the values obtained in this section were slightly higher than those obtained in Section 5.2. The reason for this is unclear.

Capacitance, like resistance is a parameter that can't be directly compared between films of different thickness, due to its dependence on film thickness. However it can be used to calculate the relative permittivity, ε_r, which is a material dependant parameter. The results for ε_r for the hole only and electron only devices show a clear difference between the conventional and treated films. In both instances the value for the treated film is greater than for the conventional. This indicates a higher polarisability in the treated film, indicative of possible film morphology changes. As discussed previously, in polymeric materials delocalisation of electrons in the π molecular orbitals relative to the positively charged atoms, act as diploes and their separation is proportion to their delocalisation length along the polymer backbone. To achieve higher values for ε_r requires a larger polarisability in the treated films. This is achieved through longer effective conjugation lengths. The fabrication of

treated films doesn't in any way alter the chain length of the PmPV, but the proposed increased interchain separation achieved in the treated films could act to increase the effective conjugation length. This is because interchain interactions act to trap charge, thus reducing the effective conjugation length. Interchain interactions are inversely proportional to interchain separation[36], hence an increase in interchain separation acts to increase the effective conjugation length. The alteration of ε_r requires a change in either chemical structure or film morphology or both. No changes in chemical structure take place during the preparation of treated films, indicating that any observed changes are due to changes in film morphology. This result again supports the experimental evidence presented in previous chapters for increased interchain separation. It should be pointed out that ε_r is related to both the orientation of permanent dipoles and the induced polarisation of individual atoms or ions. It is not related to the majority charge carrier in the material, meaning that the values measured for electron and hole only currents should be the same. This is clearly not the case for the results presented. The use of different solutions for the electron and hole work shouldn't give rise to such differences. The measured values for ε_r are larger than the value of 3 used previously. This combined with the differences between the values measured for the conventional and treated film isn't sufficient to alter the results to the extent that differences of one order of magnitude will be erased.

The graphs of V vs $1/C^2$ allow the free carrier density, p_0, to be calculated. For the results presented, the slope of the graphs is zero for all four devices. This indicates that the sample thickness represents a lower limit for the depletion region width. Using the sample thickness along with the values calculated for the relative permittivity an upper limit for the free carrier density can be calculated[37]. The hole only devices give values of 1.7e+22 and 1.3e+22 m^{-3} for the conventional and treated films respectively, which compare very favourably with the values calculated previously using SCL conduction. The electron only devices give values of 8.3e+21 and 6.2e+21 m^{-3} for the conventional and treated films respectively. These values are slightly lower than measured using SCL conduction.

The dielectric relaxation time was also measured. The values measured for holes differ between the conventional and treated films, as expected due to the different mobilities measured previously. The values measured agree very well with the values measured in Section 5.2, once again showing how different experimental techniques can be used to verify results. However the values measured using electron only currents were the same as expected for conventional and treated films, but differed slightly from those measured in Section 5.2. The large errors associated with the values measured previously could contribute to the difference in values measured by the two experimental techniques.

In the next section Light Emitting Diodes (LEDs) are fabricated to see if the improvements in photoluminescence efficiency, degradation lifetime and the increased hole mobility in treated films of PmPV will translate to longer lifetimes and more efficient LEDs.

5.4 Light Emitting Diodes

5.4.1 Introduction

Since the first reported electroluminescence from a conjugated polymer in 1990[38] there has been rapid development in the field of polymeric LEDs. During the mid 1990s research was focused on the blue end of the visible spectrum, as there were no cheaply available blue emitting inorganic semiconductors. Researchers have also been focusing on producing the red, green and blue emitting devices that fit the requirements of the CIE coordinates necessary to produce perfect white light. This is necessary for the production of high quality, full colour polymeric displays[39]. Small area, limited colour organic displays are currently being marketed. Additionally the fabrication of polymeric lasers and in particular an electrically pumped polymeric laser is another active area of research[40]. The potential applications are endless. For example an electrically pumped blue emitting organic laser will revolutionise the world of data storage and optical communications. Solid state optically pumped polymeric lasers have been demonstrated[41] along with high intensity optically[42] and electrically[43] pumped polymeric microcavities, but the fabrication of an electrically

pumped organic laser is several years away yet. Phosphorescent materials have been successfully utilised to prepare high efficiency, high brightness LEDs through the harvesting of triplet excitons[44,45].

What follows will be a brief outline of how an LED works as most of the theory involved in electroluminescence has been discussed elsewhere within this thesis.

5.4.2 Theory

Electroluminescence from conjugated polymers can be viewed as a four step process. Charge carrier injection into the conduction band and valence band is the first process. Due to the higher hole mobility in most conjugated polymers[46] the efficient injection of electrons is important, otherwise holes may pass through the device without combining with an electron. Efficient electron injection is achieved through good band matching between the polymer and the electron injecting electrode. This is achieved through the use of low workfunction metals, such as Magnesium-Silver or Calcium. Additionally the lowest unoccupied molecular orbital (LUMO) can be tuned to enable the use of more environmentally stable, but higher workfunction, metals such as aluminium. The second process is the transport of charge carriers through the device once they have been injected. This is difficult to control in single layer devices due to the different mobilities associated with different charge carriers. Electron and/or hole transporting layers can be used to aid the symmetrical injection of charge into the active layer. If suitable transporting materials can be found the injected electrons and holes will recombine in the emissive layer, thus maximising device efficiency. Only single layer devices were fabricated in this thesis, for detailed analysis of multi layer device the reader is referred to reference[47]. The third process is the formation of an exciton from the injected electrons and holes. Due to the non-geminate nature of the charges, spin statistics dictate that singlet and triplet excitons will be formed in a 1:3 ratio. This limits the efficiency of devices as only singlet excitons can decay to the ground state by emission of a photon. The fourth and final process is the decay of the singlet exciton. Not all of the singlet excitons formed will decay through the emission of a photon. Some of the excitons will get trapped and

decay by non-radiative routes and others will form triplet excitons through intersystem crossing.

All of the various processes combine to give the following equation for electroluminescence efficiency, ϕ_{EL}

$$\phi_{EL} = \chi\phi_{PL}\eta_r\eta_e \qquad \textit{Equation 5. 36}$$

where χ is the fraction of singlet excitons formed, which is 25%, ϕ_{PL} is the photoluminescence quantum efficiency, η_r is the fraction of injected charge carriers that form excitons and η_e is the fraction of emitted photons that are coupled out of the device. η_r can be maximised through careful choice of electron and hole transporting layers and η_e can be maximised through device fabrication[48].

5.4.3 Experimental Methods and Procedures

Bipolar sandwich structure devices were prepared and tested under an applied D.C. voltage so as to study the I-V characteristics of single layer PmPV LEDs. Comparisons were made between PmPV LEDs prepared by the conventional and the treated techniques. All films were prepared from a filtered (0.8μm pore diameter) 25g/l toluene solution, at 400rpm for 60 seconds.

The 30 nm thick Indium Tim Oxide (ITO) layer was bought from a commercial supplier of sheet ITO on 50 mm square glass substrates. The bottom ITO contact was etched to the required dimensions. PmPV films were then spun on top of the bottom contact using the required spinning technique. Finally the top aluminium contacts were deposited, by thermal evaporation to a thickness of 75 nm. The device structure is the same as that shown in Figure 5. 3 with the bottom metal contact being replaced by ITO.

The devices were tested in the same purpose built test rig as used for the unipolar measurements. They were contacted using conductive silver paint and pressure probes. The probes were connected to a Keithley 2400 source measure unit via coaxial cable. A large area eye response photodiode, connected to a Keithley

mulitmeter, was used to measure the output light intensity. The separation between the active area and the photodiode was 2 mm at all times. An argon feed meant that the devices were tested in an inert atmosphere, as a vacuum attachment wasn't possible. The mulitmeter and the source meter were interfaced to a computer using National Instruments protocols in visual basic. The Current-Voltage-Intensity (I-V-I) characteristics were displayed on screen in real time. Spectra were recorded using an Andor Charge Coupled Device (CCD) Camera, which was connected to an Oriel monochromator with 0.6 nm resolution. The light was collected using a liquid light guide.

Devices were initially forward biased from 0-10V to check for any shorting that sometimes occurred. Subsequent runs were taken in 0.5 V steps up to 20 V and in 1 V steps there after. Film thicknesses were measured using optical profilometry.

5.4.4 Results and Analysis

The aim of this experimental section is to prepare LEDs from PmPV using both the conventional and the treated film preparation techniques and to see if the improvement in photoluminescence efficiency, the increased film thickness and the increased hole mobility in treated films would result in brighter and more efficient LEDs. The films prepared are detailed in Table 5. 16.

There are a number of observations that can be made from the results presented in Table 5. 16. As previously discussed it had been noted that films of type T prepared at 400 rpm showed a thickness increase of ~30% over films of type C, but that in some instances this level of thickness increase was not achieved, for reasons discussed in Section 5.2.7. For the 400 rpm treated film fabricated in this experimental section a thickness increase of 14% was attained. The thickness of the conventional 400 rpm film and the 1000 rpm films is slightly larger than earlier measurements. This can be attributed to differences in the concentration of the solution and possibly to the use of a different bottom contact material. A minimum of three points were used to calculate the mean and standard deviation for the film thicknesses presented.

Table 5. 16: Specifics of PmPV films used for LED analysis. The spin speed is measured in rpm.

Specifics of PmPV Films Used For LED Analysis

Film Type	Spin Speed	Bottom Contact	Top Contact	Deposition Method	Film Thickness		% Increase
					Mean	Std. Dev.	
C	400	ITO	Al	Evaporation	417	7 nm	
T	400	ITO	Al	Evaporation	475	8 nm	+14
C	1000	ITO	Al	Evaporation	272	11 nm	
T	1000	ITO	Al	Evaporation	265	2 nm	-3

The graphs of Electric Field (E) vs Current Density (J) and Electric Field vs Light Intensity (I) show some interesting results. No light emission was detected from either of the two film types prepared at 400 rpm, in the electric field range studied. This may have been due to the large film thickness of these devices giving rise to poor output coupling efficiency and excessive heating[49]. Light emission was however observed from both film types prepared at 1000 rpm. Representative graphs for the 1000 rpm films are plotted in Figure 5. 34 and Figure 5. 35. Some interesting observations can be made from these plots. Firstly the breakdown electric field in both film types is the same. Secondly for a given electric field the output light intensity and the current density is greater in the treated film than in the conventional film. The average magnitude of this difference is two, at the breakdown electric field. The same phenomenon is noticed in the 400 rpm films, except this time only with the current density as there is no light output from these films. The breakdown field in the 400 rpm films is the same as in the 1000 rpm films although the currents densities are significantly lower.

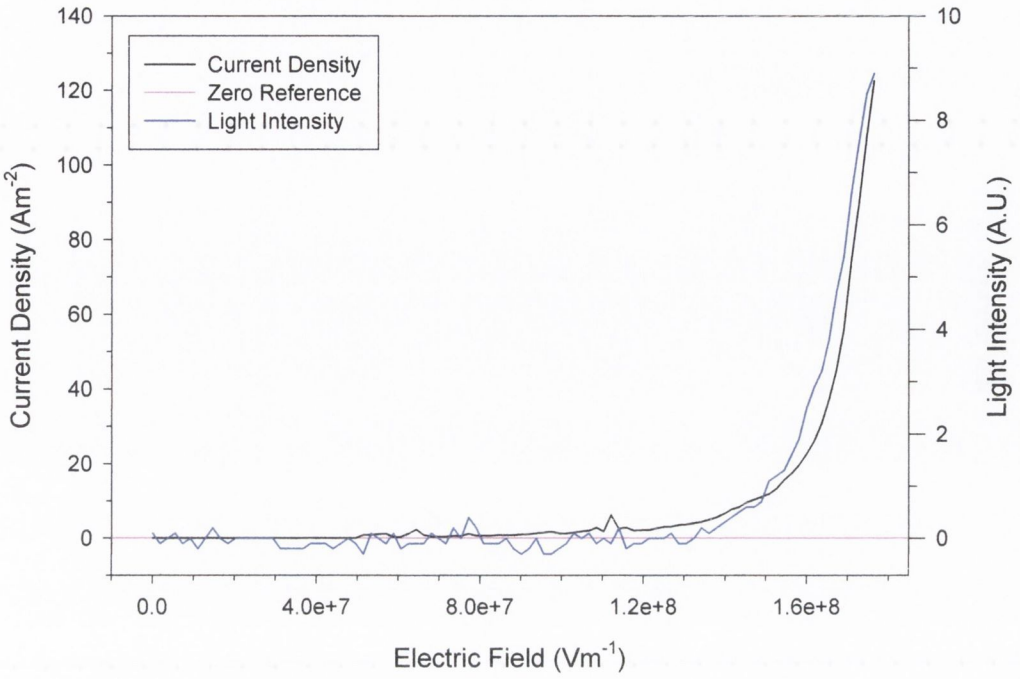

Figure 5. 34: Electric Field vs Current Density (black) and Electric Field vs Light Intensity (A.U.) (blue) for a conventional PmPV LED spun at 1000 rpm.

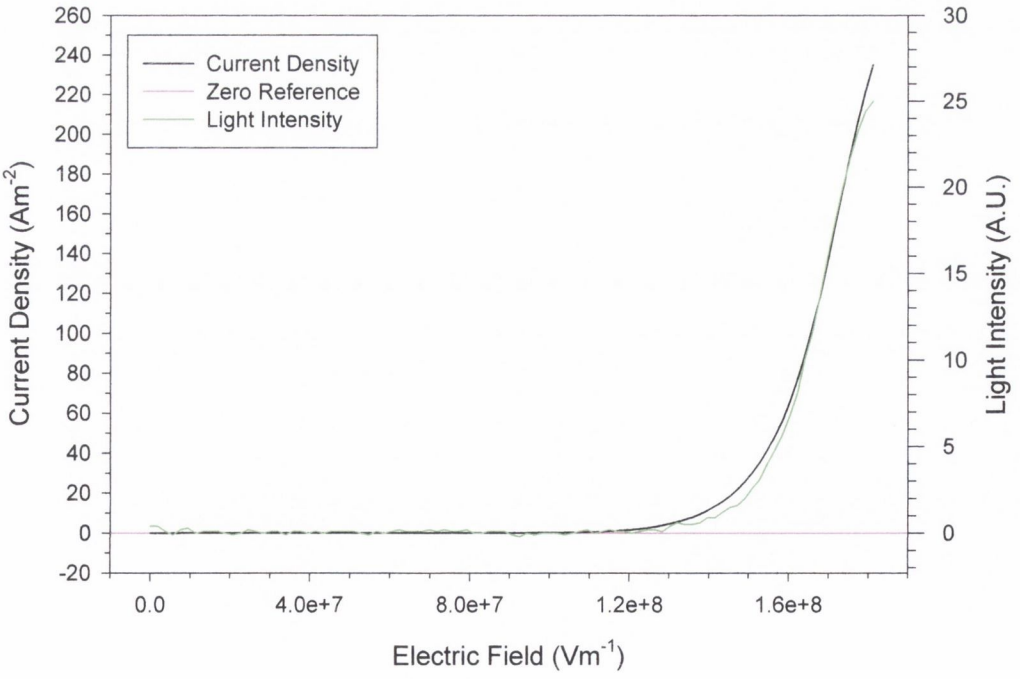

Figure 5. 35: Electric Field vs Current Density (black) and Electric Field vs Light Intensity (A.U.) (green) for a treated PmPV LED spun at 1000 rpm.

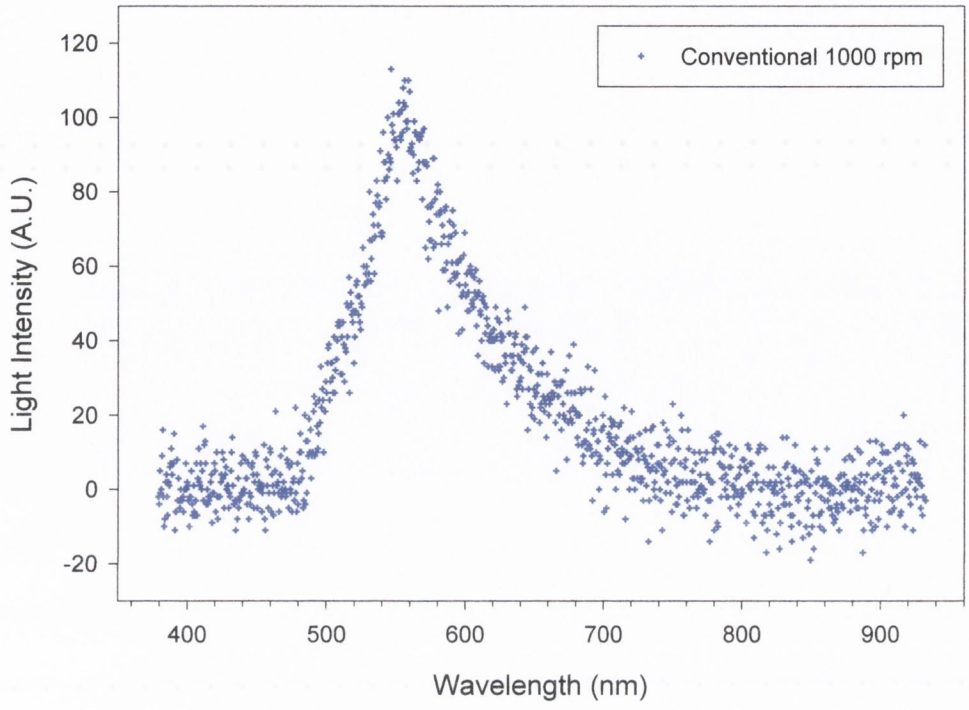

Figure 5. 36: Electroluminescence spectrum for a conventional PmPV LED at 50 Am^{-2}. The film was spun at 1000 rpm.

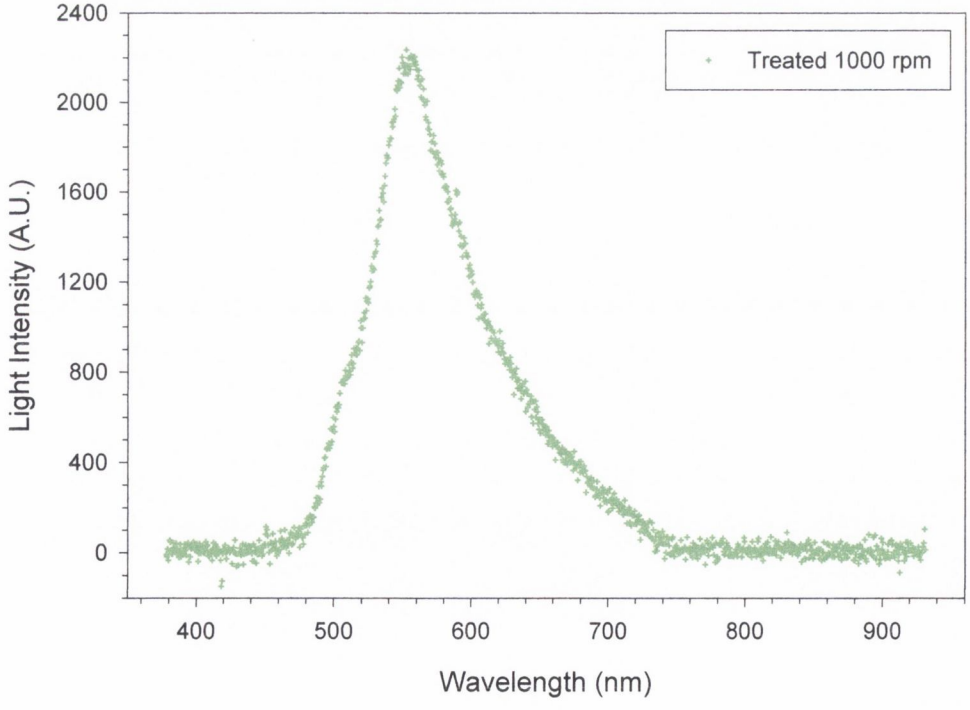

Figure 5. 37: Electroluminescence spectrum for a treated PmPV LED at 50 Am^{-2}. The film was spun at 1000 rpm.

It was noticed that the operating lifetime of the treated device was longer than that of the conventional device. This enabled the device to be held at a constant current density for longer periods before device failure. The electroluminescence spectra that were recorded are shown in Figure 5. 36 and Figure 5. 37. Both spectra were recorded at 50 Am^{-2}, but the treated film was recorded using a higher number of accumulations, due to its increased stability and lifetimes.

5.4.5 Discussion

The results show a very interesting trend, namely that the treated films can sustain a higher current density and have a higher output light intensity for a given applied electric field than the conventional films. The higher current density could be due to a higher hole mobility in the treated films. The hole mobility in 400 rpm films was measured in Section 5.2.6.2 to be one order of magnitude greater than in conventional films. The corresponding measurement was not performed on 1000 rpm films due to experimental difficulties. The increased hole mobility in treated films could be attributed to the removal of air from PmPV thin films and/or the increased interchain separation. If it were due solely to the removal of air from the films then the same mobility increase would be expected in the 1000 rpm films. This wouldn't be the case if it was due solely to increased interchain separation.

This may go some way towards explaining the increased current densities in both the 400 and 1000 rpm treated films, but is by no means certain. The mobility of electrons is unchanged in treated films meaning that no additional electrons are injected into the film. Due to their lower mobility it is the electrons that control η_r, the fraction of injected charge carriers that form excitons, hence η_r remains the same in both film types. The photoluminescence intensity increase in films showing no thickness increase is of the order of 20%. This should contribute to an increased electroluminescence efficiency. A plot of current density vs output intensity for different devices enables relative efficiencies to be established, in terms of light out per unit current. This plot is shown in Figure 5. 38 for the J-E plots shown in Figure 5. 34 and Figure 5. 35. There are some clear differences between the two film types. At low current densities the relative efficiencies in terms of light out per unit current

are similar but at current densities above 65 Am^{-2} the conventional device starts to saturate. A similar drop off isn't seen in the treated film until 220 Am^{-2}. This shows that at the top end of the operational capacity of conventional devices that the treated devices are significantly more efficient. This increase is achieved through increases in ϕ_{PL} and η_e, although the relative contributions are unclear.

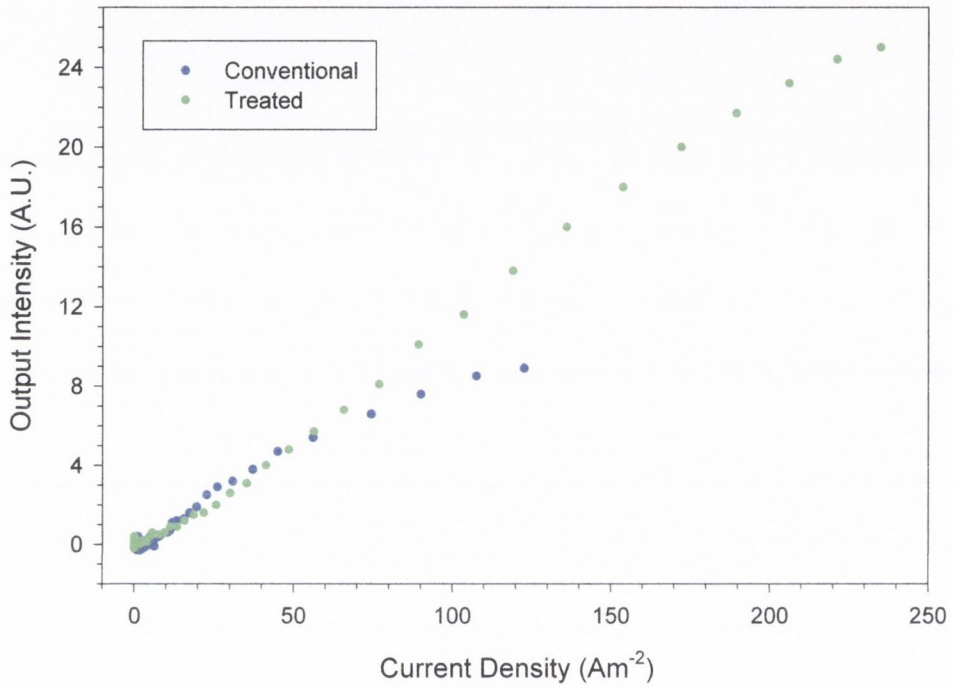

Figure 5. 38: Relative current efficiencies of the conventional (blue) and treated (green) 1000 rpm PmPV LEDs.

All the above results indicate that no one process is leading to the higher output light intensity in the treated film type device. They do however show that for the same electric field the light output is approximately twice that of the conventional device, but that the trade off is a higher current density as opposed to a significantly more efficient device at low current densities. The increase in power efficiency is shown in Figure 5. 39. The y-axis is plotted on a logarithmic scale so as it can be clearly seen that there is no light output prior to a critical turn on electric field being reached. This field is similar for both film types. The photoluminescence intensity increase for 1000 rpm treated films can account for up to one fifth of the measured electroluminescence intensity increase. Some of the additional light output may be due to better output coupling, the reason for which is unclear. Further experimental

work will have to be performed to better ascertain the origins of the increased electroluminescence output and their relative contributions.

In addition to the increased output light intensity, it was noticed that the treated devices were significantly more stable and had longer operating lifetimes than the conventional device. This was very evident when holding the devices at a constant current density while recording the electroluminescence spectra. In the conventional films the electric field required to maintain a constant J value increased dramatically resulting in rapid device failure. In the treated devices the electric field required to maintain a constant J value remained relatively constant with time. This enabled spectra to be accumulated over longer periods, resulting in the clear differences evident in the two electroluminescence spectra presented.

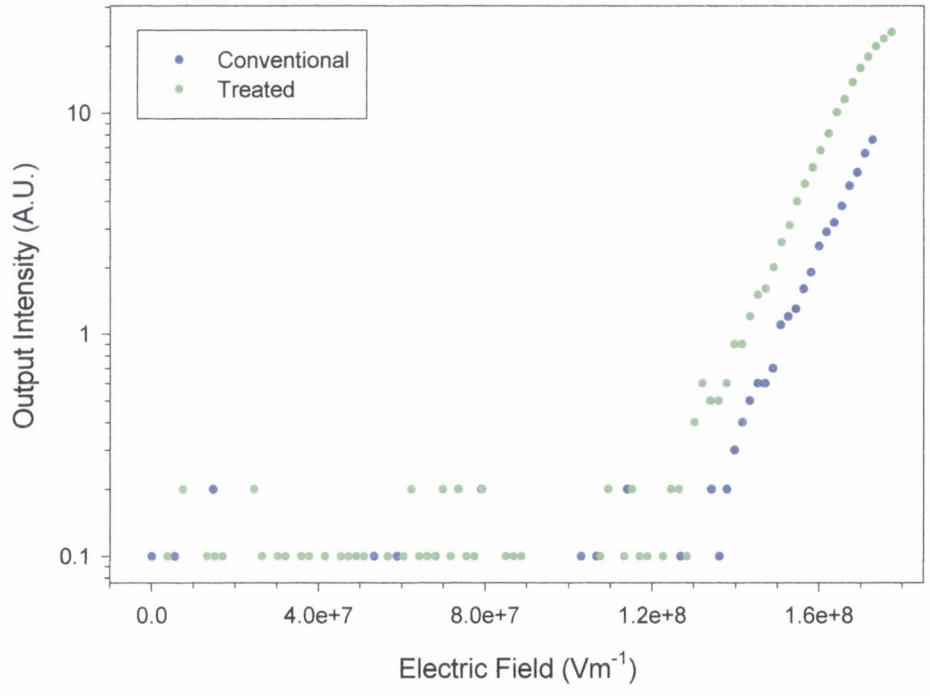

Figure 5. 39: Relative Power efficiency of the conventional (blue) and treated (green) 1000 rpm films LEDs. The y-axis is plotted on logarithmic scale so as the critical turn on electric field can be clearly seen.

The device operating lifetime is one of several requirements that must be met to enable the economic marketing of polymeric devices. The industry standard is 10000 hours. Spectral stability over the device lifetime is another important requirement. If

the spectral output changes over time then the display quality will deteriorate. Unfortunately the measured spectra were not clear enough to perform such measurements.

It should be pointed out that the device operating lifetimes in the treated devices were of the order of several minutes and significantly reduced in the conventional devices. The poor lifetimes of these PmPV devices is attributed to its low charge carrier mobility and low photoluminescence efficiency. It would be hoped that the application of the treated technique to better electroluminescence materials would hopefully lead to more dramatic results.

In total three pairs of 400 rpm films were fabricated. Light emission was not obtained in any of the devices. The information detailed in Table 5. 16 relates to the 400 rpm films that were prepared from the same solution as the 1000rpm films. The absence of any light emission from the 400 rpm films can be attributed to excessive heating due to the thickness of the devices and due to the fact that any electron-hole recombination that takes place will be at the cathode and any emitted light may not make it to the anode due to scattering. Non radiative decay processes contribute to device heating. Poor output coupling can lead to dramatically reduced external efficiencies despite possible high internal efficiencies. This is an issue that has been addressed through several different device architectures, including a minimisation of the coupling of light into the substrate[50] and through the use of hole blocking layers, which act to move the recombination of electrons and holes nearer to the anode.

5.5 Conclusions

This chapter has touched on many areas of the electrical properties of PmPV thin films enabling a detailed picture to be built and an understanding of the effects on the electrical properties through the preparation of treated films. The important point that the reader should take away with them is that the treatment of PmPV films is not detrimental to the performance of electrical devices. In each of the three experimental sections it was shown that important electrical/polymeric properties were improved in the treated devices.

The Current – Voltage measurements showed that for electrons the electrical properties remained unaffected by the fabrication of treated devices. The removal of air in the 1000 rpm films and the removal of air combined with increased interchain separation in the 400 rpm films had no effect on the electrical properties. However differences were noted for holes. Treated films prepared at 400 rpm exhibited trap free conduction, where as the corresponding conventional film showed trapping characteristics. Correspondingly the mobility and conductivity increased and the dielectric relaxation time decreased, all by one order of magnitude. The most probable cause for the elimination of traps can be attributed to the removal of a discrete trapping level caused by an interchain interaction, as shown in Figure 5. 18, due to increased interchain separation. The absence of a similar effect for electrons is unclear. The one sided increase in charge carrier mobility will be of limited benefit in bipolar devices but has the potential to be used for controlling the electrical properties in unipolar devices. However the results for the 1000 rpm treated LEDs show similar properties to the 400 rpm hole only I-V devices, in terms of higher current densities for a given electric field. This indicates that the observed differences between treated and conventional devices may be due to the removal of air from the treated films.

The impedance spectroscopy measurements provided one of the important pieces in the electrical jigsaw in terms of measuring a polymeric property that can be related to interchain separation. The calculation of the relative permittivity, which is proportional to the dielectric polarisability, enables the effective conjugation length of polymeric materials to be compared. In this case it was used to compare conventional and treated films of PmPV. The values measured for the treated film were larger, indicating a higher polarisability and hence longer effective conjugation length. Interactions between neighbouring polymer chains lead to trapping sites that trap single charge carriers and also dissociate excitons, thus effectively shortening the delocalisation length for single charge carriers and excitons. A reduction in such trapping sites through increased interchain separation acts to increase single charge carrier and exciton delocalisation lengths. This is a very important result in that it supports the findings of the previous chapter through an independent experimental technique. The experimental technique also acted to verify the similarity and the difference in the conductivity for the

conventional and treated films for electrons and holes respectively. I-V measurements performed on the same devices produced the same values for the conductivity, again showing the excellent agreement between the two experimental techniques. The results also showed that the devices were depleted of free charge indicating the formation of large depletion regions at the electrodes, considering the device thicknesses measured. The depletion regions were also significantly greater than the device thickness as no dielectric bulk values were observed upon the application of a ±4 volts D.C. potential. The excellent agreement between the equivalent circuit values and the frequency dependant values allowed extensive use of the equivalent circuit in the analysis of the results.

The fabrication of single layer LEDs using both film preparation techniques showed that significant improvement in output light intensity could be achieved, but unfortunately without any significant improvements in efficiency. Additionally the absence of any light emission from the 400 rpm devices curtailed detailed analysis of the effects of interchain separation on output light intensity and device efficiency.

In conclusion the preparation of treated devices from PmPV had a positive effect on device performance. This is shown by the higher hole mobilities that were measured and the brighter LEDs that were fabricated. In addition the calculation of the relative permittivity provided an alternate route to support the increased interchain separation in treated 400 rpm PmPV films.

5.6 References

1. J. G. Simmons, 'Theory of metallic contacts on high resistivity solids – I Shallow Traps,' J. Phys. Chem. Solids 32 (1771) 1987-1999.

2. J. G. Simmons, 'Theory of metallic contacts on high resistivity solids – II Deep Traps,' J. Phys. Chem. Solids 32 (1771) 2581-2593.

3. L. Solymar and D. Walsh, 'Electrical Properties of Materials.' Oxford University Press, 6th Edition (1998).

4. Fowler R H and Nordheim L, Proc. R. Soc. London. Ser. A. 119 (1928) 173.

5. N. F. Mott and R. W. Gurney, 'Electronic Processes in Ionic Crystals,' Dover Publications (1940).

6. C. D. Child, 'Discharge From Hot Cao,' Phys. Rev. 32 (1911) 492-511.

7. K. C. Kao and W. Hwang, 'Electrical Transport in Solids; with particular reference to organic semiconductors', Pergamon Press (1981).

8. Mark P and Helfrich W, J. Appl. Phys. 33 (1962) 205.

9. W. Hwang and K. C. Kao, 'Studies of the theory of single and double injections in solids with a gaussian trap distribution'. Solid State Electronics 19 (1976) 1045-1047.

10. M. Pope and C. E. Swenberg, 'Electronic processes in organic crystals'. 1st Edition, Oxford University Press (1982).

11. W. R. Grove, 'On the electro-chemical polarity of gases,' Phil. Trans. Roy. Soc. London 142 (1852) 87.

12. Arnold Aronson, The basics of sputtering equipment, Material research corporation. 4th ed. (1987).

13. J. Plocharski, H. Drabik, H. Wycislik and T. Ciach, 'Electroheological properties of polyphenylene suspensions,' Synth. Met. 88 (1997) 139-145.

14. A. J. Campbell, D. D. C. Bradley, and H. Antoniadis, 'Quantifying the efficiency of electrodes for positive carrier injection into poly(9,9-dioctylfluorne) and representative copolymers,' J. Appl. Phys. 89 (2001) 3343-3351.

15. S. W. Ko, B-J Jung, T. Ahn and H-K Shim, 'Novel poly(*p*-phenylenevinylene)s with an electron-withdrawing cyanophenyl group,' Macromolecules 35 (2002) 6217-6223.

16. A. J. Campbell, D.D.C. Bradley and D. G. Lidzey, ' Space-charge limited conduction woth traps in poly(phenlene vinylene) light emitting diodes.' J. Appl. Phys. 82 (1997) 6326-6342.

17. E. M. Conwell and Y. N. Gartstein, 'Factors determining polaron mobility in light emitting diodes.' Proceeding of SPIE International Society for Optical Engineering 2528 (1995) 23-31.

18. R. N. Marks, D. D. C. Bradley, R. W. Jackson, P. L. Burn and A. B. Holmes, 'Charge injection and transport in poly(p-phenylene vinylene) light emitting diodes.' Synth. Met. 57 (1993) 4128-4133.

19. H. Meyer, D. Haarar, H. Naarmann and H. H. Horhold, 'Trap distribution for charge carriers in poly(paraphenylene vinylene)and its substituted derivative DPOP-PPV.' Phys. Rev. B 52 (1995) 2587-2598.

20. P. W. M. Blom, M. J. M. de Jong and J. J. M. Vleggaar, 'Electron and hole transport in poly(*p*-phenylene vinylene) devices'. Appl. Phys. Lett. 68 (1996) 3308-3310.

21. C. R. Belton, Ph.D Thesis submitted to Trinity College Dublin (2001).

22. J. E. Bauerle, 'Study of solid electrolyte polarisation by a complex admittance method'. J. Physics & Chemistry of Solids 30 (1969) 2657-2670.

23. S. Karg, W. Riess, V. Dyakonov and M. Schwoerer, 'Electrical and optical characterisation of poly(phenylene-vinylene) light emitting diodes'. Synth. Met. 54 (1993) 427-433.

24. S. Forero-Lenger, J. Gmeiner, W. Brütting and M. Schwoerer, 'Impedance spectroscopy of polymeric light emitting devices based ondifferent poly(*p*- phenylene-vinylene) derivatives'. Synth. Met. 111-112 (2000) 165-168.

25. Webster's Dictionary, Encyclopædia Britannica (1976).

26. H. D. Young, 'University Physics'. 8th edition, Addison-Wesley (1992).

27. K. S. Cole and R. H. Cole, 'Dispersion and absorption in dielectrics I – Alternating current characteristics,' J. Chem. Phys. 9 (1941) 341.

28. W. Bruetting, E. A. Lebedev, S. Karg, T. Dittrich, V. Petrova-Koch and M. Schwoerer, 'Charge carrier mobility in poly(p-phenylenevinylene),' SPIE-Int. Soc. Opt. Eng. Proceedings of Spie - the International Society for Optical Engineering 3281 (1998) 257-265.

29. H. C. F. Martens, P. W. M. Blom and H. F. M. Schoo, 'Comparative study of hole transport in poly(p-phenylene vinylene) derivatives,' Phys. Rev. B - Cond. Matt. 61 (2000) 7489-7493.

30. H. C. F. Martens, J. N. Huiberts and P. W. M. Blom, 'Simultaneous measurement of electron and hole mobilities in polymer light-emitting diodes'. Appl. Phys. Lett. 77 (2000) 1852-1854.

31. I. H. Campbell, D. L. Smith and J. P. Ferraris, 'Electrical impedance measurements of polymer light-emitting diodes'. Appl. Phys. Lett. 66 (1995) 3030-3032.

32. S. H. Kim, K-H. Choi, H-M. Lee, D-H. Hwang, L-M. Do, H. Y. Chu and T. Zyung, 'Impedance spectroscopy of single and double layer polymer light emitting diode'. J. Appl. Phys. 87 (2000) 882-888.

33. H-W. Rhee, K. S. Chin, S. Y. Oh and J-W. Choi, 'Application of impedance technique to OLED'. Thin Solid Films 363 (2000) 236-239.

34. D. W. Marquardt, 'An Algorithm for Least Squares Estimation of Parameters.' Journal of the Society of Industrial and Applied Mathematics, 11 (1963) 431-441.

35. 'Numerical recipes in C: the art of scientific computing,' 2nd ed. Cambridge University Press (1992).

36 T-Q. Nguyen, R. C. Kwong, M. E. Thompson and B. J. Schwartz, 'Improving the performance of conjugated polymer-based devices by control of interchain interactions and polymer film morphology.' Appl. Phys. Lett. 76 (2000) 2454-2456.

37. A. J. Campbell, D. D. C. Bradley, J. Laubender and M. Sokolowski, 'Thermally activated injection limited conduction in single layer N,N'-diphenyl-N,N'-bis(3-methylphenyl)1-1'-biphenyl-4,4'-diamine light emitting diodes.' J. Appl. Phys. 86 (1999) 5004-5011.

38. J. H. Burroughes, D. D. C. Bradley, A. R. Brown, R. N. Marks, K. Mackay, R. H. Friend, P. L. Burn and A. B. Holmes, 'Light-emitting diodes based on conjugated polymers', Nature 347 (1990) 539-541.

39. H. Kobayashi, S Kanbe, S. Seki, H. Kigchi, M. Kimura, I. Yudasaka, S. Miyashita, T. Shimoda, C. R. Towns, J. H. Burroughes and R. H. Friend, 'A novel RGB multicolour light emitting polymer display.' Synth Met. 111-112 (2000) 125-128.

40. Commission of the European Community ESPRIT project 28580 (LUPO).

41. V. G. Kozlov, V. Bulovic, P.E. Burrows and S. R. Forrest, 'Laser action in organic semiconductor waveguide and double-hetrostructure devices.' Nature 389 (1997) 362-364.

42. N. Tessler, G. J. Denton and R. H. Friend, 'Lasing from conjugated polymer microcavities.' Nature 382 (1996) 695-697.

43. R. B. Fletcher, D. G. Lidzey, D. D. C. Bradley M. Bernius and S. Walker, 'Spectral properties of resonant-cavity, polyfluorene light emitting diodes.' Appl. Phys. Lett. 77 (2000) 1262-4.

44. M. A. Baldo, D. F. O'Brien, Y. You, A. Shoustikov, S. Sibley, M. E. Thompson and S. R. Forrest, 'Highly efficient phosphorescent emission from organis electroluminescent devices.' Nature 395 (1998) 151-154.

45. P. A. Lane, L. C. Palilis, D. F. O'Brien, C. Giebeler, A. J. Cadby, D. G. Lidzey, A. J. Campbell, W. J. Blau and D. D. C. Bradley, 'Origin of electrophosphorescence from a doped polymer light emitting diode.' Phys. Rev. B Cond. Matt. 63 (2001) 5206-5212.

46. D. D. C. Bradley, 'Conjugated polymer electroluminescence.' Synth. Met. 54 (1993) 401-415.

47. D. F. O'Brien 'Conjugated Polymer Electroluminescence,' Ph.D Thesis, University of Sheffield (1997).

48. A. N. Safonov, M. Jory, B. J. Matterson, M. G. Salt, J. A. E. Wasey, W. L. Barns and I. D. W. Samuel and W. L. Barnes, 'Modification of polymer light emission by lateral microstructure.' Synth. Met. 116 (2001) 145-148.

49. N. Tessler, N. T. Harrison, D. S. Thomas and R. H. Friend, 'Current heating in polymer light emitting diodes,' Appl. Phys. Lett. 73 (1998) 732-734.

50. J. M. Lupton, B. J. Matterson, I. D. W. Samuel, M. J. Jory and W. L. Barnes, Bragg scattering from periodically microstructured light emitting diodes, Appl. Phys. Lett. 77 (2000) 3340-3342.

Chapter 6

Conclusions and Future Work

6.1 Conclusions

Brighter, longer lived, more energy efficient and spectrally stable light emitting devices (LEDs) are the requirements necessary if organic polymers are to be utilised successfully in commercially available and economically affordable LEDs. This thesis makes significant strides towards these requirements for the luminescent polymer poly(m-phenylenevinylene-co-2,5-dioctlyoxy-p-phenylenevinylene) [PmPV]. Several aspects of LED fabrication were addressed in an effort to understand and improve their performance. The photoluminescence degradation and efficiency were studied and using a novel thin film preparation technique these properties were significantly improved. The morphology of the thin films was altered by the use of this technique, resulting in increased interchain separation. Application of this spinning technique to the fabrication of LEDs was found to improve the power efficiency of single layer PmPV devices. The fabrication of unipolar devices showed that the electrical properties of PmPV didn't deteriorate through the use of this spinning technique and that some properties, including the hole mobility, were improved by one order of magnitude.

The presence of oxygen and water in the atmosphere act to degrade device performance in both optical and electrical applications. Device encapsulation is essential for material stability and consistent device operation, but does not tackle the material properties of efficiency or photo-degradation lifetime. A number of thin film preparation techniques were employed to improve these properties prior to encapsulation. At this point one technique, known as the *treated* technique was thought to have altered the morphology of PmPV films. The effects associated with this included an increased photoluminescence efficiency of at least 27% combined with longer photo-degradation lifetimes and most significantly an increase in film thickness coupled with spectral

broadening towards the blue end of the spectrum, due to a disruption of chain aggregation in the solid state. It was these effects that warranted further study, as their implications for optoelectronic devices is far reaching.

Comparisons between PmPV films and blend films prepared using polystyrene, measured using photoinduced absorption techniques, showed that the polaron yield in thin polymer blend films, with a large interchain separation, is eliminated. The polaron signal in the treated film type was still clearly evident but significantly reduced compared to conventional PmPV films. This indicated that the changes in film morphology in the treated film were due to increased interchain separation. This reduction in polaron yield through increased interchain separation provided an explanation for the photoluminescence efficiency increase measured in the treated films. Measurement of the relative permittivity using impedance spectroscopy also provided supporting evidence to verify changes in film morphology. The relative permittivity of a dielectric is related to the polarisability, enabling the effective conjugation length to be compared between materials. The treatment of PmPV films increased its relative permittivity indicating an increase in polarisability and hence an increased delocalisation length for charge carriers through reduced interchain coupling, which acts to reduce delocalisation lengths by trapping charge.

The polaron absorption was observed to be at a comparatively high energy relative to other similar PPV derivatives. Two polaron absorptions were observed in a solution doping measurement, although it was noted that the higher energy transition dominated. The reason for the domination of one transition over another is unknown. A possible explanation, based on the breaking of symmetry due to the meta linkage in PmPV, was offered for the observation of the two transitions. The high energy of the polaron absorption meant that it overlapped the photoluminescence spectrum, effectively eliminating PmPV for solid state lasing applications. This highlighted the possible limitations of meta linkages for improving luminescence efficiency although further studies are required. Electrically pumped solid state organic lasers will require not only the removal of the overlap between the photoluminescence and polaron absorption but the elimination of polaron formation, as it dramatically reduces photoluminescence efficiency. The same can be said about eliminating triplet yields.

Device operating voltages can be reduced considerably if the conductivity can be increased. This is often achieved through the use of dopants. This however can lead to problems as some dopants can diffuse rapidly through a device, while others contain unwanted impurities. A thin film fabrication technique that improves charge carrier mobility instead of increasing charge carrier density would provide an alternative route. The mobility of holes in treated films of PmPV was found to have increased by one order of magnitude relative to untreated films. The same result was not achieved for electrons thus eliminating the possibility of the fabrication of LEDs with significantly enhanced efficiency through increased electron mobility. The treatment of PmPV films was found to have no detrimental affects on the electrical properties of PmPV films, indicating that the incorporation of treated films into both unipolar and bipolar devices should help improve device efficiencies.

The differences between conventional and treated PmPV thin films were measured using both direct current measurements and alternating current measurements. This allows results to be verified by alternate means, providing a valuable tool in experimental analysis.

In conclusion the photoluminescence efficiency of PmPV thin films was increased through the development of a film preparation technique that fabricated films with increased interchain separation. It was shown that these films were spectrally stable and photo-degraded less rapidly when exposed to laser light at 457.9 nm in both air and inert atmospheres. The increased photoluminescence efficiency was shown to be a consequence of a reduction in the polaron yield, which verified the increased interchain separation in the treated films. The treatment of PmPV films was shown not to be detrimental to the performance of electrical devices and in some instances significantly improved polymeric properties essential for the fabrication of efficient devices. The calculation of the relative permittivity using electrical measuring techniques supported the results obtained optically for increased interchain separation.

This thesis provides an insight into some of the requirements necessary for developing high efficiency devices through optimisation of thin film preparation techniques. The

results provide an understanding of some of the requirements necessary for device preparation and the design of polymeric materials more suited to the fabrication of high efficiency electrical and optical devices.

6.2 Future Work

There are several areas where work still needs to be performed in relation to this thesis. Firstly electrical degradation measurements need to be performed for both unipolar and bipolar currents. These measurements will involve passing constant current densities through the devices for a number of hours and monitoring the drive voltage required to maintain the constant current density. Reflection FTIR spectra, taken through thin top contacts on the unipolar devices, will enable the degradation effects to be studied at the molecular level. Any differences between different charge carriers and electrical and optical degradation can then be studied. Photoluminescence spectra, taken through the thin top contacts on the unipolar devices and through either contact on the bipolar devices will enable efficiency and spectral changes to be monitored. These measurements will indicate if the treatment of PmPV films also improves electrical degradation and stability in addition to improving these properties optically.

The second significant area of work still to be done is the application of the treated technique to other polymeric materials and in particular materials with excellent light emitting properties such as poly(9,9-dioctyl fluorene) (PFO). The possibilities for this study include; Altering sidechains and the length of sidechains, comparisons between meta and para linkages on the backbones, the use of small molecules, comparisons between the monomer and its corresponding polymer, including a conjugation length study. This number of possible studies is outside the scope of this thesis, but would provide a valuable insight into the polymeric properties best suited to optimising the treatment of thin films.

Appendix A

List of Publications

'Amplified spontaneous emission and optical gain spectra from stilbenoid and phenylene vinylene derivative model compounds.'

K. P. Kretsch, C. Belton, S. Lipson, W. J. Blau, F. Z. Henari, H. Rost, S. Pfeiffer, A. Teuschel, H. Tillmann and H-H. Horhold.

J. Appl. Phys. 86 (1999) 6155-6159

'Investigation of efficiency and photostability in polymer films.'

S. M. Lipson, D. F. O'Brien, H. J. Byrne, A. P. Davey and W. J. Blau.

Synth. Met. 111-112 (2000) 553-557

'Optical gain spectra from doped polymeric waveguides.'

K. P. Kretsch, C. Belton, S. Lipson, W. J. Blau, F. Z. Henari, S. Pfeiffer, H. Tillmann and H-H. Horhold.

Synth. Met. 111-112 (2000) 567-570

'Improvement of luminescence efficiency and photostability in polymer thin films.'

S. M. Lipson, D. F. O'Brien, H. J. Byrne, A. P. Davey and W. J. Blau.

Thin Solid Films 370 (2000) 262-267

'Photophysics of a poly(phenylenevinylene) with alternating meta-phenylene and para-phenylene rings.'

P. A. Lane, S. M. Lipson, A. J. Cadby, D. F. O'Brien, H. Mellor, S. J. Martin, D. G. Lidzey, D. D. C. Bradley and W. J. Blau.

Phys. Rev. B Cond. Matt. 62 (2000) 15718-15723

'The Photophysics of Thin Polymer Films of poly(meta-phenylene-co-2,5-dioctoxy-para-phenylenevinylene).'

S. M. Lipson, A. J. Cadby, P. A. Lane, D. F. O'Brien, D. D. C. Bradley and W. J. Blau.

Chem. Monthly 132 (2001) 151-158

'Increased luminescence efficiency in PmPV thin films by modified thin-film preparation techniques.'

S. M. Lipson, D. F. O'Brien, A. Drury, H. J. Byrne and W. J. Blau.

Synth. Met. 119 (2001) 569-570

'Studies of a poly(phenylenevinylene) without C_{2h} symmetry.'

P. A. Lane, S. M. Lipson, A. J. Cadby, D. F. O'Brien, H. Mellor, S. J. Martin, W. J. Blau and D. D. C. Bradley.

Synth. Met. 119 (2001) 661-662

'Investigation of photoluminescence efficiency in thin polymer films of poly(m-phenylenevinylene-co-2,5-dioctyloxy-p-phenylenevinylene).'

D. F. O'Brien, S. M. Lipson, A. J. Cadby, P. A. Lane, D. D. C. Bradley and W. J. Blau.

Synth. Met. 121 (2001) 1405-1406

'Optical properties of alkoxy-substituted Poly (p-phenylene 1,3,4-oxadiazoles) of extended conjugated chain to be employed in electro-optical devices.'

P. Mormile, L. Petti, M. Gillo, P. Laurienzo, M. Malinconico, A. Roviello, S. Lipson and W. J. Blau.

Submitted to Applied Physics B: Lasers & Optics.

'Model study in molecular engineering for nonlinear photonic devices: poly (arylene ethynylene) and poly (arylene vinylene) copolymers.'

K. G. Ryder, S. M. Lipson, A. Drury, S. M. O'Flaherty and W. J. Blau.

Accepted for the Proceedings of SPIE's 46th Annual Meeting and International Symposium on Optical Science and Technology. 29th July-3rd August 2001, San Diego USA.